

Preparation and Characterization of Metal-Organic Framework Membranes for Gas Separation

Von der Naturwissenschaftlichen Fakultät
der Gottfried Wilhelm Leibniz Universität Hannover
zur Erlangung des Grades

Doktor der Naturwissenschaften

Dr. rer. nat.

genehmigte Dissertation

von

Dipl.-Chem. Helge Bux

geboren am 20.03.1982 in Hannover

2011

Referent: Prof. Dr. Jürgen Caro
Korreferent: Prof. Dr. Jörg Kärger

Tag der Promotion: 15.07.2011

Preface

This thesis represents original work which was conducted while I was a member of the scientific research staff at the “Gottfried Wilhelm Leibniz University Hannover”, under the supervision of Prof. Dr. Jürgen Caro from April 2009 until May 2011.

During this period, I participated in the project “Mass Transfer in Metal-Organic Frameworks (MOFs): From Molecular Diffusion to Membrane Permeation”, which was financed by the “Deutsche Forschungsgemeinschaft” (DFG) within the priority program SPP1362 “Porous Metal-Organic Frameworks” that was organized by Prof. Dr. Stefan Kaskel. This project was a collaboration between the groups of Dr. Michael Wiebcke (Institute of Inorganic Chemistry, Leibniz University Hannover), Dr. Christian Chmelik and Prof. Dr. Jörg Kärger (Institute of Applied Physics, Leipzig University), and Priv.-Doz. Dr. Siegfried Fritzsche (Institute of Theoretical Physics, Leipzig University). In addition to the very close partnership with Prof. Dr. Yanshuo Li (State Key Laboratory of Catalysis, Dalian Institute of Chemical Physics, Chinese Academy of Science), Priv.-Doz. Dr. Armin Feldhoff (Institute of Physical Chemistry and Electrochemistry, Leibniz University Hannover), Dr. Jasper M. van Baten, and Prof. Dr. Rajamani Krishna (Department of Chemical Engineering, University of Amsterdam) also contributed to the project.

Seven research articles, in which I have participated as primary or co-author, are included in this thesis. I wrote the article presented in Section 2.2 with the kind support of the co-authors. My contribution was to prepare the membrane and crystalline powders from the MOF zeolitic imidazolate framework-8 (ZIF-8). I also performed the corresponding characterization by scanning electron microscopy (SEM) and the energy-dispersive X-ray spectroscopy (EDXS). However, I kindly thank Frank Steinbach for sample preparation and technical support. Dipl.-Chem. Janosch Cravillon and Dr. Michael Wiebcke contributed the X-ray diffraction (XRD) analysis of the ZIF-8 membrane and the crystalline powder and the sorption analysis using the Brunauer-Emmett-Teller (BET) model. M. Sci. Fangyi Liang built the permeation measurement apparatus and helped me to perform the mass transfer experiments on the ZIF-8 membrane.

The article in Section 2.3 was written by Prof. Dr. Yanshuo Li. My contribution was to provide some experimental assistance, to share experimental knowledge, and to assist in writing the article.

I also wrote the article in Section 3.2 with the kind assistance of the co-authors. I conducted the preparation of the oriented ZIF-8 membranes and the corresponding crystalline ZIF-8 powders, as well as the characterizations by SEM, EDXS, and XRD. I also performed the mass transfer experiments on the ZIF-8 membrane. Priv.-Doz. Dr. Armin Feldhoff contributed the transmission electron microscopy (TEM) images of the cross-section of the oriented ZIF-8 membrane, and Prof. Dr. Yanshuo Li provided crucial impulses for the seeding process. Dipl.-Chem. Janosch Cravillon and Dr. Michael Wiebcke provided the synthesis of the ZIF-8 nanocrystals and advised me on the fields of XRD and crystallography.

The article in Section 3.3 was written by Prof. Dr. Yanshuo Li. My contribution was to perform permeation measurements on the oriented ZIF-7 membranes and to assist in writing the article.

My contribution to the article in Section 4.2, which was written by Dr. Christian Chmelik, was the synthesis and corresponding SEM and XRD characterizations of large ZIF-8 single crystals that were used to obtain diffusion and adsorption data of ZIF-8 by infrared microscopy (IRM), as well as support in writing.

I wrote the article in Section 4.3 with the kind assistance of the co-authors. I performed the membrane preparation, the corresponding characterization by SEM, and the permeation measurements. In addition, I synthesized the large ZIF-8 crystals that were used for the IRM studies and performed the corresponding SEM characterization of the crystals. The above-mentioned IRM investigations were performed by Dr. Christian Chmelik, whereas Dr. Jasper M. van Baten and Prof. Dr. Rajamani Krishna contributed vital data from grand canonical Monte Carlo (GCMC) simulations.

Prof. Dr. Jürgen Caro and I wrote the last article in Section 4.4 with kind support of the co-authors. I synthesized the large ZIF-8 single crystals for the IRM investigations that were carried out by Dr. Christian Chmelik. Additionally, I prepared the ZIF-8 membrane, conducted the corresponding membrane permeations measurements, and performed the SEM investigation on the membrane and the single crystals. Prof. Dr. Rajamani Krishna contributed the GCMC data.

Finally, I kindly thank Prof. Dr. Jürgen Caro for his excellent and outstanding support during my time as a doctoral student in his group at the Leibniz University Hannover, and I appreciate my assignment to the above-mentioned project. This assignment provided an

opportunity for me to obtain valuable insight into two truly thrilling fields: metal-organic frameworks and microporous membranes. I also thank my project colleagues and collaboration partners, namely, Prof. Dr. Yanshuo Li, Priv.-Doz. Dr. Armin Feldhoff, Dipl.-Chem. Janosch Cravillon, Dr. Michael Wiebcke, Dr. Christian Chmelik, Prof. Dr. Jörg Kärgner, Dipl.-Phys. Loreen Hertäg, Dipl.-Phys. Markus Knauth, Priv.-Doz. Dr. Siegfried Fritzsche, Dr. Jasper M. van Baten, and Prof. Dr. Rajamani Krishna for the fruitful collaboration. In particular I thank Prof. Dr. Jörg Kärgner for evaluating this work as second referee. A special acknowledgement is given to Prof. Dr. Yanshuo Li for the lively discussions and the exchanges of knowledge.

I thank all current and former members of the Caro group, particularly Dr. Daniel Albrecht, M. Sci. Fangyi Liang, Frank Steinbach, Dipl.-Chem. Konstantin Efimov, and Dipl.-Chem. Oliver Merka for their kind support in technical aspects as well as Kerstin Janze and Yvonne Gabbey-Uebe for their administrative support. I also like to thank the technical staff of the institute, namely, Mr. Becker, Mr. Bieder, Mr. Egly, Mr. Ribbe, and Mr. Rogge.

Finally, I thank my parents Elke Jacob-Bux and Hermann Bux, my brother Fabian Bux, and my partner in life Amanda Zen for providing me motivation.

Abstract

The following thesis is dedicated to the preparation and characterization of microporous metal-organic framework (MOF) membranes on a laboratory scale. The prototypical MOFs ZIF-7 and ZIF-8 (ZIF = zeolitic imidazolate framework) were chosen for the investigations. The thesis includes seven articles, published in subject-specific, internationally renowned journals. The articles are reprinted and arranged in a logical, rather than a time-based order.

ZIF-7 and ZIF-8 membranes were prepared by two different routes. Continuous, polycrystalline layers of ZIF-8 could be solvothermally grown by in-situ crystallization on top of macroporous titania supports after finding a suitable, phase-pure synthesis in methanol. By microwave-assisted heating, the heat rate and temperature during the synthesis could be controlled, thus allowing a high reproducibility of the experiments. A more general preparation approach was obtained by seeding α -alumina supports from colloidal nanocrystal suspensions containing the polymeric additive polyethyleneimine. This method produced oriented, continuous thin-films of ZIF-7 and ZIF-8 after a subsequent secondary growth. The membranes and the secondary growth processes were studied in detail by analytical techniques such as ex-situ X-ray diffraction (XRD), scanning electron microscopy (SEM), energy-dispersive X-ray spectroscopy (EDXS), transmission electron microscopy (TEM), and selected-area electron diffraction (SAED). Unary and equimolar binary mass transfer experiments on the membranes were performed using the Wicke-Kallenbach technique. The latter technique was coupled with online gas chromatography (GC), which allowed the quantitative analysis of the permeate concentration in the sweep gas stream. In these experiments, the pure component and gas mixture permeances as well as the corresponding separation factors of standard light gases (e.g., hydrogen, oxygen, carbon dioxide, and methane) were investigated as a function of feed-pressure and temperature. The observed mass transfer through the ZIF-8 membranes was interpreted on the basis of diffusion and adsorption data, which were derived from a combination of infrared microscopy (IRM) on large ZIF-8 single crystals and grand canonical Monte Carlo (GCMC) simulations. The observed separation factors could be understood by a simple, Fick-based diffusion model. This model provided predictions of the membrane selectivity as function of pressure and temperature, which were in good agreement with the experimental measurements.

Keywords:

Membranes, Metal-Organic Frameworks, Zeolitic Imidazolate Frameworks, Diffusion, Adsorption

Zusammenfassung

Die folgende Dissertation behandelt die Präparation und Charakterisierung von mikroporösen Membranen aus metallorganischen Gerüststrukturen (MOFs). Die prototypischen MOFs ZIF-7 und ZIF-8 (ZIF = zeolithartige Imidazol-Strukturen) wurden für die Untersuchungen ausgewählt. Die Arbeit enthält sieben Artikel, welche in international renommierten Fachzeitschriften veröffentlicht wurden und hier in logischer statt chronologischer Reihenfolge nachgedruckt sind.

Durch unterschiedliche Methoden konnten ZIF-7 und ZIF-8 Membranen präpariert werden. Polykristalline, durchgängige Schichten von ZIF-8 konnten in-situ mittels Solvothermalsynthese auf makroporösen Titandioxid-Trägern gezüchtet werden, nachdem eine geeignete, phasenreine Synthese in Methanol gefunden worden war. Durch dielektrisches Heizen mittels Mikrowellenstrahlung konnten während der Synthese die Aufheizrate und die Temperatur kontrolliert und entsprechend gut reproduzierbare Ergebnisse erzielt werden. Ein genereller Ansatz zur Synthese von MOF-Membranen stellte schließlich die Tauchbeschichtung von porösen Korund-Trägern mit nanokristallinen Keimkristallen aus entsprechenden Suspensionen dar, nachdem den Suspensionen das Polymeradditiv Polyethylenimin zugesetzt worden war. Nach anschließendem Wachstum der Keimkristalle unter solvothermalen Bedingungen konnten polykristalline Dünnschichten erhalten werden. Der Wachstumsprozess der Membranschichten sowie die Membranen selbst wurden ex-situ durch Röntgendiffraktometrie (XRD), Rasterelektronenmikroskopie (REM), energie-dispersive Röntgenspektroskopie (EDXS), Transmissionselektronenmikroskopie (TEM) und Feinbereich-Elektronenbeugung (SAED) untersucht. Unäre und equimolar-binäre Stofftransport-Experimente an den ZIF-Membranen wurden mittels der Wickelkallenbach-Methode durchgeführt. Die Permeat-Konzentrationen im Spülgas wurden „online“ mittels Gaschromatographie gemessen. In den Experimenten wurden sowohl die Einzelstoff- und Gemischpermeanzen als auch die entsprechenden Stofftrennungsfaktoren als Funktion der Temperatur und des Speisedruckes bestimmt. Der beobachtete Stofftransport durch ZIF-8-Membranen wurde auf Basis von Adsorptions- und Diffusionsdaten interpretiert, welche aus Infrarot-Mikroskopie (IRM) an großen ZIF-8 Einkristallen sowie großkanonischen Monte Carlo (GCMC) Simulationen ermittelt wurden. Die beobachtete Trennung an den ZIF-8 Membranen konnte aus den Diffusions- und Adsorptionsdaten mittels einem auf dem 1. Fick'schen Diffusionsgesetz basierenden, einfachen Modell hinreichend genau vorhergesagt werden.

Stichwörter:

Membranen, Metall-organische Gerüststrukturen, Zeolitische Imidazol-Strukturen,
Diffusion, Adsorption

Contents

1	Introduction	1
1.1	Motivation	1
1.2	Metal-Organic Frameworks	4
1.2.1	Introduction and Terminology	4
1.2.2	Naming and Classification into Subtypes	5
1.2.3	Structure Principles of MOFs	6
1.2.4	Chemical and Physical Properties	7
1.2.5	Structure and Properties of the Zeolitic Imidazolate Frameworks ZIF-7 and ZIF-8	8
1.2.6	ZIF-7 and ZIF-8 as Promising Materials for Molecular Sieving	11
1.3	Mass Transport in Microporous MOF Membranes	12
1.3.1	General Aspects	12
1.3.2	Adsorption in Microporous Materials	13
1.3.3	Transport Diffusion through Microporous Membranes	16
1.4	Preparation of MOFs by Microwave-Assisted Heating	18
1.4.1	Theoretical Aspects of Dielectric Heating of Liquids	18
1.4.2	Practical Aspects of MW-Assisted Heating	19
1.5	Bibliography	22
2	Preparation and Characterization of ZIF-7 and ZIF-8 Membranes	29
2.1	Summary	29
2.2	Zeolitic Imidazolate Framework Membrane with Molecular Sieving Properties by Microwave-Assisted Solvothermal Synthesis	30
2.3	Molecular Sieve Membrane: Supported Metal-Organic Framework with High Hydrogen Selectivity	34
3	Understanding Oriented Growth Processes in Polycrystalline MOF Films	39
3.1	Summary	39
3.2	Oriented Zeolitic Imidazolate Framework-8 Membrane with Sharp H_2/C_3H_8 Molecular Sieve Separation	40
3.3	Controllable Synthesis of Metal-Organic Frameworks: From MOF Nano- rods to Oriented MOF Membranes	50
4	Understanding Mass Transfer through MOF Membranes on the Basis of ZIF-8	57
4.1	Summary	57
4.2	Mass Transfer in a Nanoscale Material Enhanced by an Opposing Flux	58

4.3 Novel MOF-Membrane for Molecular Sieving Predicted by IR-Diffusion Studies and Molecular Modeling	64
4.4 Ethene/Ethane Separation by the MOF Membrane ZIF-8: Molecular Correlation of Permeation, Adsorption, Diffusion	68
5 Closing Remarks	75
Appendix	79
Publications	79
Contributions to Conferences	80
Curriculum Vitae	83
Erklärung zur Dissertation	85

1 Introduction

1.1 Motivation

The selective removal of one or more chemical species from fluid (liquid or gas) mixtures by membranes is established in various industrial fields of separation, replacing classical purification processes in chemistry (e.g., distillation) [1]. Membranes are applied in reverse osmosis (RO; e.g., sea water desalination), nanofiltration (NF; e.g., water removal to concentrate sugars), ultrafiltration (UF; e.g., oil/water emulsions separation), and microfiltration (MF; e.g., wastewater treatment) [1, 2]. Industrial fields, in which membranes more recently were introduced are gas separation (GS; e.g., natural gas refining) and pervaporation (PV; e.g., alcohol extraction from organic solvents) [2]. Membranes allow simple, continuous, and low-energy separation processes that can be used in combination with chemical reactions in one step for process intensification (membrane reactors). In addition, membranes can outperform the classical distillation because they are capable of separating azeotropic mixtures or species with similar boiling points that are distillatively in-separable.

Membranes may consist of dense materials, such as organic polymersⁱ, or inorganic materials, such as perovskitesⁱⁱ or palladium alloysⁱⁱⁱ. However, a more reasonable approach is the concept of using porous materials that are applicable for the separation of a broad range of chemical species. Within the divergent group of porous materials, two types may generally be distinguished: a) non-crystalline (non-regular) porous materials, such as porous carbons or silica prepared by the sol-gel route, and b) crystalline (regular) porous materials, such as microporous^{iv} zeolites or mesoporous^{iv} MCMs (MCM = Mobile crystalline materials). Micropores may exhibit three kinds of separation mechanisms: a) favored or exclusive adsorption of a species from a mixture, b) diverging mobilities of species within the pores, or c) steric or size exclusion, known as molecular sieving. The latter is the simplest and the most efficient mechanism because, theoretically, it shows 100% selectivity. However, molecular sieving reliably works only through a regular micropore network without any size distribution, as it is inherent to the crystallographic structure of the above mentioned zeolites.

ⁱ Similar to a liquid, a polymer can absorb molecular species from fluid phases in its bulk matrix.

ⁱⁱ Perovskites exclusively incorporate and transport ionic oxygen by lattice vacancies.

ⁱⁱⁱ Palladium alloys exclusively incorporate and transport atomic hydrogen in their crystal lattice.

^{iv} Micropores and mesoporous are considered here according IUPAC regulations with < 2 nm and $2 \leq 50$ nm pore diameter, respectively.

The application of molecular sieve zeolite membranes has been intensively investigated for more than 20 years on the laboratory scale and has primarily focused on GS. Though the membranes partly show remarkable selectivities, zeolite membranes have failed to find their place in industrial GS until recently. This apparent contradiction can be related to the intrinsic properties of zeolites and practical issues in transferring the idealized, laboratory scale model system to practice relevant process conditions. In contrast to the widely used polymer membranes, zeolite membranes are much more expensive, and their method of production and their operation is more challenging. Zeolite membranes represent composites consisting of a thin and brittle polycrystalline layer that is mechanically stabilized against cracking on top of a macroporous stiff support^v. Once grown, the polycrystalline zeolite layer is inflexible. Consequently, the shape of the composite membrane is restricted to the original shape of the support that is commonly flat, tubular, or in the geometry of a capillary or hollow fiber. In contrast, polymers can be spun as flexible hollow fibers or tape-casted as thin-films. Polymer foils can be easily shaped subsequent to the preparation, for example, as spiral-wound membrane module that has higher surface areas per unit volume in comparison with conventional membrane geometries [1].

The fabrication process of zeolite membranes necessarily includes a calcination step to remove the structure directing agent (SDA) that forms the pores, except for a few zeolites that can be prepared without SDA such as LTA and FAU^{vi}. Because the support must withstand calcination at temperatures of 450 - 500 °C in air and for material compatibility, ceramics, such as alumina or titania, are commonly used. However, stress may be induced in the membrane-support boundary region during calcination and dehydration due to different expansion coefficients, which form cracks within the membrane layer [3]. A general problem of membranes is the filter cake-like aggregation of macroscopic particles on top of the membrane (membrane fouling), which results in a reduced performance [1, 4]. Zeolites, however, with their small channels, are additionally subject to internal pore-blocking. Small molecules, which are normally highly mobile within the pores as a pure component, may be substantially hindered in their diffusion while in mixture with a second, bulky species that blocks the pores. This phenomenon can reduce drastically the efficiency of molecular sieving [5-7]. Because of the above-mentioned drawbacks of microporous zeolite

^v Usually macroporous alumina or metal supports are fabricated by sintering particles that are a few μm in size.

^{vi} The three-digit letter code stands for LTA = Linde type A or FAU = faujasite, see ref [36].

membranes, it is not surprising that GS is currently still dominated by polymer membranes [1, 2].

Nevertheless, ultra-hydrophilic LTA zeolite membranes have recently found their niche in steam permeation, as demonstrated by the industrial pilot plant of Mitsui for the dewatering of bioethanol beyond the azeotropic point [8]. The process is, however, based on the strong and exclusive adsorption of water in defect-pores (thus blocking these pores for non-selective transport) rather than by true molecular sieving. Whereas the hydrated LTA membrane shows water/ethanol selectivity > 1000 under process operation, no shape-selectivity is found for the dehydrated LTA membrane after Ca^{2+} exchange^{vii} in the n-butane/i-butane separation.

Metal-organic frameworks (MOFs), which are new types of microporous hybrid materials, have recently emerged from intersecting the classically divided fields of organic and inorganic chemistry [9]. MOFs can be pre- and post-modified with functional groups, while the basic structure is not altered (isorecticular design) [10-13]. The modification allows the fine-tuning of pore size and the control of adsorption affinities, resulting in a previously unattainable pore customizability. MOFs show unique properties, such as ultra-high inner surfaces and structural flexibility (e.g., pore or “gate” opening for only specific molecular species). These remarkable properties of MOFs are of great interest for membrane applications. The critical and energy-intensive calcination step, as necessary for most zeolites, may be avoided because most syntheses are template-free, and only the solvent must be removed for activation. To avoid any damage of the MOF upon solvent removal, it is crucial to develop specific MOF syntheses with volatile solvents that are easy to remove (e.g., methanol), thus eliminating the need to work with more bulky solvents such as dimethylformamide (DMF) or diethylformamide (DEF). The hybrid organic-inorganic nature of MOFs is expected to be compatible with a broad range of support materials, which consequently allows to use low-cost, non-ceramic supports as mechanic stabilization. MOFs, as crystalline microporous materials with hybrid properties, fill a gap between pure inorganic zeolites and pure organic polymers, and thus might be a revolutionary material for membranes in GS.

^{vii} In LTA, Na^+ ions are located directly at the 8-ring windows that connect adjacent large cages (α -cavities). Because Ca^{2+} ions occupy different positions away from the windows within the cages, ion-exchange of Na^+ against Ca^{2+} opens these windows for hydrocarbon diffusion.

1.2 Metal-Organic Frameworks

1.2.1 Introduction and Terminology

Although there is no IUPAC definition thus far [14], the term “metal-organic framework” is commonly used in the literature for the entire class of crystalline hybrid organic-inorganic compounds, consisting of metal cations or metal clusters (including metal oxide clusters) connected at least partly with each other by organic, multidentate ligands (linkers) [9]. Figure 1 shows the basic construction principle of MOFs. It should be noted that, particularly for large-pored MOFs, interpenetration or interweaving of MOF networks may occur [15].

The term “MOF” itself can be traced back^{viii} to publications from Yaghi et al. in 1995 [16, 17]. In their work, Yaghi et al. reported the syntheses and characterizations of $\text{Cu(I)}(4,4'\text{-BPY})_{1.5}\cdot(\text{NO}_3)(\text{H}_2\text{O})_{1.25}$ (BPY = bipyridine) and $\text{Co(II)}(\text{BTC}')(\text{PYR})_2\cdot(\text{PYR})_{0.67}$ (BTC' = single protonated 1,3,5-benzenetricarboxylate, PYR = pyridine). The former metal-organic compound was reported to exhibit an ordered network with open cavities, formed from Cu^+ and BPY. The charge of the network is balanced by NO_3^- anions hosted

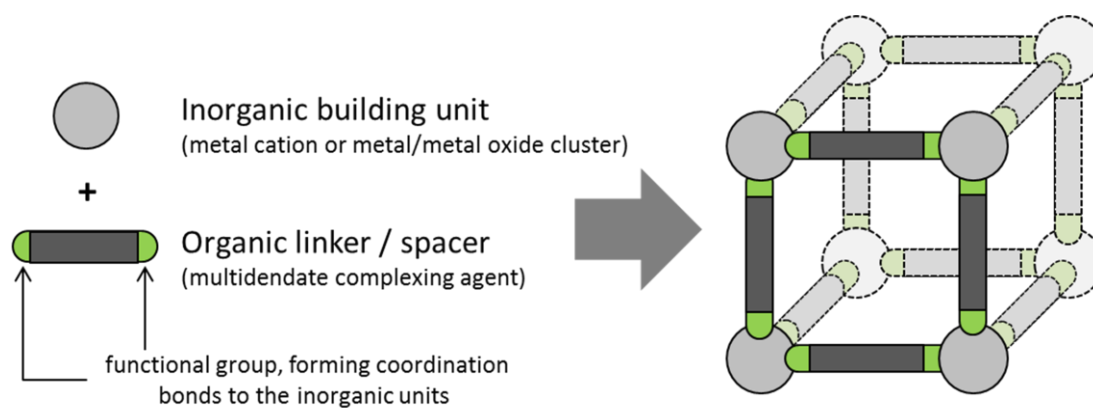


Figure 1. Structure principle of MOFs, which is demonstrated by the example of a bidentate linker that is octahedrally coordinating the inorganic centers, thus forming a simple cubic network. MOF-5 ($\text{Zn(II)}_4\text{O}(\text{BDC})_3$, BDC = 1,4-benzenedicarboxylate) exhibits this type of simple network, where the inorganic building units and the linker resemble tetrahedral (Zn_4O)⁶⁺ clusters and BDC, respectively.

^{viii} According to a search of the term “metal-organic framework” in the ISI Web of Knowledge (www.isiknowledge.com).

in the cavities, whose accessibility was validated by ion-exchange experiments. The latter metal-organic compound was reported to exhibit a charge-neutral, layer-like structure. According to Yaghi et al., the framework showed selective and reversible uptake of aromatic molecules, such as benzonitrile, whereas acetonitrile was not adsorbed. However, it should be noted that, by this time, polymeric metal-organic coordination compounds had been well-known for 30 years [9, 18, 19]. By 1959, Kinoshita et al. published the metal-organic compound $\text{Cu(I)(ADN)}_2 \cdot (\text{NO}_3)$ (ADN = adiponitrile), which, according to their structural analysis, crystallizes in a distorted, diamond-like framework topology [20]. However, no sorption or ion-exchange experiments were performed to validate the pore accessibility.

1.2.2 Naming and Classification into Subtypes

Following the nomenclature of zeolites, MOFs are often denoted by a three-digit letter code and a number, for instance, MIL-53 (Cr(III)(OH)(BDC) , BDC = 1,4-benzenedicarboxylate) [21]. The code may indicate the origin, for example, MIL stands for “Materials of Institute Lavoisier” [9]. Yaghi et al. exclusively label some of their compounds by the abbreviation MOF, such as MOF-5 ($\text{Zn(II)}_4\text{O(BDC)}_3$) or MOF-177 ($\text{Zn(II)}_4\text{O(BTB)}_2$, BTB = 1,3,5-benzenetricarboxylate) [22, 23].

There are some basic approaches to divide MOFs into certain classes and sub-groups. Kitagawa et al. [18] classified MOFs into different generations: The 1st MOF generation includes all types of networks that are unstable and collapse if guest species, originated from the synthesis process, are removed; the 2nd generation includes MOFs with rigid networks, showing no degradation of the network during the reversible adsorption of guests; the 3rd generation exhibits stable networks such as generation 2 but reversible structural changes (flexibility) during guest uptake (see Section 1.2.4). Furthermore, Férey characterized MOFs based on the dimension in connectivity of the inorganic sub-network [9]. Following this classification, networks, as shown in Figure 1, would be characterized as 0D MOF because the inorganic building units are spaced by linkers. In contrast, the network of MIL-53 [21] consists of 1D-chains of corner sharing, octahedral coordination polyhedrons ($\text{Cr(III)(OR)}_4(\text{OH})_2$, $\text{R} = \text{C}_8\text{H}_4\text{O}_2$), and these chains are connected by the BDC-linkers. Consequently, MIL-53 is classified as 1D MOF.

In addition, some authors organize MOFs in sub-groups, depending, for example, on structural motifs or the structural relation to other crystalline materials. Two closely related

groups are the “zeolite-like metal-organic frameworks” (ZMOFs) [24, 25] and “zeolitic imidazolate frameworks” (ZIFs) [26-30], which are both characterized by their networks, which assemble zeolite-related topologies. ZIFs are limited to tetrahedrally N-coordinated, metal-imidazolates as structure-building elements (detailed information can be found in Section 1.2.5). ZMOFs consist of carboxy-imidazolates that coordinate the metals with both their heterocyclic nitrogen and their carboxylate groups. In comparison to the above-mentioned ZIFs, this results in an extended coordination sphere and higher metal coordination numbers of 6 or 8. Another sub-group is referred to as paddle-wheel MOFs, which are most typically represented by HKUST-1^{ix} ($\text{Cu(II)}_3(\text{BTC})_2$, BTC = 1,3,5-benzenetricarboxylate) [31]. The name of the group is derived from the structure forming motif that visually resembles the paddle-wheel of a steamship. The motif consists of a diatomic metal-cluster, which is coordinated by 4 multidentate carboxylate-linkers. Both metal cations are square-planar coordinated by 4 oxygen, and both square-planar coordination spheres are aligned parallel and ecliptic.

1.2.3 Structure Principles of MOFs

Though there are a vast number of MOFs with different networks, the complex structures may be reduced to basic structure principles that are originally derived for pure inorganic crystalline materials, such as zeolites. O’Keeffe et al. proposed to simplify MOF structures to a number of highly symmetrical, (n, m) -connected nets [32-34]. Here, n and m denote the number of connections from two separate nodes, N and M , to neighboring nodes. The nodes and the edges of a net are not limited to single atoms or single bonds, respectively. Nodes may be “decorated” with, for example, clusters or complex polyhedrons, and edges may be “expanded” to include multiple bonds or linker molecules (for a detailed explanation of the terms, see ref. [32]). A special form of “decoration” is the replacement of an n -connected node by a polyhedron of n -vertices, which is termed “augmentation”. Following the principle proposed by O’Keeffe, MOF-5 could be denoted as a decorated, expanded, 6-connected, simple cubic network. A net within a group of n -connected nets is additionally denoted by its vertex symbol that is derived by identifying the angles per node, the sizes of the smallest rings adjacent to the angles, and the number of rings equal in size shared by an angle [35]. It is denoted as follows: $A_X \cdot B_Y \cdot \dots \cdot N_M$, where each place repre-

^{ix} HKUST = Hong Kong University of Science and Technology.

sents a specific angle α from the total amount of q angles (opposed angles are paired together). The value N is the smallest ring size at α , and M denotes the number of N -rings sharing this angle [36]. The number of angles q per node can be calculated from the connectivity n to be 3 for a 3-connected net, 6 for a 4-connected and $q = 0.5n \cdot (n-1)$ for a n -connected net.

In contrast to O’Keeffe’s approach, Férey proposed to characterize MOF networks by dissecting structures into smaller building units (BUs), defined as the smallest single unit that can describe the framework by periodically arranging or condensing [37]. This concept is widely used to describe zeolite structures, where three types of BUs are classified: a) primary building units (PBUs; tetrahedral SiO_4 polyhedra for zeolites), b) secondary building units (SBUs; representing the above-mentioned BUs), and c) composite building units (CBUs; motifs that frequently appear in more than one structure) [36]. The arrangement of the BUs, regardless whether they resemble single atoms, clusters, or more complex polyhedrons, may be topologically described by known, simple patterns. For example MOF-5 (and isorecticular frameworks [38]) may be described by an octahedral BU, which consists of a Zn_4O -cluster coordinated by 6 linkers. Condensing and arranging of 8 BUs by a simple cubic structure produces the MOF-5 network.

1.2.4 Chemical and Physical Properties

MOFs are light materials with low densities and may exhibit high inner surface areas. In particular, MOF-177 [23, 39, 40] and UMCM-2^x ($\text{Zn}_4\text{O}(\text{TDC})(\text{BTB})_{4/3}$, TDC = 1,4-thieno[3,2-b]thiophene-2,5-dicarboxylate) [41] exhibit extraordinary high inner surfaces of 3200 - 4500 $\text{m}^2 \text{g}^{-1}$ and $\sim 5200 \text{m}^2 \text{g}^{-1}$, respectively (determined using the model of Brunauer, Emmett, and Teller, BET model, see Section 1.3.2), and thus outperform microporous zeolites, mesoporous MCMs, and even activated carbons.

A number of MOFs exhibit network dynamics or network flexibilities [42] that can be generally divided into two types: i) the dynamic tilting, flipping or rotation of linkers around a bond axis; and ii) the entire reversible contraction or relaxation of the network (often termed “breathing”) that is accompanied by major structural changes, however, without breaking bonds or the loss of the crystallinity. The latter breathing effect is often

^x UMCM = University of Michigan Crystalline Material.

triggered only by specific kinds of strongly interacting molecular species. For example, carbon dioxide is absorbed at low pressures in $\text{Cu(II)(4,4'-BIPY)(DHBC)}_2 \cdot 2\text{H}_2\text{O}$ (DHBC = 2,5-dihydroxybenzoate, BIPY = 4,4'-bipyridine) [43]. However, nitrogen is not able to trigger the “gate opening” within the same pressure range, and adsorption is observed only at high pressures above 50 atm. It is assumed that the above-mentioned linker dynamics occur in a broad range of MOFs, and have been experimentally demonstrated for the benzene-rings in MIL-47, MIL-53 [44], and MOF-5 [45] by $^2\text{H-NMR}$.

Although the thermal stability of MOFs greatly depends on the specific compound, MOFs can be thermally stable roughly up to 300 °C under air. However, in a non-oxidizing N_2 atmosphere the decomposition temperatures can be up to 500 °C [26, 46]. It should be noted that these values are derived either by using thermogravimetric analysis (TGA) or in-situ X-ray diffraction (XRD), but strictly speaking, only the latter method allows a valid statement because it directly shows the structural degradation. With regard to their chemical stability, MOFs often show resistance against organic solvents, even at elevated temperature [26, 47]. The chemical resistance of MOFs against acids, however, suffers from the basic sites of the metal-organic coordination bonds, and even contact with humidity may lead to amorphization, such as for MOF-5 [48]. Recently, Tan et al. [49] summarized the mechanical properties of a number of selected MOFs, including measurements of the Young's modulus^{xi}, which is reciprocally related with the elasticity of a compound, and the hardness^x, which indicates the plasticity. Generally, the Young's moduli and hardnesses of MOFs overlap at the upper boundary with those of the more stiff and brittle zeolites and at the lower boundary with the more elastic and ductile polymers.

1.2.5 Structure and Properties of the Zeolitic Imidazolate Frameworks ZIF-7 and ZIF-8

As mentioned in Section 1.2.2, ZIFs are a sub-group of MOFs constructed from single metal cations (Me) that are N-coordinated and connected by imidazolates (IM). The PBUs are tetrahedral MeIM_4 polyhedrons, and the angle in the bridging $\text{IM}_3\text{Me-IM-MeIM}_3$ elements is close to 145° [26]. These two geometrical settings are also found for $\text{O}_3\text{Si-O-SiO}_3$

^{xi} The Young's modulus is defined as the axial stress necessary per amount of axial deformation relative to the original dimension. According to Tan et al. [49] it was derived from relaxation measurements by using nanoindentation. The latter method was also used for determination of the hardness that is the ratio of the applied load and the imprint area from the plastic deformation [49].

in zeolites. Therefore, it is not surprising that ZIF networks frequently resemble zeolite structures topologically. The networks of ZIF-7 ($\text{Zn}(\text{BIM})_2$, BIM = benzimidazolate) and ZIF-8 ($\text{Zn}(\text{MIM})_2$, MIM = 2-methylimidazolate) are both topologies of the sodalite structure [26, 29, 30]. Following the structure principles described in Section 1.2.3, the cubic sodalite structure may be dissected into a truncated octahedron. This SBU is often termed as β -cage and consists of six 4-membered rings and eight 6-membered rings, which are connected by edge-sharing. The sodalite structure emerges by face-sharing and the cubic centered arrangement of the β -cages. Alternatively, the entire net can be denoted by the vertex symbol (4·4·6·6·6·6) [32, 36]. Within the ZIF-7 and ZIF-8 topologies, the 24 corners of the β -cage are occupied by Zn^{2+} , whereas the bridging MIM linkers represent the edges. Therefore, the structure can be described as an expanded sodalite network. Whereas the structure of ZIF-8 (Figure 2) is cubic (space group $I\bar{4}3m$), the structure of ZIF-7 (Figure 3) exhibits a hexagonal distorted sodalite topology (space group $R\bar{3}$).

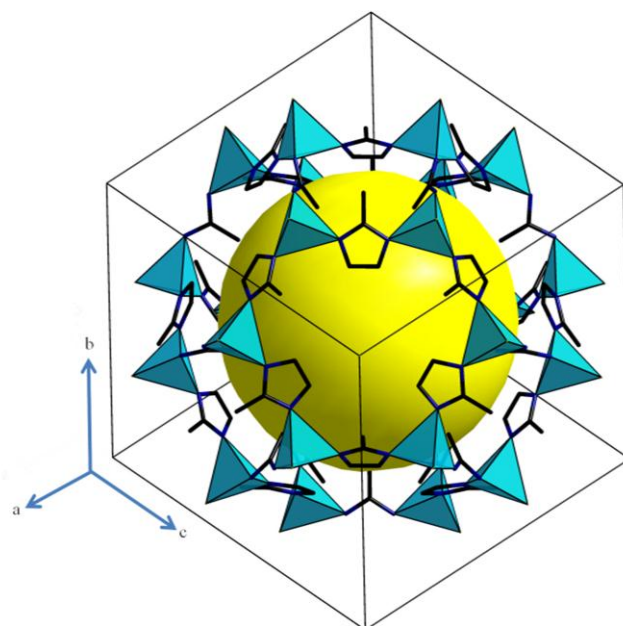


Figure 2. View along [111], showing the structure-forming SBU (β -cage) in the cubic ZIF-8 unit cell. The turquoise tetrahedrons represent ZnN_4 units, which are spaced by the MIM linkers. This results in a topological expansion with respect to the original sodalite structure, in that the SiO_4 tetrahedrons are directly connected by corner sharing. (The structure image was rendered according to crystallographic data from ref. [26])

ZIFs commonly exhibit rigid frameworks, and thus far, no breathing effects accompanied by major structural changes have been observed for ZIF-7 or ZIF-8. Nevertheless, recent studies indicate that ZIF-7 and ZIF-8 are both subject to linker dynamics, for instance, Zhou et al. [50] found quasi-free rotation of the methyl-group at C2 in ZIF-8 by using neutron scattering. In addition, Gücüyener et al. [51] postulated from measured ethane/ethene isotherms a gate-opening effect that was attributed to the linker rotation.

Though both ZIF-7 and ZIF-8 are even at elevated temperatures chemically long-term stable against organic solvents, such as boiling benzene and methanol, ZIF-7 undergoes a phase transition in boiling water [26]. As shown by Park et al. [26] using ex-situ powder XRD, ZIF-8 retains its crystallinity in boiling water for at least one week, and also seem to be resistant at least for 1 day in 8 M sodium hydroxide solution. Low et al. [52] studied the hydrothermal stabilities of a selected number of MOFs by high-throughput screening in combination with quantum mechanical calculations of activation energies E_{disp} , which are

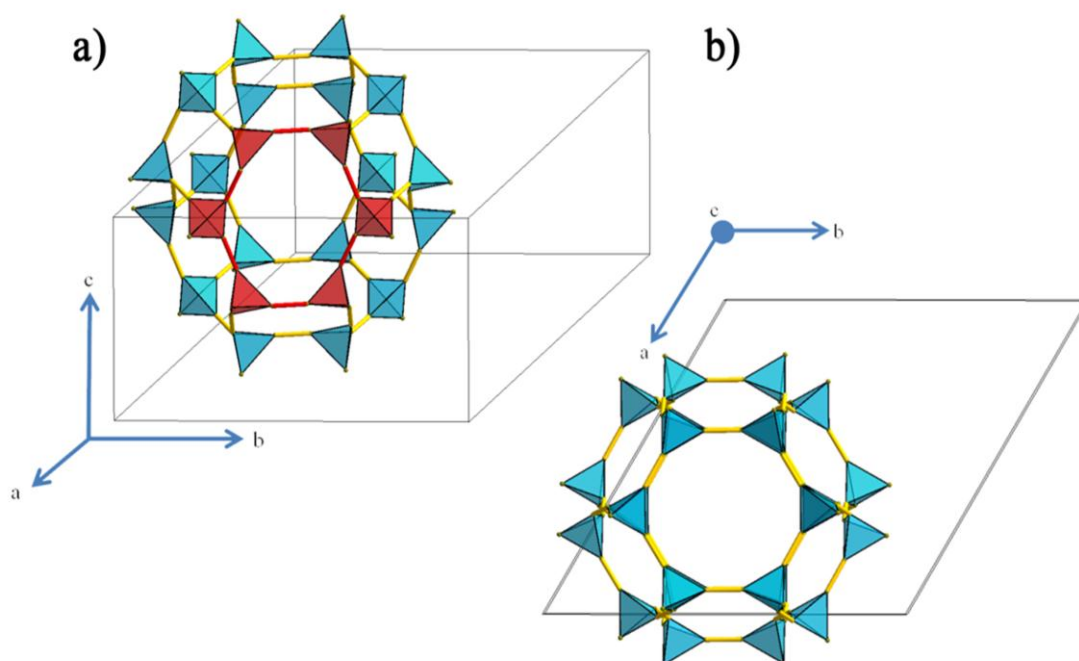


Figure 3. The β -cage of ZIF-7 within the hexagonal unit cell, exhibiting both non-distorted and distorted 6-membered rings. The turquoise and red tetrahedrons consist of ZnN_4 units spaced by BIM linkers (for clarity, the BIM linkers are drawn here as rods). Panel a): Top view on a distorted 6-membered ring (highlighted in red). Panel b): View along the c -axis, showing a non-distorted 6-membered ring. (The structure image was rendered according to crystallographic data from ref. [26]).

necessary to detach the ligands from the metals or metal-clusters and insert water between the coordination bonds. Among the studied MOFs, ZIF-8 shows the highest activation energy and highest stability against hydrothermal treatment^{xii}. In addition to the thermodynamic stability against water, ZIF-8 shows a strong hydrophobicity that prevents water from being absorbed. The thermal stabilities of ZIF-7 in air and nitrogen are apparently very similar, and the decomposition in both atmospheres indicated by TGA was found at ~ 500 °C [26, 53]. In contrast, ZIF-8 shows a lower decomposition temperature in air (~ 350 °C) [54] compared to nitrogen (~ 450 °C) [26].

According to Tan et al. [49], ZIF-8 is one of the most elastic MOFs showing a Young's modulus E of ~ 3 GPa (also see Section 1.2.4). By comparison, ceramic alumina shows a Young's modulus of $E \sim 300$ GPa. In contrast, ZIF-7 appears to be more stiff ($E \sim 6$ GPa) and exhibits a moderately higher hardness H of ~ 0.7 GPa compared to ZIF-8 ($H \sim 0.4$) [49].

The micropore properties of ZIF-8 have been well investigated. The calculated inner surfaces by the BET model (see Section 1.3.2) and the micropore volumes, respectively, range from ~ 950 m² g⁻¹ and ~ 0.36 m³ g⁻¹ for nanocrystals [55] up to ~ 1600 m² g⁻¹ and ~ 0.77 cm³ g⁻¹ for microcrystalline powders [26, 29, 54]. The nitrogen and argon adsorption isotherms of ZIF-8 at 77 K and 87 K, respectively, show a characteristic 2-step behavior that was interpreted by Yaghi et al. [26] as a reorganization of the guest molecules within the pores. Furthermore, Wu et al. [56, 57] identified hydrogen and methane adsorption sites within the ZIF-8 network by neutron-scattering experiments. The preferred sites of hydrogen and methane in ZIF-8 were found near the C4-C5 π -bond of the linker, which is contrary to their findings for MOF-5, where preferred adsorption sites were determined to be near the Zn₄O-clusters. For ZIF-7, such detailed studies have yet to be performed.

1.2.6 ZIF-7 and ZIF-8 as Promising Materials for Molecular Sieving

The zeolite sodalite is only of minor relevance for molecular sieving because the original zeolitic structure exhibits very narrow pores (~ 2.8 Å for the hydroxy-form [58]) that

^{xii} Low et al. [52] specify E_{disp} for ZIF-8 with ~ 245 kJ/mol and for MOF-5 (as one of the less water-stable MOFs) with ~ 49 kJ/mol.

barely allows the passing of the smallest molecule, i.e. hydrogen (molecule size $\sim 2.9 \text{ \AA}$)^{xiii}. In contrast, the expanded sodalite network of ZIF-7 and ZIF-8 shows larger pores. The pore diameters of ZIF-7 and ZIF-8 can be estimated from the crystallographic structure determined by single-crystal X-ray diffraction to be $\sim 3.0 \text{ \AA}$ and $\sim 3.4 \text{ \AA}$, respectively [26]. Both diameters prove themselves to be very convenient for molecular sieving in two important industrial processes: a) the water gas shift (WGS) reaction and b) natural gas refining. The former process is used for large-scale hydrogen production by transforming carbon monoxide with water into hydrogen and carbon dioxide. Finally, hydrogen ($\sim 2.9 \text{ \AA}$) must be separated from the by-product carbon dioxide ($\sim 3.3 \text{ \AA}$) to be used in further processes (e.g., as a supply in the Haber-Bosch process^{xiv} for large scale ammonia synthesis [59]). In the latter process, raw natural gas is refined by separating the gaseous alkanes as methane (3.8 \AA) from the by-products that primarily consist of corrosive carbon dioxide (3.3 \AA), and also, for example, nitrogen (3.6 \AA) [60].

1.3 Mass Transport in Microporous MOF Membranes

1.3.1 General Aspects

Following the IUPAC definition, membranes broadly include all types of flat structures that allow the (selective) mass transfer if some undefined driving force is applied [61]. Based on the broad definition, a driving force, for instance, could be electric or even magnetic in its origin. However, the following discussion is restricted to the mass transfer of a gaseous species through microporous membranes by applying a constant pressure difference Δp between the two interfaces of the membrane.

As already described in Section 1.1, crystalline, microporous membranes, such as zeolite membranes, are commonly prepared as composites that consist of a thin, polycrystalline zeolite layer grown on top of a mechanically stabilizing, macroporous support. Although the support layer of the composite membranes may influence the mass transfer [62],

^{xiii} The following sizes for molecules represent kinetic diameters according to D.W. Breck, *Zeolite Molecular Sieves*, Wiley, New York, 1974. The kinetic diameter is defined as the closest approach of two molecules at zero kinetic energy. For nonpolar molecules, σ may be derived by the Lenard-Jones potential from the location of the potential well minimum r_{min} as $\sigma = r_{min} \cdot 2^{-1/6}$. The value r_{min} can be determined by the Van der Waals radius of the molecule.

^{xiv} In the Haber-Bosch process, ammonia is directly synthesized from the elements of hydrogen and nitrogen. Even though the exothermal equilibrium reaction can be catalyzed by α -iron, high temperatures ($\sim 500 \text{ }^\circ\text{C}$) are necessary to obtain sufficiently high reaction rates. High pressures ($\sim 350 \text{ bar}$) prevent the shift of the equilibrium to the reactant side. The catalyst, α -iron, is generated in-situ from magnetite (inverse spinel structure $\text{Fe(III)(Fe(II)Fe(III))O}_4$) by the reduction with hydrogen at $500 \text{ }^\circ\text{C}$ [59].

here, any effects from the support are neglected. Consequently, only mass transfer through the microporous layer is considered in the following discussion. For the discussion below, this process is divided in two steps: a) mass exchange of i between the gas phase and the membrane interface by adsorption from the gas phase in the boundary region, and b) transport diffusion of i within the bulk membrane. However, it should be noted that the adsorption in micropores is necessarily tied to diffusion and the divide in two processes only of exemplary nature. Figure 4 schematically shows the mass transfer of a species i through a microporous layer in steady state.

1.3.2 Adsorption in Microporous Materials

The adsorption of a gaseous species i at the inner surface of microporous materials is an equilibrium process during which species i is bound to the inner surface either by chemisorption (covalent binding) or physisorption (van der Waals interactions). However, the latter is the general rule for gas adsorption. Both adsorption mechanisms can be distin-

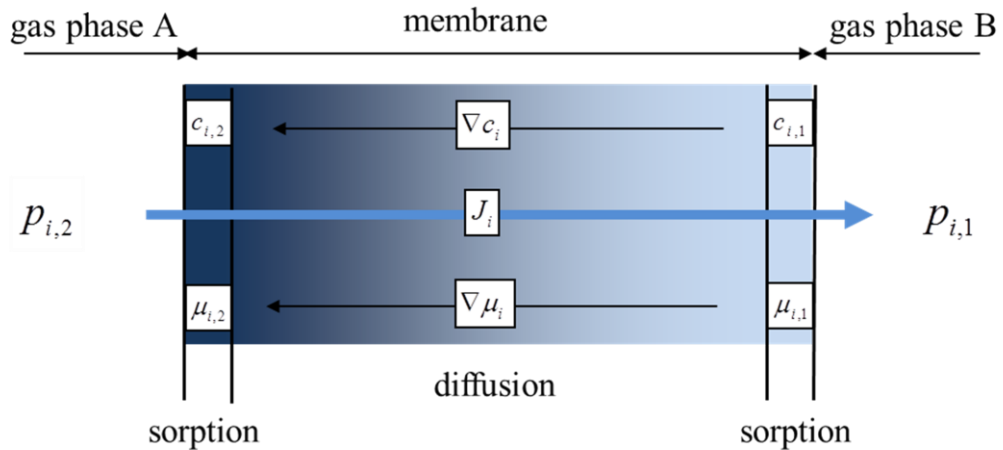


Figure 4. Schematic drawing of the mass transfer of a species i through a microporous membrane in steady state. The gas phases A and B correspond to constant pressures p_1 and p_2 , respectively. The sorption of i on both membrane faces at different partial pressures results in equilibrium concentrations $c_{i,1}$ and $c_{i,2}$ and corresponding chemical potentials $\mu_{i,1}$ and $\mu_{i,2}$, respectively. Consequently, a concentration gradient ∇c_i exists within the bulk membrane. The thermodynamic driving force of the mass transfer of i (denoted by the flux J_i) is the gradient in chemical potential $\nabla \mu_i$.

guished by the heat of adsorption that is for chemisorption and physisorption, typically 200 and 20 kJ/mol, respectively [63]. For physical adsorption, there are six types of prototypical adsorption isotherms classified by the IUPAC definition [64]. Pure microporous materials typically exhibit type-I isotherms, which show a steep (almost linear) slope at low pressure ranges. However, the slope gradually decreases with increasing pressure. At high pressures the micropores are completely filled, and consequently, further uptake is not observed.

Two physically based models, namely, the Langmuir model and the BET model, are commonly used to describe the measured adsorption isotherms. Both models are actually not explicitly designed for adsorption in micropores and completely fail to describe more complex system accurately (e.g., the breathing effects in MOFs).

The simpler Langmuir model describes the adsorption of a monolayer on top of a surface with discrete adsorption sites of the same energy. The model assumes a stationary equilibrium between the adsorption of i at a pressure p_i from the gas phase at a free adsorption site \circ and desorption of the condensed i from an occupied site \bullet into gas. Each sorption process corresponds to its own rate constant k .



Formulating the kinetics at a steady state and by the introduction of the degree of coverage θ_i as a ratio of the amount of occupied sites n_i and the monolayer filling m_i yields the well-established Langmuir isotherm [63]:

$$\theta_i = \frac{n_i}{m_i} = \frac{K_i p_i}{1 + K_i p_i} \tag{1}$$

The equilibrium constant K is the ratio of the rate constants k_{ads} / k_{des} . The basic Langmuir model sufficiently shows the physical background of the non-linear relation of pressure and loading in microporous materials. However, the small regime at low pressures of

$K_i p_i \ll 1$ may be linearly approximated by using Henry's law^{xv}, and is thus named the Henry region. The temperature dependency of the Langmuir isotherm is given by the equilibrium constant K that follows the van't Hoff equation^{xvi}, and accordingly, the equilibrium is shifted from adsorption to desorption with increasing temperature.

The advantage of the Langmuir model is that it can be easily modified, for example, to support two adsorption sites A and B with different energies (dual-site model) [65], or competing multi-component adsorption from a binary mixture of two species i and j [66]:

Dual-site Langmuir:

$$\theta_i = x_i \frac{K_{i,A} p_i}{1 + K_{i,A} p_i} + y_i \frac{K_{i,B} p_i}{1 + K_{i,B} p_i} \quad (2)$$

and $x_i = \frac{m_{i,A}}{m_i}$, $y_i = \frac{m_{i,B}}{m_i}$

Multicomponent Langmuir:

$$\theta_i = \frac{K_i p_i}{1 + K_i p_i + K_j p_j} \quad (3)$$

Although the shape of the simple Langmuir isotherm resembles the experimentally observed type-I isotherm for micropores, the Langmuir model results in errors if it is used to calculate the inner surface area from the filling of a monolayer m_i because the complete filling of the micropores does not necessarily correspond with the filling of a monolayer. Although it does not take into account the limiting micropore filling, the multilayer model of Brunauer, Emmett, and Teller (BET) is often used for the determination of the surface area [67]:

$$\theta_i = \frac{V_i}{V_{i,m}} = \frac{C_i p_i}{(p_0 - p) [1 + (C_i - 1)(p / p_0)]} \quad (4)$$

^{xv} Henry's law describes originally the relation between the vapor pressure p_i and the mole fraction x_i of a species i in solution: $p_i = x_i \cdot \kappa_i$, where κ_i is the Henry constant [63].

^{xvi} $\frac{d \ln K}{dT} = \frac{\Delta H_{ads}^\circ}{RT^2}$, where H_{ads}° is the heat of adsorption at standard temperature and pressure.

where V_i , V_0 , C_i , and p_0 denotes the adsorbed gas volume of i at equilibrium pressure, the gas volume necessary for filling a monolayer, the adsorption constant of i , and the saturation pressure of i at the specific temperature for surface area measurements (that is commonly the boiling point of i at 101.3 kPa), respectively. However, because the micropore filling is commonly obtained at very low relative pressures $p/p_0 < 0.01$, a valid analysis can only be performed below this region. Nevertheless, the BET surface areas are only indicative values and should not be taken as true quantities [68].

1.3.3 Transport Diffusion through Microporous Membranes

Following the adsorption principles explained in Section 1.3.2, if a constant pressure drop Δp_i is established across a microporous membrane, both membrane faces show different, constant θ_i values in the steady state (Figure 4). The term θ_i can be expressed as a surface concentration c_i in the unit molecules/cage by $c_i = \theta_i \cdot c_{i,0}$, where $c_{i,0}$ denotes the total amount of surface sites per cage. Consequently, a gradient ∇c_i is established across the membrane, and i diffuses from the membrane face at $c_{i,2}$ to $c_{i,1}$. If there are no external barriers that limit the mass transfer through the membrane surface, diffusion through the bulk membrane is the rate limiting step [69]. The mass transfer between both membrane faces then may be quantitatively described by the empirically founded Fick's 1st law, which can be simplified for a linear, 1D cross-sectional concentration profile [70]:

$$J_i = -D \cdot \nabla c_i \approx -D \cdot \frac{\Delta c_i}{\Delta z} \quad (5)$$

where J_i , D , and Δz denote the flux of i through the membrane, the Fickian transport diffusion coefficient of i , and the thickness of the membrane, respectively. It should be noted that D , though ideally constant, can show a strong concentration dependency experimentally and, therefore, should be denoted as $D(c)$. Though Fick's 1st law may be used for the multicomponent diffusion of, for instance, two species i and j , the corresponding mixture diffusivity $D_{i,j}(c)$ may significantly deviate from the pure component $D_i(c)$. However, the law can be extended for the diffusion of i in the presence of n multiple species j by using a diffusion matrix D_{ij} instead of a single diffusion coefficient [71]:

$$J_i = -\sum_{j=1}^n D_{ij}(c) \frac{\partial c_j}{\partial z} \quad (6)$$

Nevertheless, Fick's law may prove to be inadequate in understanding the experimental findings, for example, in counter diffusion experiments, where i may even be "dragged" by a another species in direction of its concentration gradient [72].

In contrast, the Maxwell-Stefan approach for the steady state diffusion is physically derived by the consideration of the equilibrium between a driving and a frictional force on i . The thermodynamic driving force for the situation described in Figure 4 is the gradient of the chemical potential $\nabla\mu_i$. The above-mentioned, opposed frictional force results from interactions of i with, for instance, the immobile pore surface or a mobile, second species. The frictional force is linearly related to the corresponding mole fractions x , the velocities v , and the friction coefficients that are commonly reciprocally expressed as Maxwell-Stefan diffusivities \mathcal{D} [72]:

$$-\frac{\nabla\mu_i}{RT} = \sum_{j \neq i} \frac{1}{\mathcal{D}_{ij}} \cdot x_j (v_i - v_j) \quad (7)$$

where R is the ideal gas constant. For the single component diffusion of i through a microporous matrix s , the Maxwell-Stefan equation might be formulated to resemble Fick's 1st law:

$$J_i = -\frac{\mathcal{D}_{i,s} c_i}{RT} \nabla\mu_i \quad (8)$$

where $\mathcal{D}_{i,s}$ denotes the Maxwell-Stefan diffusivity of i and s . In this simple case, the Fickian diffusivity D is related to the Maxwell-Stefan diffusivity \mathcal{D} by the thermodynamic factor:

$$D = \mathcal{D} \cdot \left(\frac{d \ln p}{d \ln c} \right) \quad (9)$$

For the binary mixture diffusion of i and j within the same matrix, the Maxwell-Stefan equation becomes much more complex to solve, but may be still written in the convenient form as follows [73-75]:

$$-\theta_i \frac{\nabla \mu_i}{RT} = \frac{\theta_j J_i - \theta_i J_j}{c_{sat} \cdot \mathcal{D}_{i,j}} - \frac{J_i}{c_{sat} \cdot \mathcal{D}_{i,s}} \quad (10)$$

where c_{sat} denote the total concentration at the complete micropore filling.

1.4 Preparation of MOFs by Microwave-Assisted Heating

1.4.1 Theoretical Aspects of Dielectric Heating of Liquids

As electromagnetic radiation with frequencies ν of 300 MHz to 300 GHz, microwaves (MWs) may induce an oscillating orientation polarization in liquids containing dipolar molecules. On a molecular level, this means that the dipolar molecules try to align themselves with the oscillating electric field. However, the typical relaxation time for molecule rotation is in the range of 10^{-12} s. Therefore, if the frequency is increased above 100 GHz, the orientation of the dipolar molecules cannot follow the rapidly oscillating electric field. Consequently, the total polarizability and the relative permittivity ϵ_r dramatically drop [63, 76]. Within a transition region at higher frequencies, the dipolar molecules may still respond to the electric field but lag behind in their orientation. This out-of-phase polarization results in a dielectric loss ϵ'' that manifests in a dielectric heating. The dielectric loss ϵ'' is commonly expressed as an imaginary part of the complex relative permittivity $\epsilon_r = \epsilon' + i\epsilon''$ [76, 77].

The efficiency of the dielectric heating depends on the balance between a) the permittivity ϵ' (that decreases at higher frequencies) and b) the loss factor ϵ'' (that runs through a

maximum at the turning point of the slope of ε'). The efficiency may be evaluated for a specific ν by the loss tangent $\tan \delta = \varepsilon'' / \varepsilon'$ [77].

In most household and laboratory MW ovens, the MWs are generated by a magnetron at a fixed ν of 2.45 GHz, even though the maximum loss tangent for pure water is not reached until 18 GHz at ambient temperature [76]. The frequency, however, is deliberately chosen to balance heating effectiveness and penetration depth, which reciprocally depends on ε'' [78]. At a constant frequency but with increasing temperature, ε' and ε'' may run through maxima. The thermal motion weakens the intermolecular dipole interactions. Consequently, the inertia against aligning within the electric field is reduced but, simultaneously, the random, thermal motion counteracts the polarization [79-81]. For water in the temperature range of 0 to 40 °C^{xvii}, these maxima appear only for frequencies above 2.45 GHz and shift with increasing ν to higher temperatures [81].

Although MWs can be used to excite the rotational states of molecules (e.g., in rotational spectroscopy in the gas phase), in the liquid state, the free rotation of solvent molecules would contradict that the frequency of 2.45 GHz is energetically far too low to i) excite even the lowest rotational states of molecules [82], and ii) to break hydrogen bonds that prevent free rotation in liquid state [78].

1.4.2 Practical Aspects of MW-Assisted Heating

Though there are various non-classical preparation routes for crystalline MOFs [55, 83-85], the most relevant technique for MOF preparation is solvothermal synthesis, which is commonly performed by convectional heating in air-circulated ovens. The process of heat transfer from a surrounding medium (usually air) through the walls of the autoclave (usually a stainless steel housing containing a Teflon insert) to the enclosed synthesis solution is slow. Therefore, the solution is almost heated homogenously with time because the heat dissipation is faster than the heat transport into the solution. In MW-assisted heating, the material of the autoclave is commonly chosen to be transparent for MW radiation (e.g., Teflon), and the heat release generated within the solvent (as described in Section 1.4.1) is much faster. The absorption profile of the MWs within the solvent may be approximated

^{xvii} According to the graphs of ref. [81] and the corresponding model in ref. [80], for pure water and 2.45 GHz ε' and ε'' at $T = 0$ °C or $T = 40$ °C can be specified as $\varepsilon' \sim 82$ and $\varepsilon'' \sim 21$ or $\varepsilon' \sim 74$ and $\varepsilon'' \sim 6$, respectively. This clearly shows that the dielectric loss decreases with increasing temperature at least for the given temperature range and frequency.

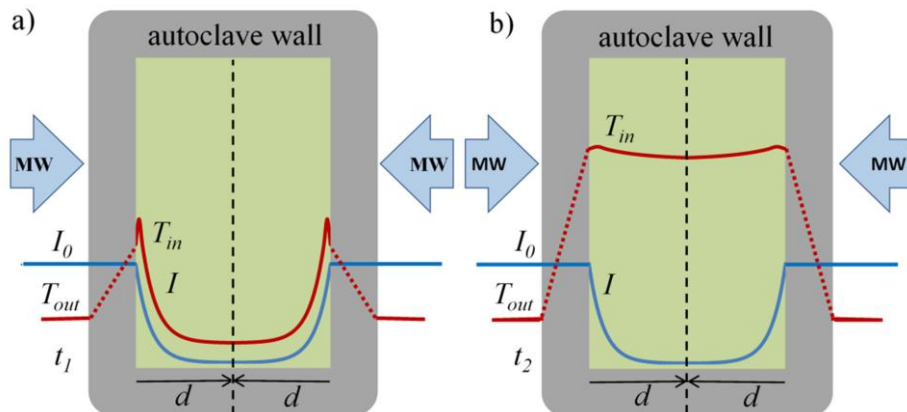


Figure 5. Cross-section schematic drawing of a solvent filled MW-autoclave showing the absorption of microwave energy and resulting temperature profiles at different times during the dielectric heating process. Following the Lambert-Beer law, with increasing distance d from the walls, the intensity I of the MWs exponentially decreases from its initial value I_0 symmetrically to the mirror plane (black, dotted line). The temperature dependencies of the absorption process and the loss tangent are neglected here. In the beginning of a rapid heating process at t_1 in panel a) the profile of the temperature T is spatially inhomogeneous within the solvent. However, at steady state conditions at $t_2 > t_1$, as shown in panel b), the temperature may be almost equally distributed. This is particular true if I_0 is dynamically controlled by a temperature regulator, as in modern laboratory microwaves. The exact heat transfer profile through the walls of the autoclave is not relevant here and shown only as a dotted line to reflect it's unknown progress.

by the Lambert-Beer law, which predicts the exponential decay in intensity I of transmitted MWs with increasing distance d from the incident MW intensity I_0 [63, 78]:

$$\log\left(\frac{I}{I_0}\right) = -k \cdot d \quad (11)$$

where k summarizes the molar extinction coefficient ε and the concentration c . Consequently, the spatial temperature profile as a function of time is inhomogeneous for short time periods during the initial heating process because the absorption of MWs occurs at the

outer solvent region near the walls of the autoclave. At the beginning of MW-heating, a few molecular layers directly attached to the Teflon wall will remain at a lower temperature because they become quenched by the cold Teflon walls (Figure 5). This effect can reduce crystallization at the walls, which is often observed in Teflon-lined, stainless-steel autoclaves. In contrast to convectional heating, the autoclave walls transfer heat from the solution to the surrounding medium outside. The maximum of temperature is consequently shifted slightly away from the absorption maximum. If steady state is established (e.g., by temperature-regulated control of the MW power), the temperature is approximately homogeneously distributed within the solution.

Though MW-assisted heating is reported to produce higher yields and to result in faster chemical reaction rates [86], a specific “microwave”-effect by electromagnetic interaction with the solvent as proposed by some authors could not be verified thus far [82, 87-90]. For instance, Obermayer et al. [91] performed 18 different reactions, each in a MW-nontransparent SiC vessel and a MW-transparent glass autoclave. The comparative analysis revealed no differences in the yields regardless of whether MWs directly heated the solvent or just the autoclave walls.

1.5 Bibliography

- [1] E. Drioli (ed.), and L. Giorno (ed.), *Comprehensive Membrane Science and Engineering*, Elsevier, Amsterdam, 2010.
- [2] S.P. Nunes (ed.), and K.V. Peinemann (ed.), *Membrane Technology in the Chemical Industry*, Wiley-VCH, Weinheim, 2006.
- [3] M. Noack, M. Schneider, A. Dittmar, G. Georgi, and J. Caro, The Change of the Unit Cell Dimension of Different Zeolite Types by Heating and Its Influence on Supported Membrane Layers. *Microporous and Mesoporous Materials* **2009**, *117* 10-21.
- [4] J. Lu, N. Liu, L. Li, and R. Lee, Organic Fouling and Regeneration of Zeolite Membrane in Wastewater Treatment. *Separation and Purification Technology* **2010**, *72*, 203-207.
- [5] H. Voß, A. Diefenbacher, G. Schuch, H. Richter, I. Voigt, M. Noack, and J. Caro, Butene Isomers Separation on Titania Supported MFI Membranes at Conditions Relevant for Practice. *Journal of Membrane Science* **2009**, *329* 11-17.
- [6] C. Chmelik, H. Voß, H. Bux, and J. Caro, Adsorption and Diffusion - Basis for Molecular Understanding of Permeation through Molecular Sieve Membranes. *Chemie Ingenieur Technik* **2011**, *83*, 104-112.
- [7] Z.A.E.P. Vroon, K. Keizer, M.J. Gilde, H. Verweij, and A.J. Burggraaf, Transport Properties of Alkanes through Ceramic Thin Zeolite MFI Membranes. *Journal of Membrane Science* **1996**, *113*, 293-300.
- [8] J. Caro, and M. Noack, Zeolite Membranes - Recent Developments and Progress. *Microporous and Mesoporous Materials* **2008**, *115*, 215-233.
- [9] G. Ferey, Hybrid Porous Solids: Past, Present, Future. *Chemical Society Reviews* **2008**, *37*, 191-214.
- [10] R. Banerjee, H. Furukawa, D. Britt, C. Knobler, M. O’Keeffe, and O.M. Yaghi, Control of Pore Size and Functionality in Isoreticular Zeolitic Imidazolate Frameworks and their Carbon Dioxide Selective Capture Properties. *Journal of the American Chemical Society* **2009**, *131*, 3875-3877.
- [11] K.K. Tanabe, Z.Q. Wang, and S.M. Cohen, Systematic Functionalization of a Metal-Organic Framework via a Postsynthetic Modification Approach. *Journal of the American Chemical Society* **2008**, *130*, 8508-8517.
- [12] Z.Q. Wang, K.K. Tanabe, and S.M. Cohen, Tuning Hydrogen Sorption Properties of Metal-Organic Frameworks by Postsynthetic Covalent Modification. *Chemistry - A European Journal*, **2010**, *16*, 212-217.
- [13] M. Eddaoudi, J. Kim, N. Rosi, D. Vodak, J. Wachter, M. O’Keeffe, and O.M. Yaghi, Systematic Design of Pore Size and Functionality in Isoreticular MOFs and Their Application in Methane Storage. *Science* **2002**, *295*, 469-472.
- [14] IUPAC, Coordination Polymers and Metal Organic Frameworks: Terminology and Nomenclature Guidelines. <http://www.iupac.org/web/ins/2009-012-2-200>.
- [15] S. Bauer, and N. Stock, MOFs - Metallorganische Gerüststrukturen. Funktionale poröse Materialien. *Chemie in unserer Zeit* **2008**, *42*, 12-19.
- [16] O.M. Yaghi, and H. Li, Hydrothermal Synthesis of a Metal-Organic Framework Containing Large Rectangular Channels. *Journal of the American Chemical Society* **1995**, *117*, 10401-10402.
- [17] O.M. Yaghi, G.M. Li, and H.L. Li, Selective Binding and Removal of Guests in a Microporous Metal-Organic Framework. *Nature* **1995**, *378*, 703-706.

- [18] S. Kitagawa, R. Kitaura, and S. Noro, Functional Porous Coordination Polymers. *Angewandte Chemie International Edition* **2004**, *43*, 2334-2375.
- [19] K. Biradha, A. Ramanan, and J.J. Vittal, Coordination Polymers Versus Metal-Organic Frameworks. *Crystal Growth & Design* **2009**, *9*, 2969-2970.
- [20] Y. Kinoshita, I. Matsubara, T. Higuchi, and Y. Saito, The Crystal Structure of Bis(Adiponitrilo)Copper(I) Nitrate. *Bulletin of the Chemical Society of Japan* **1959**, *32*, 1221-1226.
- [21] C. Serre, F. Millange, C. Thouvenot, M. Noguès, G. Marsolier, D. Louër, and G. Férey, Very Large Breathing Effect in the First Nanoporous Chromium(III)-Based Solids: MIL-53 or $\text{CrIII}(\text{OH}) \cdot \{\text{O}_2\text{C}-\text{C}_6\text{H}_4-\text{CO}_2\} \cdot \{\text{HO}_2\text{C}-\text{C}_6\text{H}_4-\text{CO}_2\text{H}\}_x \cdot \text{H}_2\text{O}_y$. *Journal of the American Chemical Society* **2002**, *124*, 13519-13526.
- [22] H. Li, M. Eddaoudi, M. O'Keeffe, and O.M. Yaghi, Design and Synthesis of an Exceptionally Stable and Highly Porous Metal-Organic Framework. *Nature* **1999**, *402*, 276-279.
- [23] H.K. Chae, D.Y. Siberio-Perez, J. Kim, Y. Go, M. Eddaoudi, A.J. Matzger, M. O'Keeffe, and O.M. Yaghi, A Route to High Surface Area, Porosity and Inclusion of Large Molecules in Crystals. *Nature* **2004**, *427*, 523-527.
- [24] Y. Liu, V.C. Kravtsov, R. Larsen, and M. Eddaoudi, Molecular Building Blocks Approach to the Assembly of Zeolite-Like Metal-Organic Frameworks (ZMOFs) with Extra-Large Cavities. *Chemical Communications* **2006**, 1488-1490.
- [25] F. Nouar, J. Eckert, J.F. Eubank, P. Forster, and M. Eddaoudi, Zeolite-like Metal-Organic Frameworks (ZMOFs) as Hydrogen Storage Platform: Lithium and Magnesium Ion-Exchange and H_2 -(rho-ZMOF) Interaction Studies. *Journal of the American Chemical Society* **2009**, *131*, 2864-2870.
- [26] K.S. Park, Z. Ni, A.P. Cote, J.Y. Choi, R.D. Huang, F.J. Uribe-Romo, H.K. Chae, M. O'Keeffe, and O.M. Yaghi, Exceptional Chemical and Thermal Stability of Zeolitic Imidazolate Frameworks. *Proceedings of the National Academy of Sciences of the United States of America* **2006**, *103*, 10186-10191.
- [27] B. Wang, A.P. Cote, H. Furukawa, M. O'Keeffe, and O.M. Yaghi, Colossal Cages in Zeolitic Imidazolate Frameworks as Selective Carbon Dioxide Reservoirs. *Nature* **2008**, *453*, 207-211.
- [28] A. Phan, C.J. Doonan, F.J. Uribe-Romo, C.B. Knobler, M. O'Keeffe, and O.M. Yaghi, Synthesis, Structure, and Carbon Dioxide Capture Properties of Zeolitic Imidazolate Frameworks. *Accounts of Chemical Research* **2010**, *43*, 58-67.
- [29] X.C. Huang, Y.Y. Lin, J.P. Zhang, and X.M. Chen, Ligand-Directed Strategy for Zeolite-Type Metal-Organic Frameworks: Zinc(II) Imidazolates with Unusual Zeolitic Topologies. *Angewandte Chemie International Edition* **2006**, *45*, 1557-1559.
- [30] X. Huang, J. Zhang, and X. Chen, $[\text{Zn}(\text{bim})_2] \cdot (\text{H}_2\text{O})_{1.67}$: A Metal-Organic Open-Framework with Sodalite Topology. *Chinese Science Bulletin* **2003**, *48*, 1531-1534.
- [31] S.S.Y. Chui, S.M.F. Lo, J.P.H. Charmant, A.G. Orpen, and I.D. Williams, A Chemically Functionalizable Nanoporous Material $[\text{Cu}_3(\text{TMA})_2(\text{H}_2\text{O})_3]_n$. *Science* **1999**, *283*, 1148-1150.
- [32] M. O'Keeffe, M. Eddaoudi, H. Li, T. Reineke, and O.M. Yaghi, Frameworks for Extended Solids: Geometrical Design Principles. *Journal of Solid State Chemistry* **2000**, *152*, 3-20.
- [33] N.W. Ockwig, O. Delgado-Friedrichs, M. O'Keeffe, and O.M. Yaghi, Reticular Chemistry: Occurrence and Taxonomy of Nets and Grammar for the Design of Frameworks. *Accounts of Chemical Research* **2005**, *38*, 176-182.

- [34] V.A. Blatov, M. O'Keeffe, and D.M. Proserpio, Vertex-, Face-, Point-, Schläfli-, and Delaney-Symbols in Nets, Polyhedra and Tilings: Recommended Terminology. *CrystEngComm* **2010**, *12*, 44-48.
- [35] M. O'Keefe, and B.G. Hyde, Crystal Structures I: Patterns and Symmetry, Mineralogical Society of America, Washington D. C., 1996.
- [36] C. Baerlocher, L.B. McCusker, and D.H. Olson, Atlas of Zeolite Framework Types, Elsevier, Amsterdam, 2007.
- [37] G. Férey, Building Units Design and Scale Chemistry. *Journal of Solid State Chemistry* **2000**, *152*, 37-48.
- [38] O.M. Yaghi, M. O'Keeffe, N.W. Ockwig, H.K. Chae, M. Eddaoudi, and J. Kim, Reticular Synthesis and the Design of New Materials. *Nature* **2003**, *423*, 705-714.
- [39] A.G. Wong-Foy, A.J. Matzger, and O.M. Yaghi, Exceptional H₂ Saturation Uptake in Microporous Metal-Organic Frameworks. *Journal of the American Chemical Society* **2006**, *128*, 3494-3495.
- [40] Y. Li, and R.T. Yang, Gas Adsorption and Storage in Metal-Organic Framework MOF-177. *Langmuir* **2007**, *23*, 12937-12944.
- [41] K. Koh, A.G. Wong-Foy, and A.J. Matzger, A Porous Coordination Copolymer with over 5000 m²/g BET Surface Area. *Journal of the American Chemical Society* **2009**, *131*, 4184-4185.
- [42] G. Férey, and C. Serre, Large Breathing Effects in Three-Dimensional Porous Hybrid Matter: Facts, Analyses, Rules and Consequences. *Chemical Society Reviews* **2009**, *38*, 1380-1399.
- [43] R. Kitaura, K. Seki, G. Akiyama, and S. Kitagawa, Porous Coordination-Polymer Crystals with Gated Channels Specific for Supercritical Gases. *Angewandte Chemie International Edition* **2003**, *42*, 428-431.
- [44] D.I. Kolokolov, H. Jovic, A.G. Stepanov, V. Guillerm, T. Devic, C. Serre, and G. Férey, Dynamics of Benzene Rings in MIL-53(Cr) and MIL-47(V) Frameworks Studied by ²H NMR Spectroscopy. *Angewandte Chemie International Edition* **2010**, *49*, 4791-4794.
- [45] S.L. Gould, D. Tranchemontagne, O.M. Yaghi, and M.A. Garcia-Garibay, Amphidynamic Character of Crystalline MOF-5: Rotational Dynamics of Terephthalate Phenylenes in a Free-Volume, Sterically Unhindered Environment. *Journal of the American Chemical Society* **2008**, *130*, 3246-3247.
- [46] S. Ma, X.S. Wang, D. Yuan, and H.C. Zhou, A Coordinatively Linked Yb Metal-Organic Framework Demonstrates High Thermal Stability and Uncommon Gas-Adsorption Selectivity. *Angewandte Chemie International Edition* **2008**, *47*, 4130-4133.
- [47] J.H. Cavka, S. Jakobsen, U. Olsbye, N. Guillou, C. Lamberti, S. Bordiga, and K.P. Lillerud, A New Zirconium Inorganic Building Brick Forming Metal Organic Frameworks with Exceptional Stability. *Journal of the American Chemical Society* **2008**, *130*, 13850-13851.
- [48] S.S. Kaye, A. Dailly, O.M. Yaghi, and J.R. Long, Impact of Preparation and Handling on the Hydrogen Storage Properties of Zn₄O(1,4-benzenedicarboxylate)₃ (MOF-5). *Journal of the American Chemical Society* **2007**, *129*, 14176-14177.
- [49] J.C. Tan, and A.K. Cheetham, Mechanical Properties of Hybrid Inorganic-Organic Framework Materials: Establishing Fundamental Structure-Property Relationships. *Chemical Society Reviews* **2011**, *40*, 1059-1080.
- [50] W. Zhou, H. Wu, T.J. Udovic, J.J. Rush, and T. Yildirim, Quasi-Free Methyl Rotation in Zeolitic Imidazolate Framework-8. *The Journal of Physical Chemistry A* **2008**, *112*, 12602-12606.

- [51] C. Gücüyener, J. van den Bergh, J. Gascon, and F. Kapteijn, Ethane/Ethene Separation Turned on Its Head: Selective Ethane Adsorption on the Metal-Organic Framework ZIF-7 through a Gate-Opening Mechanism. *Journal of the American Chemical Society* **2010**, *132*, 17704-17706.
- [52] J.J. Low, A.I. Benin, P. Jakubczak, J.F. Abrahamian, S.A. Faheem, and R.R. Willis, Virtual High Throughput Screening Confirmed Experimentally: Porous Coordination Polymer Hydration. *Journal of the American Chemical Society* **2009**, *131*, 15834-15842.
- [53] Y.S. Li, F.Y. Liang, H. Bux, A. Feldhoff, W.S. Yang, and J. Caro, Molecular Sieve Membrane: Supported Metal-Organic Framework with High Hydrogen Selectivity. *Angewandte Chemie International Edition* **2010**, *49*, 548-551.
- [54] H. Bux, F.Y. Liang, Y.S. Li, J. Cravillon, M. Wiebcke, and J. Caro, Zeolitic Imidazolate Framework Membrane with Molecular Sieving Properties by Microwave-Assisted Solvothermal Synthesis. *Journal of the American Chemical Society* **2009**, *131*, 16000-16001.
- [55] J. Cravillon, S. Munzer, S.J. Lohmeier, A. Feldhoff, K. Huber, and M. Wiebcke, Rapid Room-Temperature Synthesis and Characterization of Nanocrystals of a Prototypical Zeolitic Imidazolate Framework. *Chemistry of Materials* **2009**, *21*, 1410-1412.
- [56] H. Wu, W. Zhou, and T. Yildirim, Methane Sorption in Nanoporous Metal-Organic Frameworks and First-Order Phase Transition of Confined Methane. *The Journal of Physical Chemistry C* **2009**, *113*, 3029-3035.
- [57] H. Wu, W. Zhou, and T. Yildirim, Hydrogen Storage in a Prototypical Zeolitic Imidazolate Framework-8. *Journal of the American Chemical Society* **2007**, *129*, 5314-5315.
- [58] S. Khajavi, S. Sartipi, J. Gascon, J.C. Jansen, and F. Kapteijn, Thermostability of Hydroxy Sodalite in View of Membrane Applications. *Microporous and Mesoporous Materials* **2010**, *132*, 510-517.
- [59] E. Riedel, *Anorganische Chemie*, deGruyter, Berlin, 2002.
- [60] S. Cavenati, C.A. Grande, and A.E. Rodrigues, Separation of CH₄/CO₂/N₂ Mixtures by Layered Pressure Swing Adsorption for Upgrade of Natural Gas. *Chemical Engineering Science* **2006**, *61*, 3893-3906.
- [61] W.J. Koros, Y.H. Ma, and T. Shimidzu, Terminology for Membranes and Membrane Processes. *Pure and Applied Chemistry* **1996**, *68*, 1479-1489.
- [62] J.M. van de Graaf, F. Kapteijn, and J.A. Moulijn, Methodological and Operational Aspects of Permeation Measurements on Silicalite-1 Membranes. *Journal of Membrane Science* **1998**, *144*, 87-104.
- [63] P.W. Atkins, *Physikalische Chemie*, Wiley-VCH, Weinheim, 2001.
- [64] K.S.W. Sing, D.H. Everett, R.A.W. Haul, L. Moscou, R.A. Pierotti, J. Rouquerol, and T. Siemieniewska, Reporting Physisorption Data for Gas Solid Systems with Special Reference to the Determination of Surface-Area and Porosity. *Pure and Applied Chemistry* **1985**, *57*, 603-619.
- [65] A.L. Myers, Activity Coefficients of Mixtures Adsorbed on Heterogeneous Surfaces. *AIChE Journal*, **1983**, *29*, 691-693.
- [66] K.K.H. Choy, J.F. Porter, and G. McKay, Langmuir Isotherm Models Applied to the Multicomponent Sorption of Acid Dyes from Effluent onto Activated Carbon. *Journal of Chemical & Engineering Data* **2000**, *45*, 575-584.
- [67] S. Brunauer, P.H. Emmett, and E. Teller, Adsorption of Gases in Multimolecular Layers. *Journal of the American Chemical Society* **1938**, *60*, 309-319.

- [68] M. Thommes, Textural Characterization of Zeolites and Ordered Mesoporous Materials by Physical Adsorption. *Studies in Surface Science and Catalysis* **2007**, *168*, 495-525.
- [69] J. Kärger, and D.M. Ruthven, Diffusion in Zeolites and Other Microporous Solids, Wiley, New York, 1992.
- [70] J. Kärger, Leipzig, Einstein, Diffusion, Leipziger Universitätsverlag, Leipzig, 2007.
- [71] C. Chmelik, and J. Karger, In Situ Study on Molecular Diffusion Phenomena in Nanoporous Catalytic Solids. *Chemical Society Reviews* **2010**, *39*, 4864-4884.
- [72] J.A. Wesselingh, and R. Krishna, Mass Transfer in Multicomponent Mixtures, Delft University Press, Delft, 2000.
- [73] J.M. van de Graaf, F. Kapteijn, and J.A. Moulijn, Modeling Permeation of Binary Mixtures through Zeolite Membranes. *AIChE Journal* **1999**, *45*, 497-511.
- [74] F. Kapteijn, W.J.W. Bakker, G. Zheng, J. Poppe, and J.A. Moulijn, Permeation and Separation of Light Hydrocarbons through a Silicalite-1 Membrane: Application of the Generalized Maxwell-Stefan Equations. *The Chemical Engineering Journal and the Biochemical Engineering Journal* **1995**, *57*, 145-153.
- [75] R. Krishna, A Unified Approach to the Modelling of Intraparticle Diffusion in Adsorption Processes. *Gas Separation & Purification* **1993**, *7*, 91-104.
- [76] C. Gabriel, S. Gabriel, E. H. Grant, B. S. J. Halstead, and D. Michael P. Mingos, Dielectric Parameters Relevant to Microwave Dielectric Heating. *Chemical Society Reviews* **1998**, *27*, 213-224.
- [77] A.R. Hippel (ed.), Dielectric Materials and Applications, Artech House, Boston, 1995.
- [78] S. Grundas (ed.), Advances in Induction and Microwave Heating of Mineral and Organic Materials, InTech, Rijeka, 2011.
- [79] A. Skolunov, Frequency-Temperature Curve of the Complex Dielectric Constant and Refractive Index of Water. *Fibre Chemistry* **1997**, *29* 367-373.
- [80] T. Meissner, and F.J. Wentz, The Complex Dielectric Constant of Pure and Sea Water from Microwave Satellite Observations. *Geoscience and Remote Sensing* **2004**, *42* 1836-1849.
- [81] M. Chaplin, Water Structure and Science, <http://www.btinternet.com/~martin.chaplin/index2.html>
- [82] K.D. Raner, C.R. Strauss, F. Vyskoc, and L. Mokbel, A Comparison of Reaction Kinetics Observed under Microwave Irradiation and Conventional Heating. *The Journal of Organic Chemistry* **1993**, *58*, 950-953.
- [83] Z.Q. Li, L.G. Qiu, T. Xu, Y. Wu, W. Wang, Z.Y. Wu, and X. Jiang, Ultrasonic Synthesis of the Microporous Metal-Organic Framework Cu₃(BTC)₂ at Ambient Temperature and Pressure: An Efficient and Environmentally Friendly Method. *Materials Letters* **2009**, *63*, 78-80.
- [84] O. Shekhah, H. Wang, T. Strunskus, P. Cyganik, D. Zacher, R. Fischer, and C. Wöll, Layer-by-Layer Growth of Oriented Metal Organic Polymers on a Functionalized Organic Surface. *Langmuir* **2007**, *23*, 7440-7442.
- [85] D.J. Tranchemontagne, J.R. Hunt, and O.M. Yaghi, Room Temperature Synthesis of Metal-Organic Frameworks: MOF-5, MOF-74, MOF-177, MOF-199, and IRMOF-0. *Tetrahedron* **2008**, *64*, 8553-8557.
- [86] A. Loupy, D. Monteux, A. Petit, J.M. Aizpurua, E. Domínguez, and C. Palomo, Towards the Rehabilitation of the Leuckart Reductive Amination Reaction Using Microwave Technology. *Tetrahedron Letters* **1996**, *37*, 8177-8180.

- [87] R. Laurent, A. Laporterie, J. Dubac, J. Berlan, S. Lefeuvre, and M. Audhuy, Specific Activation by Microwaves: Myth or Reality? *The Journal of Organic Chemistry* **1992**, *57*, 7099-7102.
- [88] S.A. Galema, Microwave Chemistry. *Chemical Society Reviews* **1997**, *26*, 233-238.
- [89] P. Goncalo, C. Roussel, J. Marie Melot, and J. Vebrel, Contribution of Microwaves in Organic Synthesis: Statement of a Methodology for the Microwave-Induced Preparation of Benzofuran-2(3H)-one and Its Comparison With Classical Heating. *Perkin Transactions 2* **1999**, 2111-2115.
- [90] N. Kuhnert, Microwave-Assisted Reactions in Organic Synthesis - Are There Any Nonthermal Microwave Effects? *Angewandte Chemie International Edition* **2002**, *41*, 1863-1866.
- [91] D. Obermayer, B. Gutmann, and C.O. Kappe, Microwave Chemistry in Silicon Carbide Reaction Vials: Separating Thermal from Nonthermal Effects. *Angewandte Chemie International Edition* **2009**, *121*, 8471-8474.

2 Preparation and Characterization of ZIF-7 and ZIF-8 Membranes

2.1 Summary

As described in Sections 1.2.5 and 1.2.6, ZIF-7 and ZIF-8 are both prototypical MOFs with excellent thermal and chemical stabilities, which make them promising for the molecular sieving of light gases. The following two publications describe the preparations of the first ZIF-8 and ZIF-7 membranes by growing polycrystalline layers on top of porous ceramic supports under solvothermal conditions. The separation factors of different light gases for both membranes were measured as significantly above the expected value of the separation through cracks or pinholes, thus showing the successful formation of crack-free, continuous layers. The preparations exemplarily demonstrate the feasibility of MOF membranes that show true molecular sieving. Though both materials are closely related, completely different preparation routes were necessary to obtain single crystals or to grow continuous ZIF layers on top of the ceramic substrates. For the preparation of ZIF-8 membranes, described in Section 2.2, it was necessary to replace the solvent dimethylformamide (DMF) by methanol to obtain a phase pure crystallization. It was possible to reproducibly grow dense, polycrystalline layers of ZIF-8 on top of titania supports by using in-situ crystallization. However, the same method could not produce dense layers on top of α -alumina supports. Although the ZIF-8 synthesis in methanol could not be transferred to ZIF-7, phase-pure ZIF-7 could be conventionally obtained in DMF (Section 2.4). However, seeding and subsequent secondary growth were necessary to obtain gap-free layers of ZIF-7 on top of porous supports. Both membranes were carefully characterized by scanning electron microscopy (SEM), energy-dispersive X-ray spectroscopy (EDXS) and X-ray diffraction (XRD). Unary and equimolar binary component mass transfer experiments were performed using a modified Wicke-Kallenbach method. Whereas the ZIF-8 membranes (synthesized in methanol and dried at ambient temperature) directly showed permeation, it was necessary to online-activate the ZIF-7 membranes at 150 °C to remove water. Although both membranes showed selectivities higher than expected from Knudsen diffusion through defects, surprisingly, both membranes allowed the passing of molecules with kinetic diameters larger than the estimated pore sizes, such as methane (see Section 1.2.6). After careful consideration, this behavior was related to the framework flexibility rather than the undefined mass transport through grain boundaries.

2.2 Zeolitic Imidazolate Framework Membrane with Molecular Sieving Properties by Microwave-Assisted Solvothermal Synthesis

H. Bux, F.Y. Liang, Y.S. Li, J. Cravillon, M. Wiebcke, and J. Caro, *Journal of the American Chemical Society* **2009**, *131*, 16000-16001.

Zeolitic Imidazolate Framework Membrane with Molecular Sieving Properties by Microwave-Assisted Solvothermal Synthesis

Helge Bux,[†] Fangyi Liang,[†] Yanshuo Li,^{†,§} Janosch Cravillon,[‡] Michael Wiebcke,[‡] and Jürgen Caro^{*,†}

Institute of Physical Chemistry and Electrochemistry, Leibniz University Hannover, Callinstr. 3A, D-30167 Hannover, Germany, Institute of Inorganic Chemistry, Leibniz University Hannover, Callinstr. 9, D-30167 Hannover, Germany, and Dalian Institute of Chemical Physics, Chinese Academy of Sciences, Zhong-Shan Road 457, Dalian 116023, China

Received August 31, 2009; E-mail: juergen.caro@pci.uni-hannover.de

Metal–organic frameworks (MOFs) are new microporous inorganic–organic hybrid materials.^{1,2} Their remarkable properties allow their utilization in various applications.^{3–9} The large diversity in structures and pore sizes as well as the high surface areas and adsorption affinities make MOFs attractive as advanced separation media.¹⁰ Supported microporous membranes possess significant potential for the development of methods for energy-efficient and environmentally benign separation of gas mixtures. Although there have been attempts to synthesize MOF layers on porous supports,^{9,11,12} only a very few have reported dense coatings.^{13–17} For membrane synthesis, not only the problems with growing a dense polycrystalline layer on porous ceramic or metal supports but also the thermal and chemical stability of a MOF have to be considered. Among the zeolitic imidazolate frameworks (ZIFs), a new subclass of MOFs, there are ZIFs that exhibit exceptionally high thermal and chemical stability.^{18–22} Therefore, we focused on ZIF-8, having the formula $\text{Zn}(\text{mim})_2$ (mim = 2-methylimidazolate), which crystallizes with a sodalite-related structure (Figure 1).^{18,19} ZIF-8 not only is highly stable but also shows adsorption affinity toward hydrogen and methane.^{23–25} Because of the narrow size of the six-membered-ring pores ($\sim 3.4 \text{ \AA}$), it can be anticipated that a ZIF-8 membrane should be able to separate H_2 (kinetic diameter $\sim 2.9 \text{ \AA}$) from larger molecules. Another important feature of ZIF-8 is its hydrophobic behavior, whereas ultramicroporous zeolites are usually hydrophilic. This should give a ZIF-8 membrane an advantage over zeolites in the separation of H_2 from a mixture with steam.

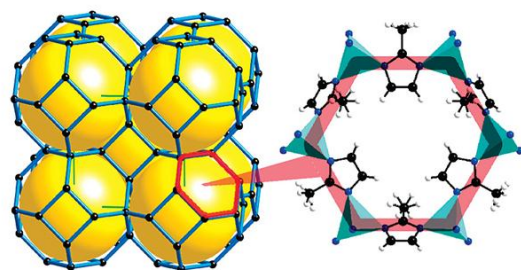


Figure 1. (left) Sodalite topology and (right) narrow six-membered-ring opening through which molecules have to pass.

Recently, we succeeded in preparing ZIF-8 nanocrystals at room temperature by modifying reported synthetic protocols^{18,19} in replacing the solvents dimethylformamide (DMF) and aqueous methanol with pure methanol.²⁶ Methanol has a much smaller

kinetic diameter than DMF. The ZIF-8 adsorption isotherm of methanol exhibits an unusual s shape,¹⁹ indicating that polar methanol only weakly interacts with the ZIF-8 framework. Therefore, methanol can be removed much more easily from the pore network than DMF, and importantly for membrane synthesis, the stress to the crystals is strongly reduced. By further modifying the synthesis in adding sodium formate and using solvothermal conditions, we were able to obtain in methanol pure-phase ZIF-8 material containing large crystals with sizes of up to $300 \mu\text{m}$ (Figure S1 in the Supporting Information). The time of synthesis could be substantially reduced to 4 h by using microwave-assisted heating.

By applying this improved synthetic protocol in membrane preparation (see the Supporting Information), we were able to obtain a crack-free, dense polycrystalline layer of ZIF-8 on a porous titania support (Figure 2). The cross section of the membrane shows a continuous, well-intergrown layer of ZIF-8 crystals on top of the support. Energy-dispersive X-ray spectroscopy (EDXS) revealed that there is a sharp transition between the ZIF-8 layer (Zn signal) and the titania support (Ti signal). A comparison of the X-ray diffraction (XRD) patterns of the ZIF-8 layer and the corresponding crystal powder sedimented during membrane synthesis indicated that the membrane layer consists of randomly oriented crystallites (Figure S2). In thermogravimetric (TG) analysis of the sedimented powder in air, no mass loss was observed at temperatures up to $\sim 360 \text{ }^\circ\text{C}$, where decomposition of the framework structure starts (Figure S3). This proves that in air, methanol has readily escaped completely from the cavities even at room temperature, yielding guest-free, activated ZIF-8.

The volumetric flow rates of the single gases H_2 , CO_2 , O_2 , N_2 , and CH_4 and of a 1:1 mixture of H_2 and CH_4 through the membrane were measured using the Wicke–Kallenbach technique (Figure S4). The permeation measurements were performed both with and without activation of the ZIF-8 membrane in fine vacuum. Nearly the same flow rates were observed in those two cases, confirming the TG results that methanol readily escapes from the pores and clearly demonstrating the advantage of replacing the DMF solvent by methanol in the synthesis.

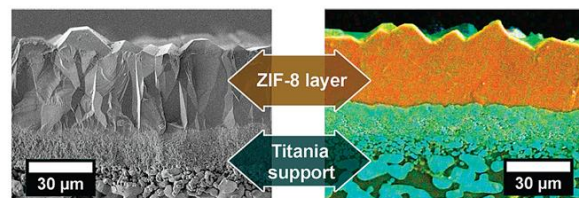


Figure 2. (left) SEM image of the cross section of a simply broken ZIF-8 membrane. (right) EDXS mapping of the sawn and polished ZIF-8 membrane (color code: orange, Zn; cyan, Ti).

[†] Institute of Physical Chemistry and Electrochemistry, Leibniz University Hannover.

[‡] Institute of Inorganic Chemistry, Leibniz University Hannover.

[§] Dalian Institute of Chemical Physics.

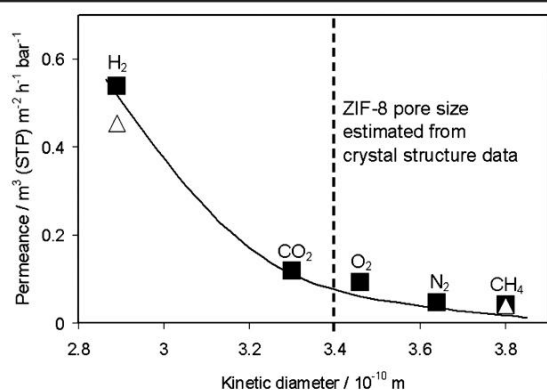


Figure 3. Single (squares) and mixed (triangles) gas permeances for a ZIF-8 membrane vs kinetic diameters.

The permeances calculated from the volumetric flow rates through the ZIF-8 membrane are presented in Figure 3 and Table S1. From both it can be seen that the permeances clearly depend on the molecular size of the gases. Although the pore size of ZIF-8 is estimated from crystallographic data to be ~ 3.4 Å, even larger molecules like CH₄ (kinetic diameter ~ 3.8 Å) can (only slowly) pass through the pore network, and consequently, there exists no sharp cutoff at 3.4 Å. This indicates that the framework structure of ZIF-8 is in fact more flexible rather than static in its nature, in accordance with recent findings by inelastic neutron scattering.²⁷

Comparison of the H₂ single-gas permeance with the H₂/CH₄ mixed-gas one revealed only a small difference, meaning that the larger CH₄ only slightly influences the permeation of the mobile H₂. This experimental finding is different from the results for mixture diffusion in zeolites, where an immobile component usually reduces the mobility of a coadsorbed, more mobile component. As an example, the presence of isobutane reduces the self-diffusivity of *n*-butane in MFI zeolites by orders of magnitude.²⁸ Our observation can be understood by considering that the pore size of ZIF-8 is narrow but the cages are large (~ 11.4 Å in diameter). Thus, although a CH₄ molecule can block the pore entrance for an H₂ molecule, as soon as it has entered the cage, it does not restrict the H₂ diffusion any more.

The separation factor $\alpha_{i,j}$ of a binary mixture is defined as the molar ratio of the components *i* and *j* in the permeate divided by the molar ratio of *i* and *j* in the retentate.²⁹ From the Wicke–Kallenbach permeation studies with gas-chromatographic control of a 1:1 H₂/CH₄ mixture, the value of α at 298 K and 1 bar was determined to be 11.2, which considerably exceeds the Knudsen separation factor for H₂/CH₄ (~ 2.8). In comparison, Guo et al.¹⁶ reported a H₂/CH₄ separation factor of ~ 6 for a supported Cu₃(btc)₂ membrane (btc = benzene-1,3,5-tricarboxylate). Very recently, Ranjan and Tsapatsis¹⁷ reported a high ideal H₂/N₂ selectivity (~ 23) but relatively low fluxes for a Cu(hfipbb)(H₂hfipbb)_{0.5} membrane [H₂hfipbb = 4,4'-(hexafluoroisopropylidene)bis(benzoic acid)].

In conclusion, we have obtained by a novel microwave-assisted solvothermal process a gas-separating ZIF membrane with selectivity for H₂ with respect to other gases. The membrane achieves a fine balance between flux and selectivity relative to other MOF membranes reported to date.^{16,17} The hydrogen permeance of our still relatively thick ZIF-8 membrane is $\sim 50\%$ of the hydrogen permeances of zeolite membranes of the same selectivity.³⁰ It is

expected that the membrane permeance can be improved by reducing the membrane thickness through further optimization of the synthesis parameters. Our ZIF-8 membrane has the additional advantage of high thermal and chemical stability, which provides the possibility of increasing the permeance at high temperature. Our work demonstrates that it is generally possible to prepare highly gas-selective MOF membranes on ceramic supports by in situ crystallization. There is some optimism that MOF membranes can represent a new generation of advanced molecular sieving membranes for gas separation.

Acknowledgment. We thank O. M. Yaghi and B. Wang for permission to use their ZIF-8 structure drawing. We thank A. Feldhoff and F. Steinbach for support in electron microscopy and F. Brieler for adsorption measurements. Y.L. thanks the Alexander von Humboldt Foundation. This work is part of DFG Priority Program 1362 (Porous Metal–Organic Frameworks).

Supporting Information Available: Synthesis protocol, measured flow rates, permeance calculation, numeric permeance data, XRD patterns of the ZIF-8 membrane and ZIF-8 crystal powder, and TG and Ar physisorption data. This material is available free of charge via the Internet at <http://pubs.acs.org>.

References

- Yaghi, O. M.; O'Keeffe, M.; Ockwig, N. W.; Chae, H. K.; Eddaoudi, M.; Kim, J. *Nature* **2003**, *423*, 705.
- Feréy, G. *Chem. Soc. Rev.* **2008**, *37*, 191.
- Kitagawa, S.; Kitaura, R.; Noro, S. *Angew. Chem., Int. Ed.* **2004**, *43*, 2334.
- Murray, L. J.; Dinca, M.; Long, J. R. *Chem. Soc. Rev.* **2009**, *38*, 1294.
- Lee, J.; Farha, O. K.; Roberts, J.; Scheidt, K. A.; Nguyen, S. T.; Hupp, J. T. *Chem. Soc. Rev.* **2009**, *38*, 1450.
- Ma, L.; Abney, C.; Lin, W. *Chem. Soc. Rev.* **2009**, *38*, 1248.
- Czaja, A. U.; Trukhan, N.; Müller, U. *Chem. Soc. Rev.* **2009**, *38*, 1284.
- Spokoiny, A. M.; Kim, D.; Sumrein, A.; Mirkin, C. A. *Chem. Soc. Rev.* **2009**, *38*, 1218.
- Zacher, D.; Shekhan, O.; Wöll, C.; Fischer, R. A. *Chem. Soc. Rev.* **2009**, *38*, 1418.
- Li, J.-R.; Kuppler, R. J.; Zhou, H.-C. *Chem. Soc. Rev.* **2009**, *38*, 1477.
- Arnold, M.; Kortunov, P.; Jones, D. J.; Nedellec, Y.; Kärger, J.; Caro, J. *Eur. J. Inorg. Chem.* **2007**, 60.
- Yoo, Y.; Jeong, H.-K. *Chem. Commun.* **2008**, 2441.
- Gascon, J.; Aguado, S.; Kapteijn, F. *Microporous Mesoporous Mater.* **2008**, *113*, 132.
- Liu, Y.; Ng, Z.; Khan, E. A.; Jeong, H.-K.; Ching, C.; Lai, Z. *Microporous Mesoporous Mater.* **2009**, *118*, 296.
- Yoo, Y.; Lai, Z.; Jeong, H.-K. *Microporous Mesoporous Mater.* **2009**, *123*, 100.
- Guo, H.; Zhu, G.; Hewitt, I. J.; Qiu, S. *J. Am. Chem. Soc.* **2009**, *131*, 1646.
- Ranjan, R.; Tsapatsis, M. *Chem. Mater.* [Online early access]. DOI: 10.1021/cm902032y. Published Online: Sept 1, 2009.
- Park, K. S.; Ni, Z.; Côté, A. P.; Choi, J. Y.; Huang, R.; Uribe-Romo, F. J.; Chae, H. K.; O'Keeffe, M.; Yaghi, O. M. *Proc. Natl. Acad. Sci. U.S.A.* **2006**, *103*, 10186.
- Huang, X.-C.; Lin, Y.-Y.; Zhang, J.-P.; Chen, X.-M. *Angew. Chem., Int. Ed.* **2006**, *45*, 1557.
- Banerjee, R.; Phan, A.; Wang, B.; Knobler, C.; Furukawa, H.; O'Keeffe, M.; Yaghi, O. M. *Science* **2008**, *319*, 939.
- Banerjee, R.; Furukawa, H.; Britt, D.; Knobler, C.; O'Keeffe, M.; Yaghi, O. M. *J. Am. Chem. Soc.* **2009**, *131*, 3875.
- Wu, T.; Zhang, J.; Zhou, C.; Wang, L.; Bu, X.; Feng, P. *J. Am. Chem. Soc.* **2009**, *131*, 6111.
- Wu, H.; Zhou, W.; Yildirim, T. *J. Am. Chem. Soc.* **2007**, *129*, 5314.
- Zhou, W.; Wu, H.; Hartman, M. R.; Yildirim, T. *J. Phys. Chem. C* **2007**, *111*, 16131.
- Wu, H.; Zhou, W.; Yildirim, T. *J. Phys. Chem. C* **2009**, *113*, 3029.
- Cravillon, J.; Münzer, S.; Lohmeier, S.-J.; Feldhoff, A.; Huber, K.; Wiebbeke, M. *Chem. Mater.* **2009**, *21*, 1410.
- Zhou, W.; Wu, H.; Udovic, T. J.; Rush, J. J.; Yildirim, T. *J. Phys. Chem. A* **2008**, *112*, 12602.
- Fernandez, M.; Kärger, J.; Freude, D.; Pampel, A.; van Baten, J. M.; Krishna, R. *Microporous Mesoporous Mater.* **2007**, *105*, 124.
- Koros, W. J.; Ma, Y. H.; Shimidzu, T. *Pure Appl. Chem.* **1996**, *68*, 1479.
- Caro, J.; Noack, M. *Microporous Mesoporous Mater.* **2008**, *115*, 215.

JA907359T

2.4 Molecular Sieve Membrane: Supported Metal-Organic Framework with High Hydrogen Selectivity

Y.S. Li, F.Y. Liang, H. Bux, A. Feldhoff, W.S. Yang, and J. Caro, *Angewandte Chemie International Edition* **2010**, *49*, 548-551.

Molecular Sieve Membrane: Supported Metal–Organic Framework with High Hydrogen Selectivity**

Yan-Shuo Li,* Fang-Yi Liang, Helge Bux, Armin Feldhoff, Wei-Shen Yang, and Jürgen Caro*

Microporous membranes with pore apertures below the nanolevel can exhibit size selectivity by serving as a molecular sieve, which is promising for overcoming Robeson's "upper-bound" limits in membrane-based gas separation.^[1] Zeolites, polymers of intrinsic microporosity (PIMs), metal oxides, and active carbon^[2a] are the typical materials used for this purpose. Metal–organic frameworks (MOFs) have attracted much research interest in recent years, and are emerging as a new family of molecular sieves.^[2b–5] MOFs are novel porous crystalline materials consisting of metal ions or clusters interconnected by a variety of organic linkers. In addition to promising applications in adsorptive gas separation and storage or in catalysis, their unique properties, such as their highly diversified structures, large range in pore sizes, very high surface areas, and specific adsorption affinities, make MOFs excellent candidates for use in the construction of molecular sieve membranes with superior performance.^[6,7] The preparation of MOF membranes for gas separation is rapidly becoming a research focus. A number of attempts have been made to prepare supported-MOF membranes,^[8–12] however, progress is very limited and so far there are only very few reports of continuous MOF films on porous supports being used as separating membranes. Recently, Guo et al. reported a copper-net-supported HKUST-1 ($\text{Cu}_3(\text{BTC})_2$; BTC = benzene-1,3,5-tricarboxylate) membrane exhibiting a H_2/N_2 selectivity of 7^[13] (separation factor of H_2 over N_2 is calculated as the permeate-to-retentate composition ratio of H_2 , divided by the same ratio for N_2 as proposed by IUPAC^[2b]); this is the first MOF membrane to show gas-separation performance beyond Knudsen diffusion behavior.

Very recently, Ranjan and Tsapatsis prepared a microporous metal–organic framework [MMOF, $\text{Cu}(\text{hfpbb})(\text{H}_2\text{hfpbb})_{0.5}$; $\text{hfpbb} = 4,4'$ -(hexafluoroisopropylidene)bis(benzoic acid)] membrane by seeded growth on an alumina support.^[14] The ideal selectivity for H_2/N_2 , based on single permeation tests, was 23 at 190 °C. This higher selectivity, compared to the report from Guo et al., might be a result of the smaller effective pore size (ca. 0.32 nm of MMOF versus 0.9 nm of HKUST-1),^[15] which results in a relatively low H_2 permeance of this MMOF membrane ($10^{-9} \text{ mol m}^{-2} \text{ s}^{-1} \text{ Pa}^{-1}$ at 190 °C). The authors attributed this finding to the blockage of the one-dimensional (1D) straight-pore channels in the membrane. Therefore, with regard to H_2 separation, small-pore MOFs having three-dimensional (3D) channel structures are considered to be ideal membrane materials. Zeolitic imidazolate frameworks (ZIFs), a subfamily of MOFs, consist of transition metals (Zn, Co) and imidazolate linkers which form 3D tetrahedral frameworks and frequently resemble zeolite topologies.^[16–18] A number of ZIFs exhibit exceptional thermal and chemical stability.^[16] Another important feature of ZIFs is their hydrophobic surfaces, which give ZIF membranes certain advantages over zeolite membranes and sol–gel-derived silica membranes in the separation of H_2 in the presence of steam.^[19]

Very recently we reported the first result from permeation measurements on a ZIF-8 membrane.^[20] The ZIF-8 membrane showed a H_2/CH_4 separation factor greater than 10. Whereas the ZIF-8 pores (0.34 nm) are slightly larger than the kinetic diameter of CO_2 (0.33 nm), and are very flexible, the H_2/CO_2 separation on this ZIF-8 membrane showed Knudsen selectivity. In the current work, we therefore chose ZIF-7 as a promising candidate for the development of a H_2 -selective membrane to satisfy the above requirements. ZIF-7 ($\text{Zn}(\text{bim})_2$) is formed by bridging benzimidazolate (bim) anions and zinc cations with sodalite (SOD) topology.^[16,18] The pore size of ZIF-7 (the hexagonal window size in the SOD cage) estimated from crystallographic data is about 0.3 nm, which is just in between the size of H_2 (0.29 nm) and CO_2 (0.33 nm). We could therefore expect a ZIF-7 membrane to achieve a high selectivity of H_2 over CO_2 and other gases through a molecular sieving effect.

In many cases, it was reported that the heterogeneous nucleation density of MOF crystals on ceramic supports is very low,^[8,9,14] which makes it extremely difficult to prepare supported-MOF membranes by an in situ synthesis route. Chemical modifications of substrate surfaces have been proposed to direct the nucleation and orientation of the deposited MOF layers.^[21,22] Based on our knowledge in the development of zeolite membranes,^[23,24] we adopted a seeded secondary growth method for the ZIF-7 membrane prepara-

[*] Prof. Dr. Y.-S. Li, F.-Y. Liang, H. Bux, A. Feldhoff, Prof. Dr. J. Caro Institute of Physical Chemistry and Electrochemistry and the Laboratory for Nano and Quantum Engineering (LNQE) in cooperation with the Center for Solid State Research and New Materials, Leibniz Universität Hannover Callinstrasse 3A, 30167 Hannover (Germany) Fax: (+49) 511-762-19121 E-mail: yanshuo.li@pci.uni-hannover.de juergen.caro@pci.uni-hannover.de

Prof. Dr. Y.-S. Li, Prof. Dr. W.-S. Yang State Key Laboratory of Catalysis Dalian Institute of Chemical Physics Chinese Academy of Sciences Zhong-Shan Road 457, 116023 Dalian (China)

[**] Y.-S. Li is grateful for the financial support from the Alexander von Humboldt Foundation. DFG Priority Program 1362 "Porous Metal–Organic Frameworks" is acknowledged for financial support. The authors thank F. Steinbach for support in electron microscopy and K. Efimov for TGA measurements.

Supporting information for this article is available on the WWW under <http://dx.doi.org/10.1002/anie.200905645>.

tion to eliminate the influence of the surface chemistry and to promote the growth of ZIF-7 on the supports; this approach has been well-established in the research of zeolite membranes.^[25] To this end, an effective seeding method is necessary.^[10] In addition, we used a microwave dielectric heating technique to shorten the secondary growth time so as to reduce the thickness of the crystallized ZIF-7 layer, which is essential to ensure a high flux, especially for the ultramicroporous ZIF-7 membranes.

ZIF-7 nanoseeds were synthesized at room temperature using a modified synthetic protocol according to a report from Yaghi and co-workers,^[16] in which the linker (bim) to zinc ratio was increased from 0.74 to 6.5. Similar to the case of the room-temperature synthesis of ZIF-8 nanocrystals,^[26] it was speculated that the excess bim could act both as a linker in its deprotonated form and as a growth terminator and stabilizing agent in its neutral form. Compared with reported structural data, the obtained product is pure ZIF-7 according to the powder X-ray diffraction (PXRD; see Figure S1 in the Supporting Information). The average particle size of the ZIF-7 is 30 nm as estimated from the broadening of the XRD peaks (calculated based on Scherrer's equation), which is in agreement with the direct determination of the particle size by transmission electron microscopy (TEM; see Figure S2 in the Supporting Information).

The synthesized ZIF-7 nanoseeds can be dispersed in methanol or *N,N*-dimethylformamide (DMF) to form stable colloidal dispersions. When these colloidal dispersions are used to seed alumina supports, however, the seed layer can easily peel away from the supports. To address this problem, we dispersed the ZIF-7 nanoseeds in a polyethyleneimine (PEI) solution to obtain a viscous seeding solution (containing 4 wt% ZIF-7 and 2 wt% PEI). Although ZIF-7 cannot be dispersed in the aqueous phase because of its hydrophobic property, it can be homogeneously dispersed in an aqueous PEI solution by using ultrasonic treatment. This dispersion may possibly arise because PEI can coordinate with the zinc atoms at the surface of the nanoseeds, thereby making them compatible with the aqueous solution.^[27] Furthermore, PEI can effectively enhance the linkage between the seeds and the support through H-bonding interactions. A dip-coating technique was used for the surface seeding of the alumina support (20 s). No obvious ZIF-7 phase can be detected by XRD (see Figure S3 in the Supporting Information), indicating that the seed layer is very thin and, consequently, does not alter the permeation patterns of the seeded support. The seeded alumina support showed a high flux of H₂ and a low H₂/N₂ selectivity of 2.8, indicating that the seed layer does not act as a gas-transport barrier and shows no gas separation.

Microwave-assisted solvothermal synthesis was carried out to perform the secondary (seeded) growth. The seeded support was placed vertically in a clear synthesis solution with a molar composition of Zn²⁺/bim/DMF = 0.75:1:150, and then heated by a microwave at 100 °C for three hours. After secondary growth, a large-scale ordered polycrystalline ZIF-7 layer without any pinholes or cracks formed on the alumina support. The SEM top view (Figure 1 a) shows that the ZIF-7 grains are 1–2 μm in size and intergrown. Owing to the very thin seed layer and the short seeded secondary growth time by

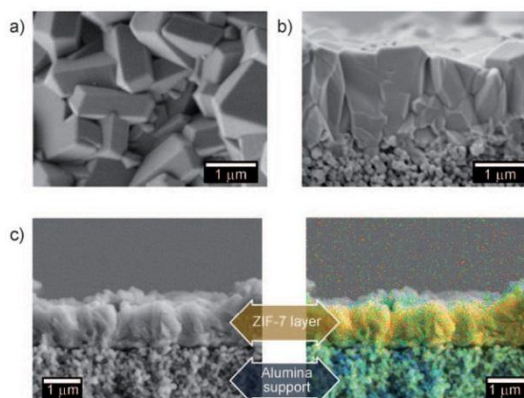


Figure 1. a) Top view and b) cross-section SEM images of the ZIF-7 membrane; c) EDXS mapping of the ZIF-7 membrane; orange Zn, cyan Al.

microwave heating, the ZIF-7 top layer is about 1.5 μm thick (Figure 1 b), which is much thinner than the MOF layers reported thus far.^[8,10–12] Energy-dispersive X-ray spectroscopy (EDXS) reveals that there is a sharp transition between the ZIF-7 layer (Zn signal) and the alumina support (Al signal; Figure 1 c). The XRD pattern of the ZIF-7 membrane shows that the ZIF-7 layer consists of randomly oriented grains and is free of impurity phases (see Figure S3 in the Supporting Information).

The synthesized ZIF-7 membrane is impermeable to all gases, including H₂, since it still contains the guest molecules within its cavities. An on-stream activation was carried out to open the pores and to monitor the activation process simultaneously by using a Wicke–Kallenbach permeation cell with a 1:1 mixture of H₂ and N₂ on the feed side (see Figure S4 in the Supporting Information). Figure 2 represents the variation of the H₂ and the N₂ permeances from their binary mixture during the on-stream activation process. Coinciding with the thermogravimetric (TG) analysis (see Figure S5 in the Supporting Information), the guest molecules began to leave the cavities when the cell was heated up to 100 °C, at which point the ZIF-7 membrane became gas permeable. At 165 °C this partially activated ZIF-7 membrane showed a H₂ permeance of about $7 \times 10^{-9} \text{ mol m}^{-2} \text{ s}^{-1} \text{ Pa}^{-1}$ and a H₂/N₂ separation factor of 8. The complete activation was accomplished after the temperature had been maintained at 200 °C for around 40 hours, and the H₂ permeance reached a plateau value of approximately $8 \times 10^{-8} \text{ mol m}^{-2} \text{ s}^{-1} \text{ Pa}^{-1}$ and the H₂/N₂ separation factor was 7.7.

For applications at elevated temperature, the activated ZIF-7 membrane was tested in single-gas and mixed-gas permeation at 200 °C using the Wicke–Kallenbach technique (see Figure S4 in the Supporting Information). Figure 3 (also see Table S1 in the Supporting Information) gives the permeances of H₂, CO₂, N₂, and CH₄ as single gases as well as from their 1:1 mixtures through the ZIF-7 membrane as a function of the kinetic diameter of the gas molecules. For both single- and mixed-gas permeation, there is a clear cut-off between H₂ and CO₂. The H₂/CO₂ ideal selectivity (calculated

Communications

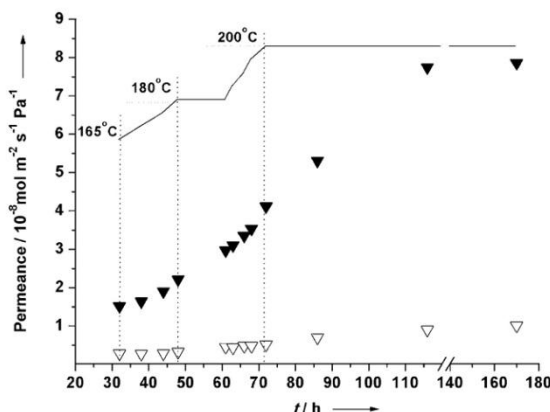


Figure 2. H₂ (solid triangles) and N₂ (triangles) permeances from the 1:1 mixture through the ZIF-7 membrane during the on-stream activation process with increasing temperature.

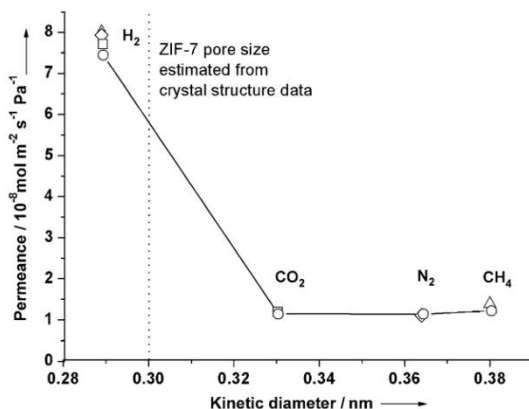


Figure 3. Permeances of single gases (circles) and from 1:1 mixtures (squares: H₂/CO₂ mixture, rhombuses: H₂/N₂ mixture, triangles: H₂/CH₄ mixture) of the ZIF-7 membrane at 200°C as a function of molecular kinetic diameters.

as the ratio of single-gas permeances) and separation factor are 6.7 and 6.5, respectively, which exceed the Knudsen separation factor (ca. 4.7). This result is consistent with our previous speculation that separation H₂/CO₂ by molecular sieves can be fulfilled by using ultramicroporous ZIF-7 membranes. For the 1:1 binary mixtures, the H₂/N₂ and H₂/CH₄ separation factors determined by the Wicke–Kallenbach method are 7.7 and 5.9, respectively (at 200°C and 1 bar), both are higher than the corresponding Knudsen separation factors (3.7 and 2.8, respectively). It follows from Figure 3 that the permeances are almost the same for H₂ as single gases and H₂ in the 1:1 binary mixtures. This experimental finding indicates a rather independent transport mechanism for the components of a mixture which can be correlated with ZIF-7 structure. ZIF-7 crystallizes in the sodalite structure with a hexagonal arrangement of the cavities octahedrally intercon-

nected by narrow windows interconnecting the cavities, which are responsible for the molecular sieving effect. The non-zero permeances of CO₂, N₂, and CH₄ can be attributed to a certain influence of the non-size-selective mass transport through the imperfect sealing or through the grain boundaries of the polycrystalline ZIF-7 layer. Nevertheless, the H₂/CO₂ separation factor of the ZIF-7 membrane in the current work is by far the highest value reported for a MOF membrane, and the membrane performance had already exceeded the latest Robeson's "upper-bound" line (see Figure S6 in the Supporting Information).^[29] Notably, in the present study the same ZIF-7 membrane had been tested for more than one week at 200°C and showed no degradation. This indicates that the ZIF-7 membrane has a good thermal stability.

In conclusion, an ultramicroporous zeolitic imidazolate framework, ZIF-7, was tested for its gas-separation properties in membrane applications by synthesizing it on a porous alumina support using a microwave-assisted secondary growth technique. In terms of H₂ separation, the ZIF-7 membrane has several advantages: 1) its pore dimension approaches the size of H₂, therefore a high H₂ selectivity could be obtained without any sophisticated pore-size engineering as is essential for zeolite membranes targeting H₂/CO₂ separation;^[30,31] 2) it is thermally stable for use at elevated temperatures (ZIF-7 is stable at least to 500°C in air according to the TG analysis, see Figure S5 in the Supporting Information); and 3) its hydrophobic property endows it with very good hydrothermal stability. Apart from exploring promising membrane materials, the present work also demonstrates a general approach towards the fabrication of high-quality MOF membranes on ceramic supports, namely polymers with coordination abilities (such as PEI in current work) which can be used to aid the seeding procedure, and the fast microwave synthesis is superior for reducing the membrane thickness. As shown in this work, and considering the very versatile structures and the development on the rational design of MOFs,^[32] as well as the recent advances in molecular simulation studies,^[33] MOF membranes might be able to revolutionize gas separations by using molecular sieves.

Experimental Section

Asymmetric alumina disks (Inocermic) were used as supports in current work. The disk has a diameter of 18 mm and thickness of 1 mm. The pore size of the top layer is 70 nm.

ZIF-7 nanoseeds were synthesized at room temperature. A typical synthesis procedure is as follows: 100 mL DMF (>99.8%, Arcos) was added to a solid mixture of 0.302 g Zn(NO₃)₂·6H₂O (>99%, Aldrich) and 0.769 g benzimidazole (>99%, Aldrich) with stirring (molar composition of the synthesis solution: Zn²⁺/bim/DMF = 0.154:1:200). After the reaction mixture had been kept at room temperature for 48 h, the product was separated using a centrifuge, and then washed with DMF.

The solution used for seeding was prepared by dispersing ZIF-7 nanoseeds into polyethyleneimine (PEI) solution. In a typical synthesis 0.2 g PEI (50 wt% in water, Aldrich) was dissolved in 4 mL NaHCO₃ solution (50 mM), and then 0.18 g of the as-synthesized ZIF-7 nanocrystals was added to the mixture, which was then treated under ultrasonic conditions for 20 min. The obtained seeding solution can be stored in a glass bottle for the later use.

An alumina support was dip-coated in the above seeding solution for 20 s. After briefly drying at room temperature for 2 h, the seeded support was dried in an oven (80 °C) overnight before secondary growth.

For the microwave-assisted secondary growth, 30 mL DMF was added into a solid mixture of Zn(NO₃)₂·6H₂O (0.57 g) and bim (0.31 g) with stirring (molar composition of the synthesis solution: Zn²⁺/bim/DMF = 0.75:1:150). This clear solution was transferred into a Teflon autoclave in which a seeded support was placed vertically. Afterwards the autoclave was heated in a microwave oven (Ethos 1, MLS) at a power of 300 W to 100 °C in 10 min, and then kept at 100 °C for 3 h. After cooling, the membrane was washed with methanol and dried at 50 °C overnight.

The experimental characterization techniques, including XRD, TEM, SEM, EDXS and TGA methods, as well as permeation measurements are described in detail in the Supporting Information.

Received: October 8, 2009

Published online: November 26, 2009

Keywords: gas separation · membranes · metal-organic frameworks · microwave chemistry · supported structures

- [1] L. M. Robeson, *J. Membr. Sci.* **1991**, *62*, 165.
- [2] a) Y. S. Lin, I. Kumakiri, B. N. Nair, H. Alsayouri, *Sep. Purif. Methods*, **2002**, *31*, 229; b) S. Kitagawa, R. Kitaura, S. Noro, *Angew. Chem.* **2004**, *116*, 2388; *Angew. Chem. Int. Ed.* **2004**, *43*, 2334.
- [3] M. Yaghi, M. O'Keeffe, N. W. Ockwig, H. K. Chae, M. Eddaoudi, J. Kim, *Nature* **2003**, *423*, 705.
- [4] G. Férey, *Chem. Soc. Rev.* **2008**, *37*, 191.
- [5] S. L. James, *Chem. Soc. Rev.* **2003**, *32*, 276.
- [6] J.-R. Li, R. J. Kuppler, H.-C. Zhou, *Chem. Soc. Rev.* **2009**, *38*, 1477.
- [7] D. Zacher, O. Shekha, C. Wöll, R. A. Fischer, *Chem. Soc. Rev.* **2009**, *38*, 1418.
- [8] M. Arnold, P. Kortunov, D. J. Jones, Y. Nedellec, J. Kärger, J. Caro, *Eur. J. Inorg. Chem.* **2007**, *1*, 60.
- [9] Y. Yoo, H. K. Jeong, *Chem. Commun.* **2008**, 2441.
- [10] J. Gascon, S. Aguado, F. Kapteijn, *Microporous Mesoporous Mater.* **2008**, *113*, 132.
- [11] Y. Liu, Z. Ng, E. A. Khan, H. K. Jeong, C. Ching, Z. P. Lai, *Microporous Mesoporous Mater.* **2009**, *118*, 296.
- [12] Y. Yoo, Z.-P. Lai, H. K. Jeong, *Microporous Mesoporous Mater.* **2009**, *123*, 100.
- [13] H. Guo, G. Zhu, I. J. Hewitt, S. L. Qiu, *J. Am. Chem. Soc.* **2009**, *131*, 1646.
- [14] R. Ranjan, M. Tsapatsis, *Chem. Mater.* **2009**, *21*, 4920.
- [15] L. Pan, D. H. Olson, L. R. Ciemnomolonski, R. Heddy, J. Li, *Angew. Chem.* **2006**, *118*, 632; *Angew. Chem. Int. Ed.* **2006**, *45*, 616.
- [16] K. S. Park, Z. Ni, A. P. Côté, J. Y. Choi, R. Huang, F. J. Uribe-Romo, H. K. Chae, M. O'Keeffe, O. M. Yaghi, *Proc. Natl. Acad. Sci. USA* **2006**, *103*, 10186.
- [17] X.-C. Huang, Y.-Y. Lin, J.-P. Zhang, X.-M. Chen, *Angew. Chem.* **2006**, *118*, 1587; *Angew. Chem. Int. Ed.* **2006**, *45*, 1557.
- [18] X.-C. Huang, J.-P. Zhang, X.-M. Chen, *Chin. Sci. Bull.* **2003**, *48*, 1531.
- [19] P. Klüsgens, M. Rose, I. Senkowska, H. Fröde, A. Henschel, S. Siegle, S. Kaskel, *Microporous Mesoporous Mater.* **2009**, *123*, 100.
- [20] H. Bux, F.-Y. Liang, Y.-S. Li, J. Cravillon, M. Wiebecke, J. Caro, *J. Am. Chem. Soc.*, DOI: 10.1021/ja907359t.
- [21] S. Hermes, F. Schröder, R. Chelkowski, C. Wöll, R. A. Fischer, *J. Am. Chem. Soc.* **2005**, *127*, 13744.
- [22] E. Biemmi, C. Scherb, T. Bein, *J. Am. Chem. Soc.* **2007**, *129*, 8054.
- [23] J. Caro, M. Noack, *Microporous Mesoporous Mater.* **2008**, *115*, 215.
- [24] Y.-S. Li, W.-S. Yang, *J. Membr. Sci.* **2008**, *316*, 3.
- [25] M. A. Snyder, M. Tsapatsis, *Angew. Chem.* **2007**, *119*, 7704; *Angew. Chem. Int. Ed.* **2007**, *46*, 7560.
- [26] J. Cravillon, S. Münzer, S. J. Lohmeier, A. Feldhoff, K. Huber, M. Wiebecke, *Chem. Mater.* **2009**, *21*, 1410.
- [27] V. N. Kislenco, L. P. Oliynyk, *J. Polym. Sci. Part A* **2002**, *40*, 914.
- [28] W. J. Koros, Y. H. Ma, T. Shimidzu, *Pure Appl. Chem.* **1996**, *68*, 1479.
- [29] L. M. Robeson, *J. Membr. Sci.* **2008**, *320*, 390.
- [30] M. Hong, J. L. Falconer, R. D. Noble, *Ind. Eng. Chem. Res.* **2005**, *44*, 4035.
- [31] M. Kanezashi, J. O'Brien-Abraham, Y. S. Lin, *AIChE J.* **2008**, *54*, 1478.
- [32] M. O'Keeffe, *Chem. Soc. Rev.* **2009**, *38*, 1215.
- [33] M. Zhou, Q. Wang, L. Zhang, Y.-C. Liu, Y. Kang, *J. Phys. Chem. B* **2009**, *113*, 11049.

3 Understanding Oriented Growth Processes in Polycrystalline MOF Films

3.1 Summary

In an attempt to find a general approach for MOF membrane preparation, the seeding procedure for ZIF-7 membranes (described in Section 2.3) could be successfully transferred completely to ZIF-8, as shown in Section 3.2. The subsequent secondary growth surprisingly resulted in a highly $\{100\}$ -oriented, continuous polycrystalline layer on top of porous α -alumina supports. For ZIF-7, crystals with a well-defined morphology could be obtained after substitution of the classical zinc source, zinc nitrate hexahydrate, against anhydrous zinc chloride. The hexagonal prismatic, rod-like ZIF-7 crystals were observed to grow c -out-of-plane on top of previously seeded α -alumina supports. The growth process as function of time was studied in detail for both, ZIF-7 and ZIF-8, by ex-situ XRD, SEM, transmission electron microscopy (TEM), and selected area electron diffraction (SAED). The observed preferred crystal orientation within the ZIF layers could be consistently explained by the evolutionary growth model of van der Drift, which predicts the dominance (or “survival”) of only those seed nuclei with their directions of fastest growth perpendicular to the starting plane. For ZIF-7, it could be shown that the direction of fastest growth is perpendicular to $\{003\}$ under equilibrium conditions, which results in a rod-like morphology with an elongated c -axis. For ZIF-8, the rhombic dodecahedral equilibrium morphology indicated growth rate dominance in the direction $\langle 100 \rangle$, thus forming a “coniferous forest”-like texturized, polycrystalline layer surface, consisting of intergrown pyramidal tops. The crystal preferred orientation (CPO) index (which is a quantitative value of the quality of orientation) indicated a high degree of orientation for the ZIF-8 layers. Though ZIF-7 grows much more anisotropically, a moderate distribution of the c -axis tilt angle relative to the support was found in SEM. These observations are consistent with simulations for zeolites that demonstrate a direct correlation between lateral growth and the distribution of orientations surviving during evolutionary growth (Section 3.2). Both studies provided insight into the growth process of ZIFs. However, in terms of membrane performance, the orientations of the membrane layers were either in the best case negligible for ZIF-8 or even disadvantageous for ZIF-7. Nevertheless, the importance of control of the growth process and crystal orientation in MOF membrane preparation could be demonstrated exemplarily.

3.2 Oriented Zeolitic Imidazolate Framework-8 Membrane with Sharp H₂/C₃H₈ Molecular Sieve Separation

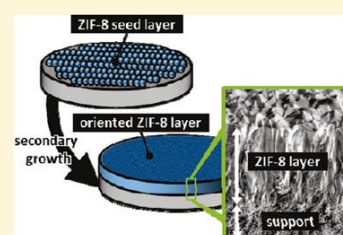
H. Bux, A. Feldhoff, J. Cravillon, M. Wiebcke, Y.S. Li, and J. Caro, *Chemistry of Materials* **2011**, *23*, 2262-2269.

Oriented Zeolitic Imidazolate Framework-8 Membrane with Sharp H₂/C₃H₈ Molecular Sieve SeparationHelge Bux,^{†,*} Armin Feldhoff,^{†,*} Janosch Cravillon,[‡] Michael Wiebcke,[‡] Yan-Shuo Li,[§] and Juergen Caro[†][†]Institute of Physical Chemistry and Electrochemistry, Leibniz University Hannover, Callinstr. 3A, D-30167 Hannover, Germany[‡]Institute of Inorganic Chemistry, Leibniz University Hannover, Callinstr. 9, D-30167 Hannover, Germany[§]Dalian Institute of Chemical Physics, Chinese Academy of Sciences, Zhong-Shan Road 457, Dalian 116023, China

Supporting Information

ABSTRACT: A highly oriented zeolitic imidazolate framework 8 (ZIF-8) composite membrane was prepared by seeding and secondary growth. By dip-coating, preformed ZIF-8 nanocrystals were attached to the surface of a porous α -alumina support using polyethyleneimine as the coupling agent. After solvothermal treatment, a continuous and well-intergrown ZIF-8 layer was obtained. X-ray diffraction analysis of the membrane showed preferred orientation of the {100} plane parallel to the support. Further time-dependent investigations by scanning and transmission electron microscopy as well as X-ray diffraction indicated that the preferred orientation develops during an evolutionary growth process. In gas mixture permeation experiments, the membrane showed good performance in H₂/hydrocarbon separation. A sharp molecular sieve separation is observed for an equimolar H₂/C₃H₈ mixture with a separation factor above 300.

KEYWORDS: metal–organic frameworks, zeolitic imidazolate frameworks, membrane, oriented growth



INTRODUCTION

In the past 10 years, porous metal–organic frameworks (MOFs) have established themselves in materials science.^{1–3} The 3-D framework structures are formed by metal clusters or cations connected by organic linker molecules. On the basis of the organic–inorganic hybrid character, MOFs have promise in a wide range of applications, e.g., gas storage,^{4,5} medical applications,^{6–8} catalysis,⁹ sensor technology,^{10,11} and molecular separation.^{12–14}

Basically, there are three options to use MOFs for molecular separation of liquid or gas mixtures: (i) by retaining one or more species from the liquid or gas phase by preferential adsorption in the pores, (ii) by different diffusivities of the species in the MOF, which is in the extreme case sterical size exclusion (molecular sieving) of one or more species, and (iii) the combination of (i) and (ii). One of the primary features that makes MOFs highly interesting for molecular separation is the so-called isorecticular design.¹⁵ Linker molecules can be modified with functional groups or even completely substituted, maintaining the basic framework structure while altering adsorption and diffusion properties.¹⁶

Membranes in general represent a cost and energy effective solution for industrial gas and liquid separation modified support. The mixture separation performance of membranes is characterized by the separation factor α_{ij} , which is defined after IUPAC as the ratio of the molar fraction of species *i* and *j* in the permeate, divided by the ratio of the molar fraction of species *i* and *j* in the retentate.¹⁷ Currently, there are increasing numbers of successful attempts to prepare molecular sieving MOF membranes as thin, polycrystalline layers on top of macroporous support materials, showing separation factors up to 25.^{18–27}

For the preparation of MOF membranes, usually two basic techniques known from zeolite membrane fabrication are applied: (i) secondary growth crystallization, where in a first step a seed layer is attached to the support and, subsequently, in a second step, grown to a continuous polycrystalline layer under solvothermal conditions, and (ii) in situ crystallization, where the polycrystalline layer is grown on the bare or chemically modified support in a one-step one-pot solvothermal synthesis. In situ crystallizations seem to be simple and, thus, the favored preparation route. However, they have the disadvantage of critically depending on high rates of heterogeneous nucleation on the support surface to successfully obtain continuous, well-intergrown MOF layers. Whether or not a high surface nucleation rate occurs depends on various factors, e.g., the surface chemistry of the support material (zeta potential, surface acidity, etc.). In secondary growth crystallizations, nucleation and crystal growth are decoupled, and hence, high nucleation rates and chemical interactions with the support material are less crucial.

Recently, we reported on the preparation of ceramic-supported zeolitic imidazolate framework (ZIF) membranes. ZIF-type MOFs frequently crystallize within zeolite-like tetrahedral framework structures, e.g., ZIF-7 and ZIF-8 with sodalite (SOD) and ZIF-22 with Linde type A (LTA) topologies.^{28–30} A number of ZIFs show excellent chemical and thermal stabilities, which is advantageous for membrane applications. ZIF-8 (Zn(mim)₂, mim = 2-methylimidazolate) membranes^{31,32} and ZIF-22 (Zn(Sabim)₂, Sabim = 5-azabenzimidazolate) membranes³³ were prepared by in situ crystallization,

Received: February 22, 2011

Revised: March 1, 2011

Published: March 22, 2011

while secondary growth was used for the preparation of ZIF-7 ($\text{Zn}(\text{bim})_2$, bim = benzimidazolate) membranes.^{34–36} The ZIF-7 and ZIF-22 membranes (both with pore sizes of ~ 3.0 Å) showed in the separation of an equimolar H_2/CO_2 mixture (kinetic diameters: 2.9 Å/ 3.3 Å)³⁷ separation factors of $\alpha = 13.6$ at 220 °C and $\alpha = 7.2$ at 50 °C, respectively. Because the pores of ZIF-8, as determined from crystallographic data, are larger (3.4 Å),²⁸ the membrane had a lower H_2/CO_2 separation factor ($\alpha = 4.5$ at 25 °C) compared to that of the above-mentioned narrow-pore ZIF membranes, but performed very well in the separation of H_2 from CH_4 (kinetic diameters: $2.9/3.8$ Å)³⁷ with $\alpha = 11.2$ at 25 °C.

Under certain synthesis conditions, ZIF-7 (hexagonal space group $R\bar{3}$) with its structural anisotropy forms needle-like crystals.³⁶ Thus, a ZIF-7 membrane with preferred crystal orientation relative to the support could be obtained by secondary growth of a ZIF-7 seed layer on top of an alumina support. In contrast, the ZIF-8 and ZIF-22 (cubic space groups $I\bar{4}3m$ and $Fm\bar{3}m$, respectively) with their isotropic structures resulted in supported layers of only randomly orientated crystals by in situ crystallization. Here, we report on the preparation of a continuous and well-intergrown polycrystalline ZIF-8 layer formed by secondary growth from a nanocrystal³⁸ seed layer on top of a porous alumina support. Contrary to the previously reported in situ crystallization, a highly oriented crystal growth is observed, although the seeds are randomly oriented. We will report the detailed preparation route and discuss a possible mechanism of oriented crystal growth that is supported by time-dependent electron microscopy and X-ray diffraction studies. We further report on the H_2/CO_2 and $\text{H}_2/\text{C}_1\text{–C}_3$ hydrocarbon gas separation performance of the newly developed ZIF-8 membrane.

EXPERIMENTAL SECTION

Membrane Synthesis. Asymmetric porous $\alpha\text{-Al}_2\text{O}_3$ discs (Fraunhofer IKTS) with a diameter of 18 mm were used as supports. ZIF-8 ($\text{Zn}(\text{mim})_2$) nanocrystals were prepared as previously reported.³⁸ The seeding solution was prepared as follows: 1.210 g freshly synthesized ZIF-8 nanocrystals (still wet and in gel-like state) were dispersed into a water/polyethyleneimine (PEI) solution, which consisted of 0.120 g sodium bicarbonate (Roth, >99.5%), 1.506 g PEI ($\sim 50\%$ solution in H_2O , Fluka), and 30 mL water.^{34,35} Addition of PEI to the seeding solution is vital to ensure that the seed crystals adhere to the support surface. As proposed by Ranjan and Tsapatsis,²¹ PEI may form hydrogen bonds with both the ZIF seed crystals and free hydroxyl groups of the support surface. In addition, PEI may form Zn–N coordination bonds to zinc cations on the surface of the nanocrystals. To generate a sufficiently high concentration of surface hydroxyl groups, the alumina supports were pretreated with $\sim 6\%$ hydrochloric acid and extensively washed with water afterward. For high reproducibility, the seeds were attached to the alumina discs using an automatic dip-coating device with a defined dipping and withdrawing speed of 300 and 100 mm/min, respectively. The discs were immediately removed after dip-coating and air-dried in an oven at 80 °C for 4 h. For subsequent solvothermal secondary growth solutions of low concentration were used, typically containing 0.532 g (3.95 mmol) zinc chloride (>99% Merck), 0.487 g (5.92 mmol) 2-methylimidazole (>99%, Sigma-Aldrich), and 0.272 g (3.95 mmol) sodium formate (>99%, Sigma-Aldrich) dissolved in 80 mL methanol (99.9%, Roth). The seeded alumina discs were placed vertically in PTFE holders to avoid sedimentation of crystals, which eventually nucleated from the homogeneous solution during membrane synthesis. In addition, the holders covered the back side of the supports to prevent crystallization on the coarse side of the asymmetric supports. The holders with mounted alumina supports were placed in autoclaves so that their top layer (70 nm $\alpha\text{-Al}_2\text{O}_3$) faced the synthesis solution. The autoclaves were heated in a microwave oven to 100 °C within 10 min typically for 2 h. In further experiments, the

synthesis time was varied from 0.5 h to 4 h. After cooling to room temperature, the membranes were carefully removed from the holder, intensively washed with methanol, and dried overnight at room temperature over silica gel. In addition, the crystalline precipitates were collected from the bottom of the autoclaves, washed, and dried for further analysis.

The secondary growth experiments at 1 h, 2 h, and 4 h were repeated to investigate the reproducibility of the growth process (see Table S1 of the Supporting Information).

To prove that the seed crystals actually initiate the layer growth, a reference membrane synthesis experiment was performed. In this case, the alumina support was dip-coated in an aqueous solution containing only 5.0% but no seed crystals.

X-ray Diffraction (XRD). XRD analysis of the membranes and powder samples was carried out on a Bruker D8 Advance diffractometer in reflection mode using Cu K α radiation. The 2θ range from 5° to 50° was scanned with a step size of 0.02° .

Scanning Electron Microscopy (SEM) and Energy-Dispersive X-ray Spectroscopy (EDXS). SEM and EDXS were performed on a JEOL JSM-6700F instrument with a field emitter as the electron source. For SEM, the films and membranes were simply broken and coated with Au to improve conductivity. Usually a low accelerating voltage (1–2 kV), a low current (3–5 μA), and a lens distance of 15 mm were used. For EDXS, the voltage and current were increased to 5 kV and 10 μA , respectively.

Transmission Electron Microscopy (TEM). For the preparation of a TEM specimen, a membrane was epoxy-glued against a silicon wafer. After curing, the sandwich was wire-sawed into about 1 mm thick slabs, which contained the glue line. The specimen bar was grinded and polished down to approximately 30 μm using polymer-embedded polishing films with propylene glycol as lubricant on an Allied High Tech Multiprep/Techprep device. The thin bar was epoxy-glued onto a supporting copper slot-grid and, after curing, locally thinned to electron transparency by 3 kV Ar^+ ion sputtering in a Gatan precision ion polishing system (PIPS). Observation of a membrane microstructure in cross-section was made at a electron energy of 200 kV in scanning transmission electron microscope (STEM) bright-field mode using a JEOL JEM-2100F field-emission instrument.

Permeation Experiments. Although a total of 10 ZIF-8 membranes have been prepared, only one of these membranes, showing a distinctive crystal orientation obtained after 2 h of secondary growth, was studied in permeation experiments. The measurements were carried out following a modified Wicke–Kallenbach technique³⁹ (Figure S1 of the Supporting Information). A sweep gas at 1 bar pressure (N_2 at 100 mL/min, purity 5.0) was used to continuously remove the permeate. The sweep gas composition was analyzed by using a gas chromatograph (HP Agilent 6890N, thermal conductivity detector) equipped with a Carboxen 1000 packed column (15 ft., 1/8 in., Supelco Sigma-Aldrich). The supported ZIF-8 membrane was tightly sealed in the permeation cell by using silicone and Viton O-rings (Eriks). The effective remaining membrane area was 1.09×10^{-4} m². Different hydrocarbons ($\text{C}_1 = \text{CH}_4$, $\text{C}_2 = \text{C}_2\text{H}_6$, $\text{C}_3 = n\text{-C}_3\text{H}_8$, purity ≥ 2.5) and CO_2 (food grade purity) were measured in equimolar gas mixture with hydrogen (purity 5.0) with a constant, total pressure of 200 kPa on the feed side or 100 kPa partial pressure for each gas, respectively. The feed flow was kept constant at total flow rates between 80 and 100 mL/min. Permeances in $\text{mol m}^{-2} \text{s}^{-1} \text{Pa}^{-1}$ were calculated on the basis of the measured flow rates (in mL min^{-1}) at room temperature (298.15 K) and ambient pressure (101.3 kPa) and from the applied partial pressure at the feed side of the membrane (100 kPa).

RESULTS AND DISCUSSION

After the dip-coating process described in the Experimental Section, the presence of the crystalline and phase-pure ZIF-8 seed layer was verified by XRD, as shown in Figure 1. The relative reflection intensities on the XRD pattern of the seed layer

approximately match those on the XRD pattern of the corresponding nanocrystals powder and a simulated pattern. Because it is assumed that in the powder sample the nanocrystals are randomly oriented, the same has to hold true for the seed layer.

Figure 2 shows SEM images of the well-intergrown polycrystalline ZIF-8 layer on top of the alumina support obtained after secondary growth for 2 h in top view as well as in cross-sectional view. In contrast, the reference membrane synthesis experiment performed using a PEI-coated alumina support without seeds resulted in poorly intergrown film with obvious gaps between clearly distinguishable ZIF-8 crystals of rhombic dodecahedral shape, as shown by the SEM image in Figure 3. This demonstrates that seeding is in fact necessary to grow a continuous, gap-free layer on top of the alumina support. The well-intergrown ZIF-8 layer shown in panel (b) of Figure 2 is around 12 μm thick and, therefore, much thinner than the well-intergrown ZIF-8 layer we prepared recently by in situ crystallization ($\sim 30 \mu\text{m}$).³¹ Elemental mapping by EDXS of the cross-section (Figure S2 of the Supporting Information) reveals a clear boundary between the ZIF-layer and the support. Hence, the crystal growth in the pores of the support seems to be disfavored. This is understandable because in the sub- μm top-layer pores of the asymmetric support, crystal growth is limited by size. As soon as the growing ZIF layer is sufficiently dense, the support pores are cut

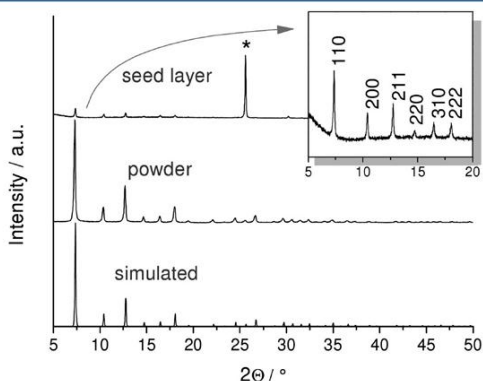


Figure 1. XRD pattern of the seed layer on top of the alumina support, XRD pattern of the corresponding nanocrystalline powder pattern, and XRD pattern simulated from crystal structure data²⁸ excluding guest species. Reflections of the alumina support are marked by an asterisk. Inset: magnification of the pattern of the seed layer including reflection indices.

from the nutrient solution and further intrapore growth is prevented. A TEM image of a very thin and polished sample from the cross-section of the membrane (Figure 4a) reveals the grain boundaries in the ZIF-8 layer. For clarity, the boundaries have been traced in panel (b) of Figure 4. Columnar crystals aligned roughly perpendicular to the support can be seen in the upper 2/3 of the layer, while in the lower 1/3 of the layer, the crystal grains are smaller and the grain boundaries are harder to trace.

The XRD patterns of the membrane and the ZIF-8 precipitate collected from the bottom of the autoclave are shown in panel (a) of Figure 5, while the XRD pattern of the reference membrane synthesis experiment is available in Figure S3 of the Supporting Information. The XRD pattern of the precipitate, which is assumed to have a random crystal orientation, and the XRD pattern of the reference experiment coincide in the reflection position and relative intensities. In contrast, the XRD pattern of the membrane exhibits a strongly increased relative intensity of the 200 reflection in relation to other reflections, which indicates a preferred crystal orientation of the {100} planes parallel to the support. A quantitative measurement of the degree of crystal orientation in the ZIF-8 layer can be obtained from the crystallographic preferred orientation (CPO) index,^{40,41} which compares the ratio of integrated intensities I_{hkl} from a pair of characteristic reflections $hkl/h'k'l'$ of the layer in relation to the integrated intensities I_{hkl} of the same pair $hkl/h'k'l'$ of the precipitate (see Equation S1 of the Supporting Information).

The CPO indices of the dominant 200 reflection in relation to the 110 (CPO_{200/110}) and the 211 reflections (CPO_{200/211}) are calculated to be 83 and 81, respectively. Both values clearly demonstrate the pronounced {100} orientation with only a low fraction of crystals taking different orientations.

At this point, it might be assumed that the slightly imperfect orientation is induced mainly from surface texture effects of the support. However, relating the columnar layer structure as observed by TEM (Figure 4) with the finding of oriented growth, it is indicated that only the upper 2/3 of the layer might be oriented, while the lower 1/3 is not or only partly oriented. Additional crystallizations with seeded supports were performed for 0.5, 1, and 4 h to study the secondary growth of the layer by XRD as function of time. Panel (b) of Figure 5 shows the XRD pattern of the obtained membranes. The corresponding CPO_{200/110} and CPO_{200/211} indices are available in Table 1. After 0.5 h, a very thin but continuous ZIF-8 layer had already formed as detected by SEM (Figure 6). The related XRD pattern of the

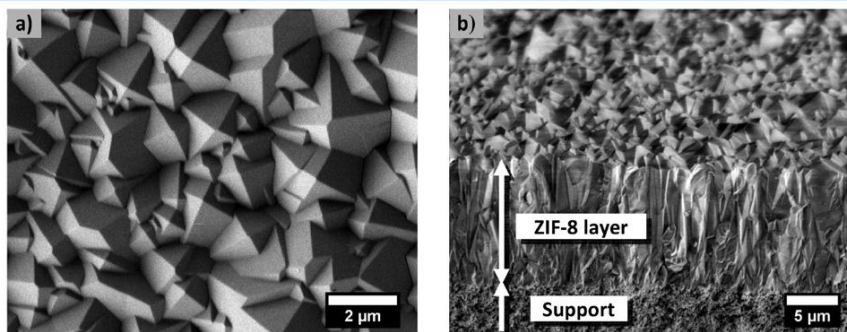


Figure 2. (a) SEM top view of the well-intergrown ZIF-8 layer after 2 h of secondary growth. (b) SEM top down view on the corresponding cross-section of the broken membrane.

membrane grown for 0.5 h matches that of the precipitate (Figure 5b), indicating random orientation of the crystals, which is quantitatively reflected by the low values of the CPO indices

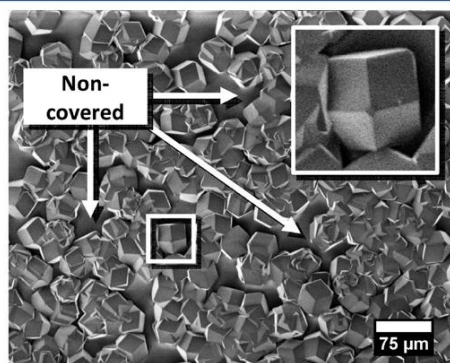


Figure 3. Supported ZIF-8 film grown from the reference membrane synthesis experiment (without seeds, only PEI-coated support) using the same solvothermal synthesis as for the seeded ZIF-8 membrane. Inset: magnification of a clearly distinguishable crystal with rhombic dodecahedral shape.

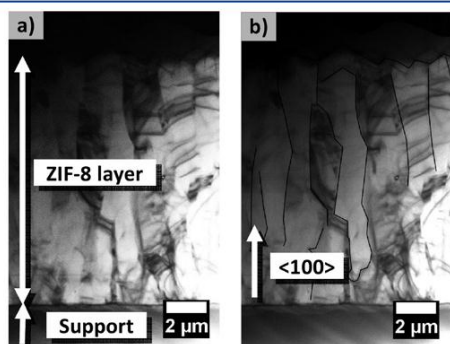


Figure 4. (a) TEM of the cross-section of the supported ZIF-8 membrane after 2 h of secondary growth as shown in panel (a) of Figure 2 and (b) with traced grain boundaries for improved visibility of the columnar growth and denoted $\langle 100 \rangle$ direction.

(Table 1). After 1 h, the 200 reflection already has increased remarkably in its relative intensity and is already stronger than the 110 reflection, which is dominating in the case of the randomly orientated powder. The CPO indices, however, are still very low, indicating that a large amount of crystals is still randomly oriented (Table 1). After 2 and 4 h of secondary growth, the intensities of all reflections apart from the 200 reflection are very low and can, according to the above measurements, be traced back mainly to the lower, less-oriented region of the ZIF-8 layer near to the support. The growth process was investigated to be generally reproducible (see Table S1 of the Supporting Information).

The preferred crystal orientation may be explained with the evolutionary selection model by van der Drift,⁴² which is commonly used to explain oriented growth of zeolite layers by secondary growth.⁴³ Starting from a randomly oriented seed layer on a planar surface, at first all seed crystals will start to grow at the same time and with the same face-dependent growth rates. After a certain time, which critically depends on the seed concentration on top of the surface, the crystals will meet their lateral neighbors. Crystals that have the fastest growth direction perpendicular or nearly perpendicular to the support surface will eventually overgrow their neighbors and thus form the top layer. The microstructure of the polycrystalline layer usually found after the evolutionary process is columnar-like in cross-sectional view. This is in fact observed for the ZIF-8 membranes (Figures 2a and 4). Ideal evolutionary selection, however, only takes place if (i) the crystals exhibit significant anisotropic growth, (ii) all crystals start to grow at the same time, and (iii) there are competing crystals in close neighborhood. A comparatively low heterogeneous nucleation rate, resulting in a lower concentration of nuclei on the support surface, might explain why in situ crystallizations under similar synthesis conditions

Table 1. Development of CPO Indices with Increasing Time of Secondary Growth

time (h)	CPO _{200/110}	CPO _{200/211}
0.5	-0.1	0.5
1	8.8	4.0
2	83.0	81.1
4	134.6	79.9

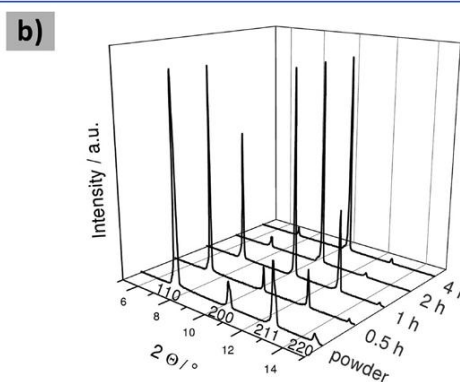
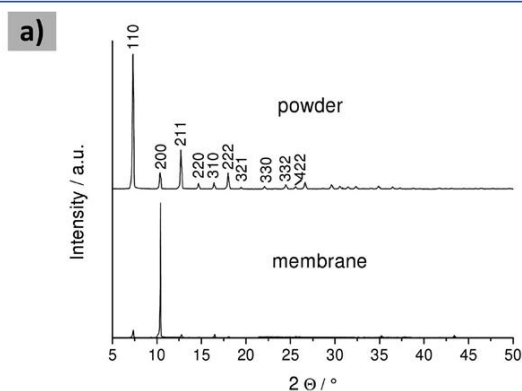


Figure 5. (a) XRD pattern of the oriented ZIF-8 layer after 2 h of secondary growth on top of the alumina support (lower pattern) and the corresponding precipitate (top pattern). The first 10 hkl -indices are denoted. (b) XRD patterns between 5° and 15° 2θ of ZIF-8 layers after secondary growth for 0.5 h, 1 h, 2 h, and 4 h in comparison with the powder pattern.

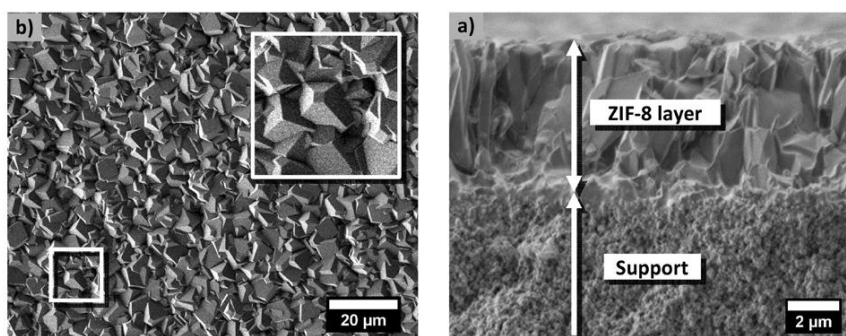


Figure 6. (a) SEM top view of the supported ZIF-8 layer which is, after secondary growth for 0.5 h, still randomly oriented. Inset: magnification showing a rhombic dodecahedral crystal with orientation near to $\langle 100 \rangle$, which might become a part of the final, oriented layer when increasing the synthesis time. (b) Corresponding cross-section of the about 5 μm thick layer formed at 0.5 h of secondary growth.

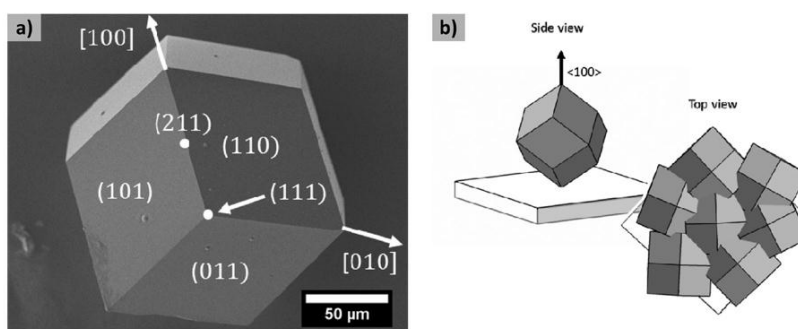


Figure 7. (a) SEM image of a ZIF-8 crystal with rhombic dodecahedral shape. The polyhedron exhibits 12 faces perpendicular to $\langle 110 \rangle$ and 24 edges perpendicular to $\langle 211 \rangle$. Six corners point along $\langle 100 \rangle$ (4-fold rotation axis), and eight corners point along $\langle 111 \rangle$ (3-fold rotation axis). (b) Schematic of an individual rhombic dodecahedral crystal as viewed perpendicular to $\langle 100 \rangle$ and microstructure of an intergrown layer of $\{100\}$ oriented rhombic dodecahedral crystals (top view).

only result in a randomly oriented layer on titania supports, as previously reported.³¹

According to the above model, our findings of strongly preferred $\{100\}$ crystal orientation is the result of fastest growth along the $\langle 100 \rangle$ direction. This is also in agreement with the crystal morphology. The equilibrium shape of ZIF-8 is apparently rhombic dodecahedral for both nanocrystals³⁸ (as those used for seeding) and large macrocrystals that are synthesized under similar conditions as the membranes (Figure 7a). Parallel work of Cravillon et al. have observed that in room-temperature syntheses cube-shaped crystals ($\{100\}$ crystal form) first develop in early stages and eventually transform into rhombic dodecahedra ($\{110\}$ crystal form).⁴⁴ The polyhedron (crystallographic point group symmetry $\bar{4}3m$) consists of 12 rhombic faces perpendicular to $\langle 110 \rangle$. When viewed along the $\langle 100 \rangle$ direction, one out of six corners is seen that lay on a 4-fold rotation axis (Figure 7b, upper left). Such corners are expected to be clearly visible in top view of a layer of intergrown micrometer-sized crystals with preferred $\{100\}$ orientation (Figure 7b, lower right), as is indeed revealed on SEM images of the ZIF-8 membranes (Figure 2a).

As proposed by Bons and Bons,⁴⁵ the final distribution of orientations, which survive the evolutionary selection, depends not only on the vertical but also on the lateral growth vector. They performed 2-D computer simulations of zeolite MFI crystals growing simultaneously in close neighborhood to each

other. Orthorhombic MFI usually grows in a coffin-like crystal shape, with the vector of fastest growth in the $[100]$ direction (c -axis). The simulation showed that with increasing lateral growth rate of MFI crystals, the fractions of crystals with orientations other than c decreases. Bons and Bons explain their results by the higher chance of c -oriented crystals to overgrow crystals with different orientations and, hence, completely stop their growth.

For the ZIF-7 membrane recently reported,³⁶ evolutionary growth of needle-like crystals was found, resulting in a c -oriented, polycrystalline layer. However, according to SEM studies, a large part of the crystals exhibited a tilted rather than a perfect c -orientation with respect to the support. These findings are in complete agreement with the model by Bons and Bons. The distinct needle-like morphology of ZIF-7 suggests that the growth rate along the c -axis is significantly larger than that along perpendicular directions, thus explaining the nonperfect c -orientation. On the other hand, for the present case of ZIF-8, a highly oriented layer is obtained, which might be unexpected at first glance because of the cubic crystal structure and, hence, “isotropic” crystal growth. However, for the observed preferred $\{100\}$ orientation, fastest growth occurs not only perpendicular but simultaneously parallel to the support surface (because, e.g., $[100]$ and $[010]$ are perpendicular to each other). Hence, the highly oriented growth is, again, in complete agreement with the model by Bons and Bons.

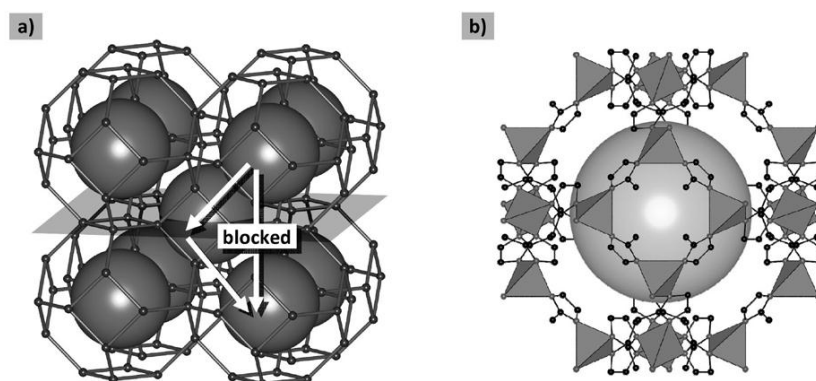


Figure 8. (a) Perspective drawing of the ZIF-8 SOD topology with a $\{100\}$ plane propagating through the structure. The arrows indicate possible pathways of a molecule through the pore system (large cages connected by six-membered ring windows). The straight passage from one cage to the one below is blocked because of the very small size of the four-membered ring windows. (b) View along $\langle 100 \rangle$ on a $[4^6 6^8]$ truncated octahedral cage of the ZIF-8 structure.

The propagation of a $\{100\}$ plane through the ZIF-8 structure with SOD topology is shown in panel (a) of Figure 8. The plane runs parallel to the very narrow four-membered ring windows, while the larger six-membered ring windows are aligned parallel to $\{111\}$ planes (Figure 8b). This means that for our $\{100\}$ oriented ZIF-8 layer the four-membered ring windows are aligned parallel to the support. However, the contribution of the four-membered ring windows to mass transport through the pore network is assumed to be negligible. As implied by the arrows in panel (a) of Figure 8, a molecule, driven by a vertical concentration gradient, cannot pass straight from one cage to the one below. Instead it has to follow a zigzag path through an adjacent cage, connected by the six-membered ring windows. The size of these windows can be estimated to be 3.4 Å from rigid framework models. Hence, in terms of diffusion through a membrane, parallel orientation of the $\{100\}$ planes (and the four-membered ring windows) to the support is rather a disadvantage, while a parallel alignment of the $\{111\}$ planes (and the six-membered ring-windows) would be the most desired orientation. However, because of the cubic symmetry of the 3-D pore network of ZIF-8, the crystal orientation is expected to be only of minor influence on the macroscopic level on membrane permeation and the separation performance.

As shown in various studies, the pore size in ZIFs seems to be larger than the value estimated from the crystallographic structures, assuming rigid framework structures. Kinetic uptake experiments and chromatographic studies showed that ethane (~ 3.8 Å),⁴⁶ propane (~ 4.0 Å),⁴⁶ and even *i*-butane can be adsorbed in ZIF-8, despite that their molecular diameters are significantly larger than the estimated six-membered pore window size of 3.4 Å.^{47–49} Recent investigations using IR microscopy for the in situ detection of molecular uptake came to the same conclusions.^{32,50} The obvious discrepancies between the predictions and the experimental findings might be explained by a dynamic flipping or rotation of the imidazolate linker. Gücüyener et al. postulated gate-opening effects in ZIF-7.⁵¹ In fact, dynamic benzene-ring flipping of the terephthalate linker in MIL type MOFs was recently found by Kolokolov et al. using ²H NMR spectroscopy.⁵² Molecular Dynamics (MD) simulations revealed huge differences in diffusion coefficients of guest molecules in rigid and flexible ZIF structures.⁵³

In Figure 9, the results of H_2/C_nX_m ($X = H, O$) and H_2/CH_4 gas mixture permeation measurements on the ZIF-8 membrane obtained after 2 h of secondary growth are reported. The permeances of H_2 and C_nX_m from the mixtures were calculated from the applied partial pressure (see Experimental Section). The corresponding mixture separation factor α was calculated following IUPAC definition.¹⁷ As already explained above, the ZIF-8 pore windows are permeable for gases with kinetic diameters larger than 3.4 Å, which is the pore size estimated from the rigid structure model. Hence, a sharp molecular sieve effect, which completely separates H_2 from CH_4 (kinetic diameter: 3.8 Å) is not observed. However, for the ZIF-8 membrane reported here, a sharp cutoff in α for H_2/C_nX_m separation is observed when increasing the hydrocarbon chain length from C_2 to C_3 (Figure 9). According to Combariza et al.,⁴⁶ the smallest pore diameters through which a molecule would fit are 3.8 Å for CH_4 and C_2H_6 and 4.0 Å for C_3H_8 . Hence, a very small difference in diameter of only 0.2 Å between C_2H_6 and C_3H_8 seems to have large effect on the molecular mobility. Of course, C_3H_8 exhibits much larger spatial dimensions than C_2H_6 , so the lower mobility might at first be not surprising. However, CH_4 and C_2H_6 exhibit a similar difference in molecular dimensions, but no such difference in mobility is found for C_2H_6 compared to that of CH_4 . This might either indicate that there is a sharp loss in gate opening flexibility at a size of ~ 4.0 Å or that there is a more complex interaction of the pore gates with penetrating molecules.

Panel (b) of Figure 9 compares the H_2 and CH_4 permeances and separation factors measured in this work with the corresponding values of the non-oriented ZIF-8 membranes on which we³¹ and McCarthy et al.²⁵ reported recently. All experiments were performed at $T = 25$ °C and at similar concentration gradients across the membrane (1 bar partial pressure at the feed side and near zero at the permeate side) and, hence, should be comparable. With respect to the H_2/CH_4 separation factor of $\alpha \approx 15$, the oriented membrane shows a slightly higher selectivity in comparison to our non-oriented ZIF-8 ($\alpha \approx 11$) membrane and the membrane prepared by McCarthy et al. (pure gas or ideal separation factor: ≈ 13). We explain this result by an improved microstructure quality of the oriented ZIF-8 membrane, i.e., a better intergrowth of the grains and consequently lower leak transport, rather than by the crystal orientation. However, in industrial applications, the

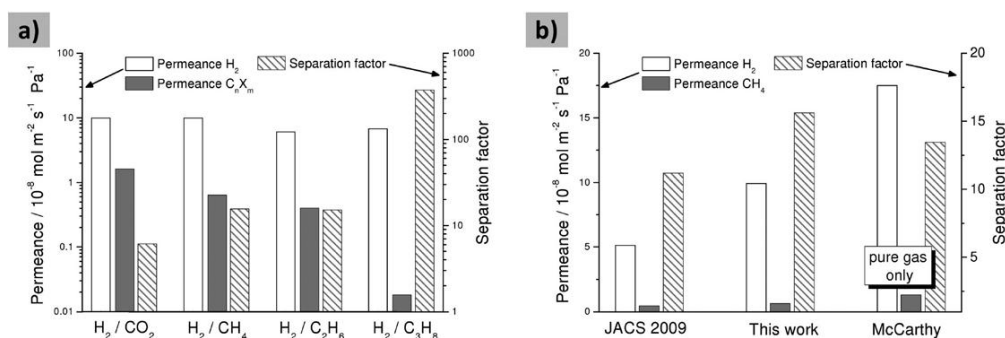


Figure 9. (a) Permeances and separation factors (in logarithmic scale) of equimolar H₂/C_nX_m gas mixtures at room temperature measured on the ZIF-8 membrane prepared by 2 h of secondary growth. (b) Comparison of the H₂/CH₄ permeances and separation factor with our previously reported ZIF-8 membrane (JACS 2009)³¹ as well as with data from the work of McCarthy et al.²⁵.

permeance (which is the pressure-normalized flux in mol m⁻² s⁻¹ Pa⁻¹) of a membrane is at least as important as its separation factor. In comparison to our non-oriented ZIF-8 membrane, the decrease in layer thickness from 30 to 12 μm resulted in an almost doubled H₂ permeance. However, following Fick's first law from which the permeance through the membrane is reciprocally correlated with the membrane thickness, we would expect an increase in the permeance by the factor 2.5. The difference between the actual and expected increase in permeance can be explained by the improved quality of the novel, oriented ZIF-8 membrane, as indicated by the higher H₂/CH₄ separation factor (Figure 9b). The permeances of the 30 μm thick membrane likely include a higher contribution of undefined mass transport through defects or leaks, which results in a lower selectivity.

The ZIF-8 membrane reported by McCarthy et al. exhibits a layer thickness of around 20 μm, while the permeances were found to be even higher than those reported here. Though McCarthy et al. performed pure gas measurements only (and we have previously shown that there is a slight but noticeable reduction of the permeances in H₂/CH₄ mixed gas separation compared to the pure gases),³¹ the deviation might be explained primarily by the different experimental measurement methods. For the permeation measurements, McCarthy et al. used an instationary time lag method,⁵⁴ where a constant gas pressure is applied to the feed side of the membrane, while the time-dependent pressure increase at the evacuated permeate side of the membrane is monitored. Permeances can be calculated from the recorded pressure-time curves, and it is ideally assumed that the permeate side pressure is near zero. In our experiments, we used a modified, stationary Wicke–Kallenbach technique (see Experimental Section), where the permeate partial pressure is kept near zero by sweeping with an inert gas. Hence, in idealized theory, the boundary conditions of permeation are the same for both experiments. However, because the porous alumina support might act as dead volume, the idealized assumption of a zero partial pressure at the permeate side might be problematic. To minimize this concentration polarization, the alumina supports have an asymmetric structure and consist of only a thin layer with a small pore size (~70 nm) supporting the ZIF-8 layer and a thick coarse layer as mechanical support with a large pore size (~10 μm). This asymmetric structure reduces the pressure loss across the membrane. Even a small increase in the residual partial pressure at the permeate side can, however, highly influence the concentration gradient (see Figure S4 of the Supporting Information) and reduce our measured permeances. Further influences of different experimental configurations

in the Wicke–Kallenbach technique are very well investigated on zeolite membranes by van de Graaf et al.⁵⁵

Recently Aguado et al. showed permeation measurements for tubular composite membranes of SIM-1 (Zn(4m5cim)₂, 4m5cim = 4-methyl-5-imidazolecarboxaldehyde) with a layer thickness of 25 μm.⁵⁶ SIM-1 is iso-structural to ZIF-8, and the membrane shows permeances of light gases in a similar order of magnitude as for the here shown ZIF-8 membranes.

CONCLUSIONS

We prepared for the first time a continuous ZIF-8 layer on top of a porous alumina support by secondary seeded growth. This method allows us to obtain much thinner ZIF-8 membranes than in previous *in situ* crystallizations. Columnar crystal grains aligned perpendicular to the support surface were observed by SEM and TEM. XRD and SEM demonstrated that the well-intergrown crystals exhibit a high degree of {100} orientation. The highly oriented growth can be well explained by the evolutionary selection model by van der Drift,⁴² which predicts that the crystals with the highest vector of vertical growth survive the selection process, and the model by Bons and Bons,⁴⁵ which correlates the degree of preferred orientation with the lateral growth vectors. Permeation measurements on the ZIF-8 membrane obtained after 2 h of secondary growth showed a slightly higher H₂/CH₄ separation factor in comparison with that of the membrane prepared by *in situ* crystallization.³¹ We explain this finding with the improved quality of the microstructure of the new membrane. Until now, ZIF-membranes showed only a smooth molecular sieve effect in the separation of lighter gases (e.g., H₂, CO₂, and CH₄), rather than a sharp cutoff at the crystallographic pore size of 3.4 Å as estimated from rigid framework structure models.⁵⁷ Here, we demonstrate that the new ZIF-8 membrane shows a sharp H₂/C₃H₈ molecular sieve separation. This indicates that the large derivations of the experimentally measured separation factors for light gases from the ones predicted recently from rigid framework structure models cannot be entirely attributed to mass transfer through, e.g., grain boundaries, cracks, or leaking gaskets.

ASSOCIATED CONTENT

S Supporting Information. Explanatory schematics (Wicke–Kallenbach technique, diffusion through membranes), additional CPO data, EDXS element mapping, and additional XRD patterns. This material is available free of charge via the Internet at <http://pubs.acs.org>.

AUTHOR INFORMATION

Corresponding Author

*armin.feldhoff@pci.uni-hannover.de (A.F.), helge.bux@pci.uni-hannover.de (H.B.).

ACKNOWLEDGMENT

This work is part of the German Research Foundation priority program SPP 1362 "Porous Metal-Organic Frameworks", organized by S. Kaskel. We gratefully acknowledge financial support.

REFERENCES

- Yaghi, O. M.; O'Keeffe, M.; Ockwig, N. W.; Chae, H. K.; Eddaoudi, M.; Kim, J. *Nature* **2003**, *423* (6941), 705–714.
- Ferey, G. *Chem. Soc. Rev.* **2008**, *37* (1), 191–214.
- Kitagawa, S.; Kitaura, R.; Noro, S. *Angew. Chem., Int. Ed.* **2004**, *43* (18), 2334–2375.
- Murray, L. J.; Dinca, M.; Long, J. R. *Chem. Soc. Rev.* **2009**, *38* (5), 1294–1314.
- Ma, S. Q.; Zhou, H. C. *Chem. Commun.* **2010**, *46* (1), 44–53.
- Horcajada, P.; Serre, C.; Maurin, G.; Ramsahye, N. A.; Balas, F.; Vallet-Regi, M.; Sebban, M.; Taulelle, F.; Ferey, G. *J. Am. Chem. Soc.* **2008**, *130* (21), 6774–6780.
- Horcajada, P.; Chalati, T.; Serre, C.; Gillet, B.; Sebrie, C.; Baati, T.; Eubank, J. F.; Heurtaux, D.; Clayette, P.; Kreuz, C.; Chang, J. S.; Hwang, Y. K.; Marsaud, V.; Bories, P. N.; Cynober, L.; Gil, S.; Ferey, G.; Couvreur, P.; Gref, R. *Nat. Mater.* **2010**, *9* (2), 172–178.
- McKinlay, A. C.; Morris, R. E.; Horcajada, P.; Ferey, G.; Gref, R.; Couvreur, P.; Serre, C. *Angew. Chem., Int. Ed.* **2010**, *49* (36), 6260–6266.
- Lee, J.; Farha, O. K.; Roberts, J.; Scheidt, K. A.; Nguyen, S. T.; Hupp, J. T. *Chem. Soc. Rev.* **2009**, *38* (5), 1450–1459.
- Harbuzaru, B. V.; Corma, A.; Rey, F.; Jorda, J. L.; Ananias, D.; Carlos, L. D.; Rocha, J. *Angew. Chem., Int. Ed.* **2009**, *48* (35), 6476–6479.
- Lu, G.; Hupp, J. T. *J. Am. Chem. Soc.* **2010**, *132* (23), 7832–7833.
- Li, J. R.; Kuppler, R. J.; Zhou, H. C. *Chem. Soc. Rev.* **2009**, *38* (5), 1477–1504.
- Gascon, J.; Kapteijn, F. *Angew. Chem., Int. Ed.* **2010**, *49* (9), 1530–1532.
- Keskin, S.; van Heest, T. M.; Sholl, D. S. *ChemSusChem* **2010**, *3* (8), 879–891.
- Eddaoudi, M.; Kim, J.; Rosi, N.; Vodak, D.; Wachter, J.; O'Keeffe, M.; Yaghi, O. M. *Science* **2002**, *295* (5554), 469–472.
- Tanabe, K. K.; Wang, Z. Q.; Cohen, S. M. *J. Am. Chem. Soc.* **2008**, *130* (26), 8508–8517.
- Koros, W. J.; Ma, Y. H.; Shimidzu, T. *J. Membr. Sci.* **1996**, *120* (2), 149–159.
- Liu, Y. Y.; Ng, Z. F.; Khan, E. A.; Jeong, H. K.; Ching, C. B.; Lai, Z. P. *Microporous Mesoporous Mater.* **2009**, *118* (1–3), 296–301.
- Yoo, Y.; Lai, Z. P.; Jeong, H. K. *Microporous Mesoporous Mater.* **2009**, *123* (1–3), 100–106.
- Guo, H. L.; Zhu, G. S.; Hewitt, I. J.; Qiu, S. L. *J. Am. Chem. Soc.* **2009**, *131* (5), 1646–1647.
- Ranjan, R.; Tsapatsis, M. *Chem. Mater.* **2009**, *21* (20), 4920–4924.
- Guerrero, V. V.; Yoo, Y.; McCarthy, M. C.; Jeong, H. K. *J. Mater. Chem.* **2010**, *20* (19), 3938–3943.
- Huang, A.; Dou, W.; Caro, J. *J. Am. Chem. Soc.* **2010**, *132* (44), 15562–15564.
- Liu, Y. Y.; Hu, E. P.; Khan, E. A.; Lai, Z. P. *J. Membr. Sci.* **2010**, *353* (1–2), 36–40.
- McCarthy, M. C.; Varela-Guerrero, V.; Barnett, G. V.; Jeong, H. K. *Langmuir* **2010**, *26* (18), 14636–14641.
- Venna, S. R.; Carreon, M. A. *J. Am. Chem. Soc.* **2010**, *132* (1), 76–78.
- Yoo, Y.; Jeong, H. K. *Cryst. Growth Des.* **2010**, *10* (3), 1283–1288.
- Park, K. S.; Ni, Z.; Cote, A. P.; Choi, J. Y.; Huang, R. D.; Uribe-Romo, F. J.; Chae, H. K.; O'Keeffe, M.; Yaghi, O. M. *Proc. Natl. Acad. Sci. U.S.A.* **2006**, *103* (27), 10186–10191.
- Hayashi, H.; Cote, A. P.; Furukawa, H.; O'Keeffe, M.; Yaghi, O. M. *Nat. Mater.* **2007**, *6* (7), 501–506.
- Phan, A.; Doonan, C. J.; Uribe-Romo, F. J.; Knobler, C. B.; O'Keeffe, M.; Yaghi, O. M. *Acc. Chem. Res.* **2010**, *43* (1), 58–67.
- Bux, H.; Liang, F. Y.; Li, Y. S.; Cravillon, J.; Wiebcke, M.; Caro, J. *J. Am. Chem. Soc.* **2009**, *131* (44), 16000–16001.
- Bux, H.; Chmelik, C.; van Baten, J. M.; Krishna, R.; Caro, J. *Adv. Mater.* **2010**, *22* (42), 4741–4743.
- Huang, A. S.; Bux, H.; Steinbach, F.; Caro, J. *Angew. Chem., Int. Ed.* **2010**, *49* (29), 4958–4961.
- Li, Y. S.; Liang, F. Y.; Bux, H.; Feldhoff, A.; Yang, W. S.; Caro, J. *Angew. Chem., Int. Ed.* **2010**, *49* (3), 548–551.
- Li, Y. S.; Liang, F. Y.; Bux, H. G.; Yang, W. S.; Caro, J. *J. Membr. Sci.* **2010**, *354* (1–2), 48–54.
- Li, Y. S.; Bux, H.; Feldhoff, A.; Li, G. L.; Yang, W. S.; Caro, J. *Adv. Mater.* **2010**, *22* (30), 3322–3326.
- Breck, D. W. *Zeolite Molecular Sieves: Structure, Chemistry, and Use*; Wiley: New York, 1974.
- Cravillon, J.; Munzer, S.; Lohmeier, S. J.; Feldhoff, A.; Huber, K.; Wiebcke, M. *Chem. Mater.* **2009**, *21* (8), 1410–1412.
- Wicke, E.; Kallenbach, R. *Colloid Polym. Sci.* **1941**, *97* (2), 135–151.
- Verduijn, J. P.; Bons, A. J.; Anthonis, M. H.; Czarnetzki, L. H. WO Patent 96/01683, 1996.
- Jeong, H. K.; Krohn, J.; Sujaoti, K.; Tsapatsis, M. *J. Am. Chem. Soc.* **2002**, *124* (44), 12966–12968.
- van der Drift, A. *Philips Res. Rep.* **1967**, *22*, 267–288.
- Caro, J.; Noack, M.; Kolsch, P. *Adsorption* **2005**, *11* (3–4), 215–227.
- Cravillon, J.; Nayuk, R.; Springer, S.; Feldhoff, A.; Huber, K.; Wiebcke, M. *Chem. Mater.*, accepted for publication, DOI: 10.1021/cm103571y.
- Bons, A. J.; Bons, P. D. *Microporous Mesoporous Mater.* **2003**, *62* (1–2), 9–16.
- Combariza, A. F.; Sastre, G.; Corma, A. *J. Phys. Chem. C* **2010**, *115* (4), 875–884.
- Luebbbers, M. T.; Wu, T. J.; Shen, L. J.; Masel, R. I. *Langmuir* **2010**, *26* (19), 15625–15633.
- Li, K. H.; Olson, D. H.; Seidel, J.; Emge, T. J.; Gong, H. W.; Zeng, H. P.; Li, J. *J. Am. Chem. Soc.* **2009**, *131* (30), 10368–10369.
- Demessence, A.; Boissiere, C.; Grosso, D.; Horcajada, P.; Serre, C.; Ferey, G.; Soler-Illia, G.; Sanchez, C. *J. Mater. Chem.* **2010**, *20* (36), 7676–7681.
- Chmelik, C.; Bux, H.; Caro, J.; Heinke, L.; Hibbe, F.; Titze, T.; Kaerger, J. *Phys. Rev. Lett.* **2010**, *104* (8), 085902.
- Güçüyener, C.; van den Bergh, J.; Gascon, J.; Kapteijn, F. *J. Am. Chem. Soc.* **2010**, *132* (50), 17704–17706.
- Kolokolov, D. I.; Jobic, H.; Stepanov, A. G.; Guillerm, V.; Devic, T.; Serre, C.; Ferey, G. *Angew. Chem., Int. Ed.* **2010**, *49* (28), 4791–4794.
- Hertäg, L.; Bux, H.; Caro, J.; Chmelik, C.; Remsunggen, T.; Knauth, M.; Fritzsche, S. *J. Membr. Sci.*, **2011**, DOI:10.1016/j.memsci.2011.01.019.
- Rutherford, S. W.; Do, D. D. *Adsorption* **1997**, *3* (4), 283–312.
- van de Graaf, J. M.; Kapteijn, F.; Moulijn, J. A. *J. Membr. Sci.* **1998**, *144* (1–2), 87–104.
- Aguado, S.; Nicolas, C.-H.; Moizan-Basle, V.; Nieto, C.; Amrouche, H.; Bats, N.; Audebrand, N.; Farrusseng, D. *New J. Chem.* **2011**, *35* (1), 41–44.
- Haldoupis, E.; Nair, S.; Sholl, D. S. *J. Am. Chem. Soc.* **2010**, *132* (21), 7528–7539.

3.4 Controllable Synthesis of Metal–Organic Frameworks: From MOF Nanorods to Oriented MOF Membranes

Y.S. Li, H. Bux, A. Feldhoff, G.L. Li, W.S. Yang, and J. Caro, *Advanced Materials* **2010**, *22*, 3322-3326.

Controllable Synthesis of Metal–Organic Frameworks: From MOF Nanorods to Oriented MOF Membranes

By Yan-Shuo Li,* Helge Bux, Armin Feldhoff,* Guo-Ling Li, Wei-Shen Yang,
and Jürgen Caro

In recent years metal–organic frameworks (MOFs) have emerged as an intriguing class of hybrid nanoporous crystalline materials as a result of their highly diversified framework topologies and tailorable organic functionality.^[1] They have shown promising applications for hydrogen storage,^[1b] gas separation,^[1c] catalysis,^[1f] molecular recognition,^[1g] and, more recently, as proton exchange membranes for high temperature fuel cells.^[1h] Recently, MOF thin films has been attracting particular attention for use as smart membranes, catalytic coatings, chemical sensors, and related nanodevices.^[2] As in the related research on zeolite thin films, morphology control is an important issue when manipulating MOF materials as molecular sieve membranes. Accordingly, two challenges present themselves: i) the preparation of size- and shape-controlled MOF nanocrystals and ii) the optimization of film microstructures, including grain size and shape, grain boundaries, and channel orientations. Stabilizing agents,^[3] coordination modulators^[4] or specific synthetic techniques, such as microwave heating,^[5] ultrasonic synthesis,^[6] and microemulsion methods,^[7] have been used in the attempt to achieve size and shape control of MOF nanocrystals. Organic self-assembled monolayers (SAMs) were used to detect the assembly of secondary building units (SBUs) so as to control the surface deposition of MOF thin films.^[8] Stepwise layer-by-layer growth of MOF thin films was introduced by Fischer and coworkers, and shown to offer better control over the film thickness and orientation.^[9] Zeolitic imidazolate framework ZIF-7 (Zn(bim)₂) with sodalite (SOD) topology is formed by bridging benzimidazolate (bim) anions and zinc cations, exhibiting a hexagonal space group (*R*3̄).^[10] Two types of hexagonal faces are included in the sodalite cages of ZIF-7 (see Figure S1 in the Supporting Information): two normal hexagonal windows (perpendicular to the <001> axes, around 0.3 nm) and six distorted ones (perpendicular to the <11̄1̄> axes, approximately 0.35 nm × 0.20 nm).

This multidimensional and anisotropic channel network makes ZIF-7 an excellent model system for fundamental studies on achieving crystallographic preferred orientation (CPO) in MOF films and investigating its effect on permeation properties, as in the case of MFI zeolite membranes.^[11] In this Communication, we report a recent advance in the control of size and shape in the synthesis of ZIF-7 nanocrystals, and the orientation modulation of ZIF-7 membranes based on evolutionary selection (van der Drifts growth) model.^[12] The resulting oriented ZIF-7 membrane is evaluated in H₂/CO₂ mixture gas separation using the Wicke–Kallenbach technique.

Using a modified synthetic protocol after the original report of Yaghi and coworkers,^[10b] we synthesized ZIF-7 nanoparticles at room temperature from a solution containing excess bim.^[2i] Figure 1a shows the transmission electron microscopy (TEM) image of the ZIF-7 nanoparticles. The average particle size is 30.7 ± 5.9 nm (Figure 1b). The high-resolution TEM (HRTEM) image in Figure 1c shows the lattice fringes for a ZIF-7 nanocrystal. The particle with hexagonal shape appears to be a single-crystal domain with high crystallinity and exhibits a 1.15 nm *d*-spacing for the (1 1 0) lattice fringes. The selected area electron diffraction (SAED) pattern from a circular area 1.2 μm in diameter shows six Debye–Scherrer rings (Figure 1d). The 110 reflection is the most intense ring, followed by the 1̄32 and 312 reflections.

In our previous work, the purified ZIF-7 nanoparticles were re-dispersed into a polyethyleneimine (PEI) solution to obtain a viscous seeding solution.^[2j,k] PEI was used to enhance the linkage between the seeds and the support. Here, we report a “one-pot” synthesis strategy that combines these two steps: zinc nitrate and bim at stoichiometric ratio (molar ratio 1:2) were directly dissolved into a PEI-dimethylformamide (DMF) solution at room temperature. The obtained colloidal solution can be directly used as a seeding sol for the membrane fabrication. By altering the molar ratio of PEI and the reaction duration we can adjust the size of the ZIF-7 nanoparticles from 40 nm to 140 nm, as shown in Figure 2. All the products are single-phase ZIF-7 materials as characterized by powder X-ray diffraction (PXRD) (see Figure S2). Some hexagonal features become distinguishable in the case of ZIF-7@PEI-3#. PEI has a high density of amino groups, therefore it can act as a base to deprotonate bim, allowing the quick generation of a large number of ZIF-7 nuclei at the early stage of crystallization, which is critical for the synthesis of nanocrystals.

The aspect ratio, that is, the ratio of the average crystal length to the average crystal width, is the most important factor in determining the CPO of the deposited films according to evolutionary selection (van der Drift growth) model. If the influence of solvent molecules is neglected, the aspect ratio of ZIF-7

[*] Prof. Y.-S. Li, H. Bux, Dr. A. Feldhoff, Prof. J. Caro
Institute of Physical Chemistry and Electrochemistry, and the
Laboratory for Nano and Quantum Engineering (LNQE)
in cooperation with the Center for Solid State Research
and New Materials
Leibniz University Hannover
Callinstrasse 3A, 30167 Hannover (Germany)
E-mail: leeys@dicp.ac.cn; armin.feldhoff@pci.uni-hannover.de
Prof. Y.-S. Li, G.-L. Li, Prof. W.-S. Yang
State Key Laboratory of Catalysis
Dalian Institute of Chemical Physics
Chinese Academy of Sciences
Zhong-Shan Road 457, 116023 Dalian (P. R. China)

DOI: 10.1002/adma.201000857

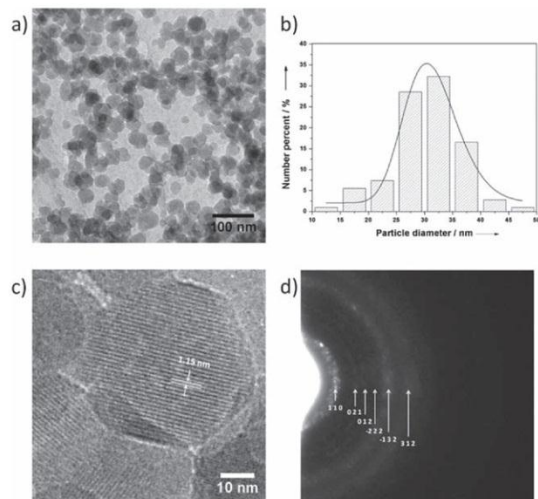


Figure 1. a) TEM bright-field image and b) particle size distribution of the ZIF-7 nanocrystals prepared by the excess ligand method. c) HRTEM image of the ZIF-7 nanocrystals, which shows a d -spacing of 1.15 nm for the (110) lattice plane. d) SAED pattern from a circular area 1.2 μm in diameter.

crystals is predicted to be close to 1 using the surface energy method (E_{SUR} , see Table S1), that is, equilibrium morphology. This low aspect ratio also accounts for the random orientation of the ZIF-7 membrane which was seeded grown from the

same synthesis system.^[2j,k] The growth rates of the low index faces were also analyzed by calculating the attachment energies (E_{att} , see Table S1) using the Hartman–Perdok method (periodic bond chain (PBC) theory).^[13] Among the low index planes, the {003} planes belong to kinked (K) faces, having the highest E_{att} , and therefore grow fastest; {110} and {101} planes belong to flat (F) faces, having the lowest E_{att} , and will be the most dominant faces in the final crystals. In the present study, we used ZnCl_2 instead of $\text{Zn}(\text{NO}_3)_2 \cdot 6\text{H}_2\text{O}$ as the zinc source. According to the hard soft acid base (HSAB) theory,^[14] both chloride and zinc are classified as “intermediate”, indicating a strong interaction between them. Therefore, the existence of chloride ions will have a great influence on the growth kinetics of ZIF-7 crystals, and result in an enlarged difference between the growth rates of {003} and {110}, {101} faces. In fact, a strong effect of anions (especially the halide anions) on the shape control of crystalline complexes or coordination polymers has been widely observed.^[15] All the ZIF-7 crystals synthesized with ZnCl_2 exhibited prismatic hexagonal shapes with high aspect ratios, whether microwave heating (Figures 3a,b) or conventional heating (Figures 3c,d) was used. Owing to the rapid and volumetric dielectric heating, the microwave-synthesized ZIF-7 crystals are much smaller than the ones synthesized with conventional heating, implying a higher nucleation rate in the former case. The sizes and aspect ratios of the ZIF-7 crystals can be adjusted by altering the amount of diethylamine (DEA) that is added as deprotonating agent. It is suspected that the distributions of the precursor species, such as the Zn-bim primary complexes, can be adjusted by control of the deprotonation degree of the linker (bim), and which in turn has an

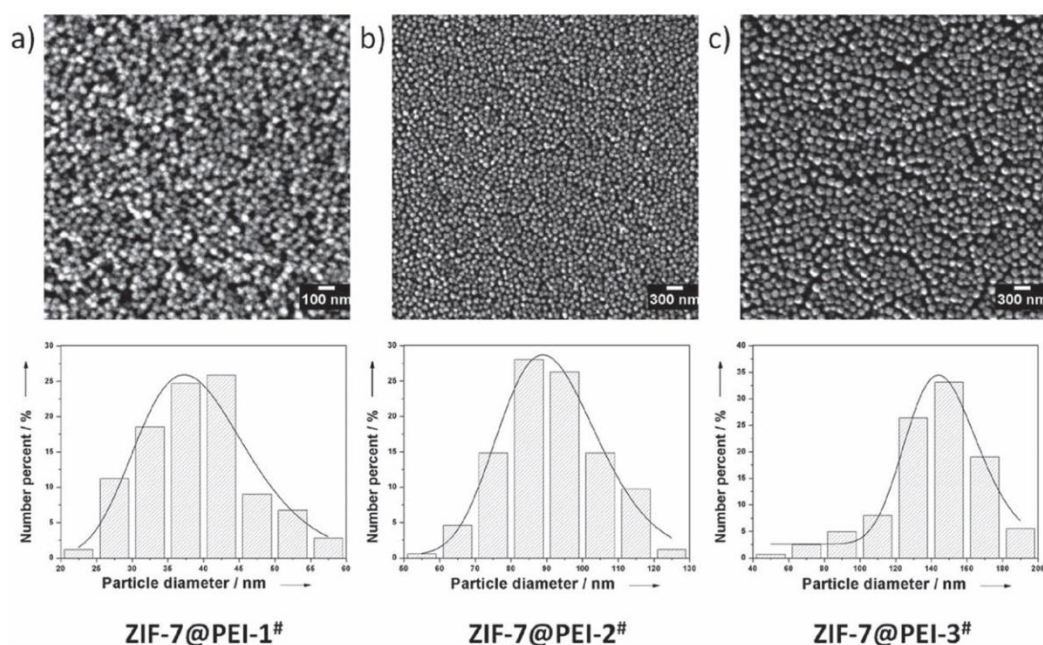


Figure 2. SEM images of the ZIF-7 nanoparticles synthesized by the “one-pot” method. Size distributions were determined by image analysis.

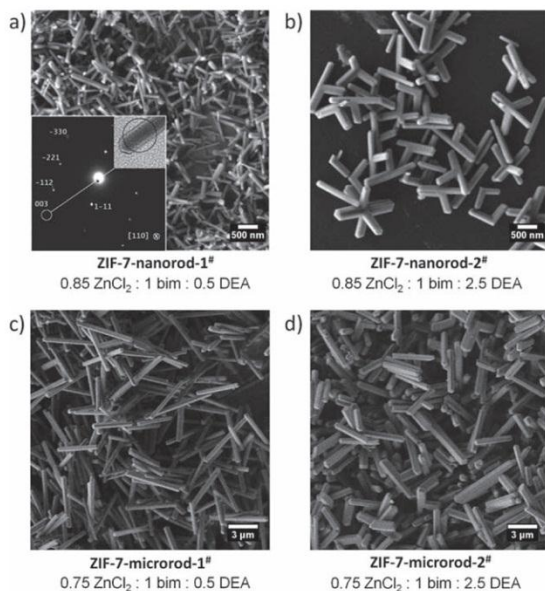


Figure 3. a–d) SEM images of the ZIF-7 nanorods and microrods. Inset in (a): Typical SAED pattern from a single nanorod (ZIF-7-nanorod-1[#]), verifying that the long axis of the rod-shaped crystal is parallel to the *c*-axis. The image descriptions give the molar ratios in the synthesis solutions.

influence on the growth kinetics. It is also notable that simultaneously parallel twins or intergrown twins can be observed in the case of microwave synthesis (Figures 3a,b). The reason for this high density of twins under microwave irradiation is still unknown. The SAED pattern (inset, Figure 3a) of ZIF-7-nanorod-1[#] demonstrates that the nanorod shown in the TEM bright-field image (inset, Figure 3a) is oriented almost along the [110] zone axis, and the longitudinal axis of the nanorod is along the *c*-axis.

In light of these morphology control studies, manipulation of the CPO of ZIF-7 membranes was attempted through evolutionary selection in a van der Drift-type growth. The nearly spherical shape of the seeding crystals (ZIF-7@PEI-2[#]) resulted in a randomly oriented seed layer (see Figure 2b and Figure 4d). Deviation from random orientation appeared after 45 min of microwave assisted secondary growth (Figure 4a). Nevertheless, the CPO distribution is broad and a very vague maximum develops at about 15°–45°. The *c*-out-of-plane orientation was significantly manifested with extended secondary growth time (Figure 4b,c); the CPO distribution became narrower and the maximum shifted to 10°. The membrane thickness increased nearly linearly with synthesis time, indicating the absence of further nucleation. The columnar grains growing from the seed layer became thicker when secondary growth was prolonged from 45 min to 225 min (Figures 4a–c). Unlike the microwave synthesis of ZIF-7 nanorods, twins were seldom observed during the microwave-assisted secondary growth, which indicates that in the former case the twinning might occur during the nucleation stage. The 030, 110, and 220 peaks are weak

for the oriented membranes, indicating that these planes are almost vertical to the substrate surface. Instead of a completely *c*-out-of-plane orientation, the ZIF-7 membranes showed an enhancement of the relative intensities of the 101, 202, 303, 012, 132, and 113 reflections with increasing secondary growth time according to the XRD characterizations (Figure 4d). It is notable that this oblique CPO should not be described as 101 CPO, but can be well explained by refined evolutionary selection in a van der Drift-type growth, taking into consideration both the fastest growth direction and the lateral growth component.^[16]

The *c*-out-of-plane oriented ZIF-7 membrane (Figure 4c) was tested for H₂/CO₂ equimolar gas mixture separation using the Wicke-Kallenbach technique with gas chromatographic control.^[2i,k] Similar to our previous report on randomly oriented ZIF-7 membrane, the oriented membrane (Figure 4c) exhibited an increase in selectivity with temperature. A H₂/CO₂ mixture separation factor of 8.4 was measured at 200 °C (see Figure S3), which is much larger than the Knudsen separation factor of 4.7. However, the H₂ permeance of the oriented membrane was one-tenth that of the randomly oriented membrane. This observation is understandable considering the anisotropic pore structure of ZIF-7 crystals. Neither the pyramidal termination {101} faces nor the prismatic {110} faces of the columnar crystals possess direct entrances (the hexagonal windows) for guest molecules (see Figure S1). This feature might result in so-called surface resistance and the grain boundary resistance associated with the mass transport through polycrystalline separating layers,^[17] which account for the lower permeance of the *c*-out-of-plane ZIF-7 membrane. Morphology-dependent gas adsorption of coordination polymers has been reported by different researchers.^[18] In the next study, we will attempt to correlate the membrane performances with both the kinetics and equilibrium of H₂ adsorption on the ZIF-7 crystals with different sizes and morphologies.

In summary, supramolecular assembly methods have been developed for the fabrication of highly oriented MOF thin films.^[8,9] A general and effective solvothermal route is introduced in the present work to tailor the crystal size and morphology of MOF materials and to manipulate the orientation of MOF films through evolutionary selection in a van der Drift-type growth originating from randomly oriented seed layers. A microstructure-related membrane performance of ZIF-7 membranes was observed, which has been extensively studied in the field of zeolite membranes,^[11] and should also be an important issue in the development of high-quality MOF membranes. Besides this, when targeting the applications of MOF thin films in catalytic coatings, chemical sensors, and related advanced nanodevices, it will also be of great significance and a big challenge to manipulate the channel orientation and grain morphology of the MOF films.

Experimental Section

Synthesis of ZIF-7 Nanoparticles: ZIF-7 nanoparticles were synthesized according to our previous report.^[2i] For the “one-pot” synthesis of ZIF-7@PEI colloids, a given amount (0.140 g, 0.140 g, and 0.360 g for ZIF-7@PEI-1[#], ZIF-7@PEI-2[#], and ZIF-7@PEI-3[#], respectively) of branched PEI (average *M_w* ~25000) was dissolved in DMF (200 mL). Zn(NO₃)₂·6H₂O (0.446 g) and benzimidazole (0.354 g) were directly mixed into this solution at room temperature. After being kept at room temperature for a certain period (5 h, 24 h, and 1 h for ZIF-7@PEI-1[#], ZIF-7@PEI-2[#], and

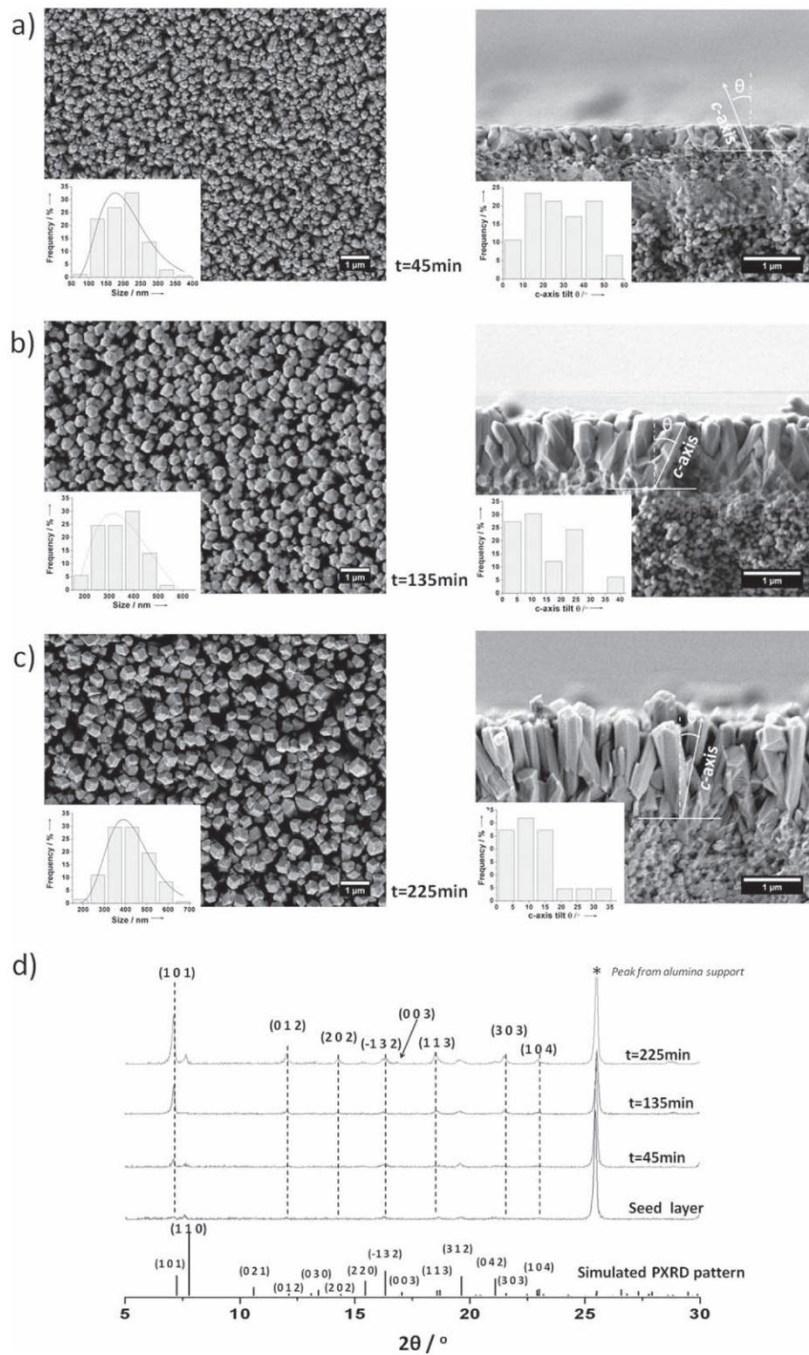


Figure 4. SEM top views and cross sections of the ZIF-7 membranes obtained after different times of microwave assisted secondary growth: a) 45 min, b) 135 min, and c) 225 min. d) the XRD patterns of the ZIF-7 membranes and the simulated PXR pattern of ZIF-7 crystal. Insets in the SEM top views give the distributions of the cross-sectional size of the columnar crystals, and the CPO distributions. The CPO is represented by the angle θ between *c*-axis and the substrate normal.

ZIF-7@PEI-3[#], respectively), the product was centrifugally concentrated to a volume of around 9 mL, containing around 2.5 wt% ZIF-7, assuming a yield of 50%.

Synthesis of ZIF-7 Nanorods and Microrods: DMF (30 mL) was added to a solid mixture of ZnCl₂ (0.295 g for nanorods or 0.265 g for microrods) and benzimidazole (0.310 g), and a given amount of diethylamine (0.093 g or 0.465 g) was added. The solvothermal synthesis was carried out in a microwave oven (Ethos 1, MLS) at 100 °C for 90 min (nanorods) or in an air oven at 130 °C for 24 h (microrods). The products were centrifuged and washed with ethanol.

Preparation of Oriented ZIF-7 Membranes: An asymmetric alumina disc (Inoceramic) was surface seeded by dip-coating in the ZIF-7@PEI-2[#] colloid for 20 s. For the secondary growth, 30 mL DMF was added to a solid mixture of ZnCl₂ (0.204 g) and benzimidazole (0.266 g), and diethylamine (0.170 g) was added. The clear solution was transferred into a poly(tetrafluoroethylene) (Teflon) autoclave in which the seeded support was placed vertically. Afterwards the autoclave was heated in a microwave oven (Ethos 1, MLS) at 100 °C for a certain period. After cooling down, the membrane was washed with methanol.

It should be noted that to guarantee a high reproducibility the anhydrous chemical reagents used for the synthesis should be handled carefully to avoid deliquescence or moisture sorption.

Experimental characterization techniques, including XRD, SEM, SAED, and HRTEM, as well as permeation measurements are described in detail in the Supporting Information.

Supporting Information

Supporting Information is available online from Wiley InterScience or from the authors.

Acknowledgements

Y.-S. Li thanks the Alexander von Humboldt Foundation for financial support and Prof. Wei-Xue Li for valuable discussion. DFG Priority Program 1362 “Porous Metal-Organic Frameworks” is thanked for financial support.

Received: March 10, 2010

Revised: March 30, 2010

Published online: June 8, 2010

- [1] a) S. Kitagawa, R. Kitaura, S. Noro, *Angew. Chem. Int. Ed.* **2004**, *43*, 2334; b) M. Yaghi, M. O’Keeffe, N. W. Ockwig, H. K. Chae, M. Eddaoudi, J. Kim, *Nature* **2003**, *423*, 705; c) G. Féry, *Chem. Soc. Rev.* **2008**, *37*, 191; d) S. L. James, *Chem. Soc. Rev.* **2003**, *32*, 276; e) J.-R. Li, R. J. Kuppler, H.-C. Zhou, *Chem. Soc. Rev.* **2009**, *38*, 1477; f) J. Lee, O. K. Farha, J. Roberts, K. A. Scheidt, S. T. Nguyen, J. T. Hupp, *Chem. Soc. Rev.* **2009**, *38*, 1450; g) X. D. Chen, C. Q. Wan, H. H. Y. Sung, I. D. Williams, T. C. W. Mak, *Chem. Eur. J.* **2009**, *15*, 6518; h) J. A. Hurd, R. Vaidhyanathan, V. Thangadurai, C. I. Ratcliffe, I. L. Moudrakovski, G. K. H. Shimizu, *Nat. Chem.* **2009**, *1*, 705.
- [2] a) D. Zacher, O. Shekhah, C. Wöll, R. A. Fischer, *Chem. Soc. Rev.* **2009**, *38*, 1418; b) M. Arnold, P. Kortunov, D. J. Jones, Y. Nedellec, J. Kärgen, J. Caro, *Eur. J. Inorg. Chem.* **2007**, *1*, 60; c) Y. Yoo, H. K. Jeong, *Chem. Commun.* **2008**, 2441; d) J. Gascon, S. Aguado, F. Kapteijn, *Microporous Mesoporous Mater.* **2008**, *113*, 132; e) Y. Liu, Z. Ng, E. A. Khan, H. K. Jeong, C. Ching, Z. P. Lai, *Microporous Mesoporous Mater.* **2009**, *118*, 296; f) Y. Yoo, Z.-P. Lai, H. K. Jeong, *Microporous Mesoporous Mater.* **2009**, *123*, 100; g) H. Guo, G. Zhu, I. J. Hewitt, S. L. Qiu, *J. Am. Chem. Soc.* **2009**, *131*, 1646; h) R. Ranjan, M. Tsapatsis, *Chem. Mater.* **2009**, *21*, 4920; i) H. Bux, F. Y. Liang, Y. S. Li, J. Cravillon, M. Wiebecke, J. Caro, *J. Am. Chem. Soc.* **2009**, *131*, 16000; j) Y. S. Li, F. Y. Liang, H. Bux, A. Feldhoff, W. S. Yang, J. Caro, *Angew. Chem. Int. Ed.* **2010**, *49*, 548; k) Y. S. Li, F. Y. Liang, H. Bux, W. S. Yang, J. Caro, *J. Membr. Sci.* **2010**, *354*, 48.
- [3] S. Hemes, T. Witte, T. Hitov, D. Zacher, S. Bahnmüller, G. Langstein, K. Huber, R. A. Fischer, *J. Am. Chem. Soc.* **2009**, *126*, 5324.
- [4] T. Tsuruoka, S. Furukawa, Y. Takashima, K. Yoshida, S. Isoda, S. Kitagawa, *Angew. Chem. Int. Ed.* **2009**, *48*, 4739.
- [5] Z. Ni, R. I. Masel, *J. Am. Chem. Soc.* **2006**, *128*, 12394.
- [6] Z. Q. Li, L. G. Qiu, T. Xu, Y. Wu, W. Wang, Z. Y. Wu, X. Jiang, *Mater. Lett.* **2009**, *63*, 78.
- [7] K. M. L. Taylor, W. J. Rieter, W. B. Lin, *J. Am. Chem. Soc.* **2008**, *130*, 14358.
- [8] a) E. Biemmi, C. Scherb, T. Bein, *J. Am. Chem. Soc.* **2007**, *129*, 8054; b) S. Hermes, F. Schröder, R. Chelmoski, C. Wöll, R. A. Fischer, *J. Am. Chem. Soc.* **2005**, *127*, 13744.
- [9] a) O. Shekhah, H. Wang, S. Kowarik, F. Schreiber, M. Paulus, M. Tolan, C. Sternemann, F. Evers, D. Zacher, R. A. Fischer, C. Wöll, *J. Am. Chem. Soc.* **2007**, *129*, 15118; b) O. Shekhah, H. Wang, T. Strunskus, P. Cyganik, D. Zacher, R. A. Fischer, C. Wöll, *Langmuir* **2006**, *23*, 7740.
- [10] a) X. C. Huang, J. P. Zhang, X. M. Chen, *Chin. Sci. Bull.* **2003**, *48*, 1531; b) K. S. Park, Z. Ni, A. P. Côté, J. Y. Choi, R. Huang, F. J. Uribe-Romo, H. K. Chae, M. O’Keeffe, O. M. Yaghi, *Proc. Natl. Acad. Sci. USA* **2006**, *103*, 10186.
- [11] a) Z. P. Lai, G. Bonilla, I. Diaz, J. G. Nery, K. Sujaoti, M. A. Amat, E. Kokkoli, O. Terasaki, R. W. Thompson, M. Tsapatsis, D. G. Vlachos, *Science* **2003**, *300*, 456; b) M. A. Snyder, M. Tsapatsis, *Angew. Chem. Int. Ed.* **2007**, *46*, 7560.
- [12] A. Van Der Drift, *Philips Res. Rep.* **1967**, *22*, 267.
- [13] P. Hartman, W. Perdok, *Acta Crystallogr.* **1955**, *8*, 521.
- [14] R. G. Pearson, *J. Am. Chem. Soc.* **1963**, *85*, 3533.
- [15] a) M. A. Withersby, A. J. Blake, N. R. Champness, P. Hubberstey, W. S. Li, M. Schröder, *Angew. Chem., Int. Ed.* **1997**, *36*, 2327; b) N. R. Brooks, A. J. Blake, N. R. Champness, J. W. Cunningham, P. Hubberstey, S. J. Teat, C. Wilson, M. Schröder, *J. Chem. Soc., Dalton Trans.* **2001**, 2530.
- [16] A. J. Bons, P. D. Bons, *Microporous Mesoporous Mater.* **2003**, *62*, 9.
- [17] a) D. A. Newsome, D. S. Sholl, *J. Phys. Chem. B* **2005**, *109*, 7237; b) A. Feldhoff, J. Caro, H. Jobic, J. Ollivier, C. B. Krause, P. Galvosas, J. Kärgen, *ChemPhysChem* **2009**, *10*, 2429.
- [18] a) H. J. Lee, W. Cho, S. Jung, M. Oh, *Adv. Mater.* **2008**, *21*, 674; b) T. Tsuruoka, S. Furukawa, Y. Takashima, K. Yoshida, S. Isoda, S. Kitagawa, *Angew. Chem. Int. Ed.* **2009**, *48*, 4739.

4 Understanding Mass Transfer through MOF Membranes on the Basis of ZIF-8

4.1 Summary

This section is dedicated to macroscopic, microscopic, and theoretical investigations to gain basic insight into the complex mechanism of mass transfer through ZIF-8 membranes. For the uptake studies from the gas phase by using infrared microscopy (IRM), large rhombic dodecahedral ZIF-8 single crystals were synthesized in methanol under solvothermal conditions by diffusion controlled in-situ mixing of the reactants (Section 4.2). The IRM investigations reported in Section 4.2, 4.3, and 4.4 shows the adsorption of molecules larger than the estimated fixed pore size of 3.4 Å, thus demonstrating the flexible nature of the pores (see section 1.2.6). Even more fascinating is the uptake behavior of the dipolar molecules, such as methanol and ethanol. The experimental sorption isotherms were found to exhibit S-shaped progressions, resembling IUPAC type-III or -V isotherms rather than the classical type-I isotherm, thus indicating strong guest-guest but weak host-guest interactions. Unusually, the transport diffusion coefficient for methanol was measured to run through a minimum at medium loadings and was even surpassed by the self-diffusion coefficient that was derived from tracer exchange experiments with deuterated methanol. Section 4.3 focuses on the unary and equimolar binary component mass transfer of methane/carbon dioxide as function of temperature through a ZIF-8 membrane. As a consequence of the framework flexibility, the separation factor was measured as 3.5, although a sharp cut-off separation would be expected from the estimated pore size for a rigid structure (see Section 1.2.6). In Section 4.4, ethane/ethene permeation experiments on a ZIF-8 membrane were performed as functions of pressure. The corresponding separation factor was calculated to be ~ 2 . The observations of the above-mentioned mass transfer experiments could be understood on the basis of IRM adsorption and diffusion data combined with the grand canonical Monte Carlo (GCMC) simulations. The low separation factors could be explained by opposed diffusion and adsorption selectivities. A simple, Fick-based model (see Section 1.3) could be used to estimate with sufficient accuracy the pure gas fluxes and mixed gas separation factors for the ZIF-8 membrane, potentially allowing a screening of MOF materials for suitable candidates.

4.2 Mass Transfer in a Nanoscale Material Enhanced by an Opposing Flux

C. Chmelik, H. Bux, J. Caro, L. Heinke, F. Hibbe, T. Titze, and J. Kärger, *Physical Review Letters* **2010**, *104*, 085902.

Mass Transfer in a Nanoscale Material Enhanced by an Opposing Flux

Christian Chmelik,^{1,*} Helge Bux,² Jürgen Caro,² Lars Heinke,^{1,3} Florian Hibbe,¹ Tobias Titze,¹ and Jörg Kärger¹
¹Leipzig University, Faculty of Physics and Geosciences, Linnéstrasse 5, D-04103 Leipzig, Germany
²Leibniz University Hannover, Institute of Physical Chemistry and Electrochemistry, Callinstrasse 3a, D-30167 Hannover, Germany
³Fritz-Haber-Institute of the Max-Planck-Society, Faradayweg 4-6, D-14195 Berlin, Germany
 (Received 16 November 2009; published 25 February 2010)

Diffusion is known to be quantified by measuring the rate of molecular fluxes in the direction of falling concentration. In contrast with intuition, considering methanol diffusion in a novel type of nanoporous material (MOF ZIF-8), this rate has now been found to be enhanced rather than slowed down by an opposing flux of labeled molecules. In terms of the key quantities of random particle movement, this result means that the self-diffusivity exceeds the transport diffusivity. It is rationalized by considering the strong intermolecular interaction and the dominating role of intercage hopping in mass transfer in the systems under study.

DOI: 10.1103/PhysRevLett.104.085902

PACS numbers: 66.30.Pa, 68.43.Jk

The elementary constituents of nature, notably atoms and molecules, undergo a perpetual random movement, referred to as diffusion [1]. Diffusion is essential for both the existence and functionality of living organisms [2] and for many technological processes including the production of electronic devices [3], plastics [4], and high-octane number gasoline [5]. Diffusion is quantified by the rate of molecular fluxes in the direction of falling concentration. IR microimaging of transient concentration profiles [6] provides a novel means for tracing such profiles [7] and is used, in this study, for the exploration of the diffusion properties of short-chain length hydrocarbons in a novel type of nanoporous material (MOF ZIF-8) [8–12].

Figure 1 provides a schematic of diffusion measurement in nanoporous solids [13,14]. Molecules are indicated by spheres, and the background symbolizes the accommodating pore network. First, we disregard the open spheres and consider the filled ones only. Their concentration $c(x)$ decreases from left to right. Following Fick's first law, the resulting flux

$$j = -D_T \frac{dc}{dx} \quad (1)$$

is proportional to the concentration gradient, with the transport diffusivity D_T as a factor of proportionality [14–16] and the concentration c referred to volume elements notably exceeding the unit cells (cavities in Fig. 1).

Now we include the “open” spheres into our consideration. They are assumed to be identical to the “filled” ones in their microdynamics, but to be distinguishable from them by the application of isotopes (“tracers”) or by spectroscopic techniques such as quasielastic neutron scattering [15] and nuclear magnetic resonance [16]. Designating flux and concentration of the open (“labeled”) molecules in the presence of their nonlabeled counterparts by an asterisk, Fick's first law now becomes

$$j^* = -D \frac{dc^*}{dx} \quad (2)$$

with D referred to as the coefficient of self- or tracer diffusion.

The relation between the self- and transport diffusivities is assessed by comparing the fluxes of the filled molecules of Fig. 1 without the open molecules (transport diffusion) and in their presence (self-diffusion). At sufficiently low concentrations, the molecules do not “feel” each other and the flux of the “filled” molecules remains totally unaffected by the presences of the “open” ones: self- and transport diffusion coincide. However, with increasing concentration, the molecules start to “compete” for the available space. Assuming identical concentration gradients and disregarding all other effects of molecular interaction (and, hence, of concentration dependence), molecular fluxes towards regions of smaller overall concentration (situation of Fig. 1 with the open spheres absent) are therefore expected to exceed those of labeled molecules (filled spheres in Fig. 1) under overall equilibrium

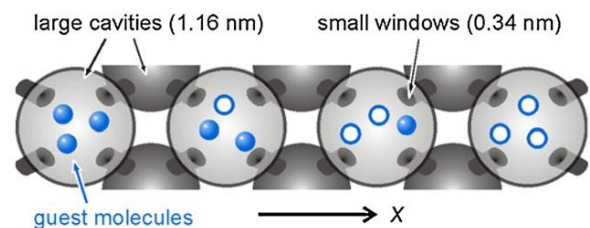


FIG. 1 (color online). Schematics of the experimental arrangement for diffusion studies in nanoporous solids: the small open and filled spheres in the (larger) spherical cages represent differently labeled but otherwise identical molecules. In *self-diffusion* measurements one considers the opposing (identical) fluxes of both types of molecules. Without the open molecules, the figure represents the situation for the measurement of *transport* diffusion. Here one considers molecular fluxes under the influence of an overall concentration gradient. The cage system symbolizes the structure of the nanoporous host system [MOF (metal-organic framework) of type ZIF-8] considered in this study.

(i.e., in the presence of the open spheres): finiteness of pore space accelerates transport diffusion in comparison with self-diffusion. To date, this effect of confinement is confirmed by all microscopic measurements of transport diffusivities in nanoporous solids which are found to be larger than or, at least, equal to the self-diffusivities [7,17–21].

It should be noted that the very first *microscopic* diffusion measurements where the self-diffusivities were found to notably exceed the transport diffusivities [22] did deviate from this pattern, in contradiction to the arguments above. However, those transport diffusivities resulted from *macroscopic* measurements which are often controlled by extracrystalline transport resistances [14]. These resistances lead to erroneously small diffusivities if not taken into account. Today, IR microimaging (IRM—see Ref. [6] and the supplementary material, Ref. [23]) allows recording the evolution of intracrystalline concentration profiles and, hence, microscopic measurements of self- and transport diffusivities under exactly the conditions implied by Fig. 1. They have thus become comparable with each other without any restriction.

Among the plethora of novel nanoporous materials appearing in recent years [24], metal-organic frameworks (MOFs) [8–12,25] are distinguished by their variety of potential applications, including environmental issues such as carbon dioxide capture and hydrogen storage. MOFs consist of precisely connected inorganic and organic moieties which may be largely varied, yielding an unprecedented variability in structure and composition. We performed our studies with MOF crystals of type ZIF-8. Their structure served as a background of Fig. 1. Mimicking the structure of zeolite sodalite, they consist of a cubic arrangement of cavities, octahedrally connected by narrow “windows,” with respective diameters of 1.16 and 0.34 nm (see [23] for more details). All experiments have been performed at room temperature, using methanol, ethane, and ethanol as probe molecules.

Figure 2 displays the concentration profiles of deuterated methanol during tracer exchange with methanol [Figs. 2(b) and 2(c)] and during uptake [Fig. 2(d)] on a MOF crystal of type ZIF-8 [Fig. 2(a)] along the segmented line of Fig. 2(b). The dodecahedral shape allows observation through two (rhombic) faces opposite to (and parallel with) each other. Figure 3(a) summarizes the self- and transport diffusivities calculated from molecular uptake over different pressure steps and from tracer exchange at different pressures (see [23] for details). As exemplified by the profiles of Figs. 2(c) and 2(d), over essentially the total range of concentrations, the self-diffusivities (i.e., the rate of tracer exchange) are notably higher than the transport diffusivities (and hence the rate of molecular uptake). This contradicts the intuitive expectation discussed above. Molecular diffusion is thus found to be not dominated anymore by finite-size effects of the pore space.

For a more fundamental discussion we recollect that, as a consequence of the different situation of measurement, there is no *a priori* means to correlate transport diffusivities and self-diffusivities except in the limit of very low concentrations [14]. Any correlation has rather to be based on model assumptions. Following Krishna [26–28], diffusion in nanopores may be treated within the frame of the Maxwell-Stefan model by equating the “generalized forces” stimulating the diffusion fluxes with the “drag” they are subject to. Thus, the drag to be overcome during self-diffusion (i.e., for opposing fluxes of differently labeled but otherwise identical molecules—see Fig. 1) is easily comprehended to consist of two contributions: one caused by the interaction with the pore walls, the other by collisions between the differently labeled molecules [27]. Representing these drags by the reciprocal values of corresponding diffusivities one may note a relation of the following structure [14,27]

$$1/D = 1/D_{T0} + \theta/\mathcal{D}_{AA}. \quad (3)$$

Here, D_{T0} is the “corrected” diffusivity, which is related to

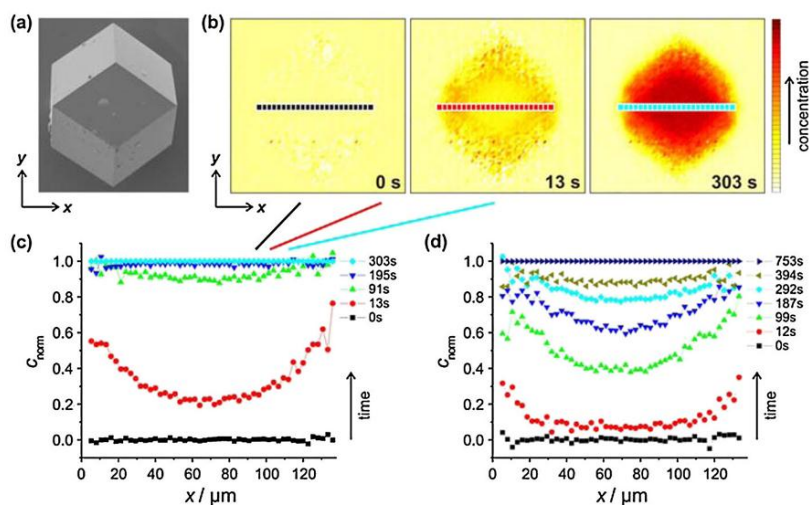


FIG. 2 (color online). Methanol in a ZIF-8 crystal recorded by IR microimaging. (a) SEM image of a dodecahedral ZIF-8 crystal. (b) Distribution of deuterated methanol before, during, and after tracer exchange with common proton-containing methanol. Crystal extension $x \times y$: $136 \times 199 \mu\text{m}^2$. (c) Transient concentration profiles plotted along the segmented line indicated in (b), i.e., along the x axis, during (tracer) exchange of methanol by deuterated methanol. (d) Analogous profiles recorded during uptake of deuterated methanol as a single component by the same crystal. Note the time scales: profile evolution in (d) proceeds remarkably slower than in (c). For data analysis, see section 3.5.3 of the supplementary material [23].

085902-2

D_T via

$$D_T = D_{T0} \frac{\partial \ln p}{\partial \ln c} \quad (4)$$

with $c(p)$ denoting the adsorption isotherm, i.e., guest concentration c in equilibrium with the surrounding pressure p . $\partial \ln p / \partial \ln c$ is referred to as the thermodynamic factor and considers the influence of deviations from ideality, i.e., from proportionality between guest concentration and gas pressure [15,28]. $1/D_{T0}$ represents the drag effects with the host [14,27]. D_{AA} is referred to as the mutual Maxwell-Stefan diffusivity. Its reciprocal value reflects the drag by counterdiffusion. Single-file diffusion, i.e., one-dimensional random walk of particles with hard-core interaction (which thus have to remain in their mutual arrangement [29,30]), represents the extreme case of infinitely large drag ($1/D_{AA} = \infty$) between counterdiffusing molecules. It is known to result in mean square displacements $\sim \sqrt{t}$ rather than $\sim t$, yielding vanishing self-diffusivities, in complete agreement with the outcome of Eq. (3).

In the limit of small guest concentrations $c \propto p$ and $\partial \ln c / \partial \ln p = 1$. This yields, with Eq. (3), equality of the self- and transport diffusivities, as argued already intuitively above, in the passage following Eq. (2). As shown in Fig. 3, in all our experiments D_T and D do indeed approach one another in the limit of θ approaching zero. As to our knowledge, never before has this limiting behavior been experimentally confirmed with similar precision.

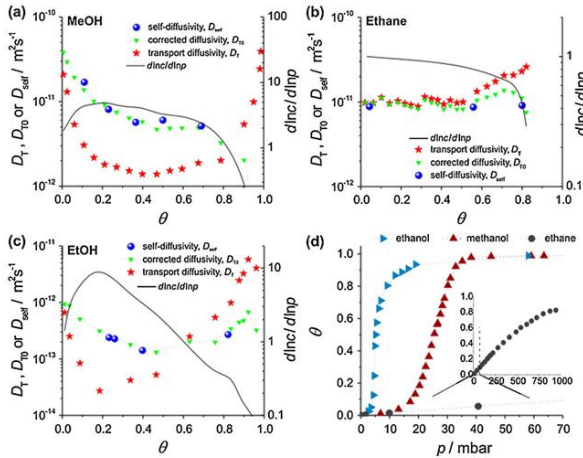


FIG. 3 (color online). Methanol, ethane, and ethanol in ZIF-8 at 298 K. Loading dependence of transport (D_T), corrected (D_{T0}), and self-diffusivity (D_{self}) of (a) methanol (MeOH), (b) ethane (C2), and (c) ethanol (EtOH). The inverse thermodynamic factor [obtained from (d)] is also shown. (d) Adsorption isotherms: the isotherms of methanol and ethanol exhibit a pronounced S shape (type III or V isotherm), whereas the isotherm of ethane shows a usual (“type I”) behavior. For all molecules the loading at saturated vapor pressure was normalized to reach $\theta = 1$.

For our further discussion we have to realize that the molecular diameters are comparable with the window sizes. The rate of molecular propagations is determined, therefore, by the passage through the windows rather than by drag effects with other molecules. The second term on the right-hand side of Eq. (3) is therefore expected to be negligibly small in comparison with the first one, so that the self- and corrected diffusivities should coincide. The experimental data of Fig. 3 are in excellent agreement with this prediction. The corrected diffusivities shown in Fig. 3 have been determined, via Eq. (4), by multiplying the transport diffusivities with the respective logarithmic derivatives of the adsorption isotherm $c(p)$ shown in Fig. 3(d). The derivatives are also displayed in Fig. 3.

The remarkable observation of self-diffusivities exceeding the transport diffusivities may thus be attributed exclusively to the thermodynamic factor, which, deviating from the common pattern, is found to be smaller rather than larger than 1. This is a consequence of the (towards the ordinate) concave shape of the adsorption isotherm. Such S-shaped isotherms (referred to as type-III or -V [24]) occur when guest-guest interactions notably exceed the guest-host interaction which, in the given case, may be easily attributed to the dipole moment of methanol. The pronounced guest-guest interaction is thus found to overcompensate the finiteness of the pore space, leading to self-diffusivities larger rather than smaller than the transport diffusivities.

Complementary diffusion measurements with ethane and ethanol [Figs. 3(b) and 3(c)] confirm our model considerations. Once again, the self- and corrected diffusivities coincide. This has to be expected since the passage through the windows between adjacent cages remains the rate-limiting process. For the nonpolar ethane, the adsorption isotherm is found to follow the conventional (Langmuir or type I) behavior. With the resulting thermodynamic factor close to 1, the transport diffusivity and the self- (or corrected) diffusivity are expected to coincide up to medium loadings which is in complete agreement with the experiment. With further increasing concentration, the thermodynamic factor increases [corresponding to the decrease of the factor $\partial \ln c / \partial \ln p$ in Eq. (4)]. Correspondingly, the transport diffusivities are also found to follow the conventional trend and exceed the self-diffusivities [Fig. 3(b)]. With ethanol [Fig. 3(c)], self-diffusion may even be found to be both faster and slower than transport diffusion. This peculiarity is associated with the fact that, over the considered concentration range, ethanol is subject to both of the so far considered types of guest interactions. For concentrations below $\theta \approx 0.6$ it resembles the behavior of methanol, yielding a concave isotherm with $\partial \ln c / \partial \ln p > 1$ and, correspondingly, self-diffusivities exceeding the transport diffusivities. For larger concentrations, by the dominating influence of the limited pore volume, everything is reversed.

It is noteworthy that, on the basis of these two governing mechanisms, namely, the effects of molecular confinement

and of molecular interaction, the experimentally observed behavior may be explained already intuitively with the schematics of Fig. 1: as soon as molecular interactions become relevant, the intermolecular attractive forces will counteract the “driving force” of the concentration gradient and reduce the flux to regions of lower guest content during transport diffusion, in comparison with self- or tracer diffusion (i.e., with uniform overall concentrations). Dominating effects of confinement, however, will make the molecules even more “willingly” propagate to regions of lower concentrations, thus enhancing the guest flux of transport diffusion in comparison with self- (or tracer) diffusion.

The observation that the rate of self-diffusion may notably surpass the rate of transport diffusion is evidence of the remarkable situation that, after pressure variation, equilibrium establishment occurs at much smaller rates than expected from the rate of molecular rearrangement, i.e., from the rate by which the guest molecules are able to exchange their positions under equilibrium. Similar behavior was recently detected during sorption hysteresis [16,31]. It was referred to the fact that system evolution during sorption hysteresis proceeds by the rearrangement of molecular ensembles rather than of (only) molecules. This mechanism is totally different, therefore, from those identified as the governing ones in the present study. Correspondingly, none of our present measurements exhibited hysteresis effects: molecular loading was a sole function of pressure, without any history dependence.

In the present study we profited from the recent advent of a powerful and most direct option to simultaneously measure self- and transport diffusion and of a novel nanoporous material of exquisite stability and homogeneity. The “anomalous” finding of self-diffusivities exceeding their counterparts of transport diffusion, refers to both fundamental research and technological application, including the message that tracer exchange rates (of, e.g., radioactive isotopes) may be dramatically underestimated if deduced from transient sorption experiments. The two peculiarities, namely, the dominating role of intercage hopping during molecular propagation and the strong guest-guest interaction, which gave rise to the observed phenomenon, may be expected to be fulfilled by quite a number of further systems. The new options of tuning the interrelation of self- and transport diffusion are far from being exhaustively explored by this study and will be, most likely, the focus of numerous ongoing studies in the fundamentals of adsorption and diffusion and in their technical exploitation.

Financial support by Deutsche Forschungsgemeinschaft (SPP 1362 “MOFs,” International Research Group “Diffusion in Zeolites,” Research Group “From Local Constraints to Macroscopic Transport” and International Research Training Group “Diffusion in Porous Materials”) is gratefully acknowledged. We are obliged to Randall Q. Snurr for stimulating discussions and critically reading our manuscript.

*Corresponding author.

chmelik@physik.uni-leipzig.de

- [1] P. Heitjans and J. Kärger, *Diffusion in Condensed Matter: Methods, Materials, Models* (Springer, Berlin, Heidelberg, 2005).
- [2] J. Howard, *Mechanics of Motor Proteins and the Cytoskeleton* (Sinauer Associates, Sunderland, 2001).
- [3] T. Y. Tan and U. Gösele, in *Diffusion in Condensed Matter: Methods, Materials, Models*, edited by P. Heitjans and J. Kärger (Springer Verlag, Berlin, Heidelberg, 2005), p. 165.
- [4] M. Doi and S. F. Edwards, *The Theory of Polymer Dynamics* (Oxford, New York, 1986).
- [5] D. Ruthven, in *Leipzig, Einstein, Diffusion*, edited by J. Kärger (Leipziger Universitätsverlag, Leipzig, 2007), p. 123.
- [6] L. Heinke *et al.*, Chem. Eng. Technol. **30**, 995 (2007).
- [7] L. Heinke *et al.*, Phys. Rev. Lett. **102**, 065901 (2009).
- [8] O. M. Yaghi *et al.*, Nature (London) **423**, 705 (2003).
- [9] H. Li *et al.*, Nature (London) **402**, 276 (1999).
- [10] L. Pan *et al.*, J. Am. Chem. Soc. **128**, 4180 (2006).
- [11] G. Férey *et al.*, Science **309**, 2040 (2005).
- [12] H. Wu, W. Zhou, and T. Yildirim, J. Am. Chem. Soc. **129**, 5314 (2007).
- [13] J. Kärger, *Leipzig, Einstein, Diffusion* (Leipziger Universitätsverlag, Leipzig, 2007).
- [14] D. M. Ruthven, in *Molecular Sieves—Science and Technology: Adsorption and Diffusion*, edited by H. G. Karge and J. Weitkamp (Springer, Berlin, Heidelberg, 2008), p. 1.
- [15] H. Jobic and D. Theodorou, Microporous Mesoporous Mater. **102**, 21 (2007).
- [16] R. Valiullin *et al.*, Nature (London) **443**, 965 (2006).
- [17] F. Salles *et al.*, Phys. Rev. Lett. **100**, 245901 (2008).
- [18] N. Rosenbach *et al.*, Angew. Chem., Int. Ed. **47**, 6611 (2008).
- [19] H. Jobic, in *Adsorption and Diffusion*, edited by H. G. Karge and J. Weitkamp (Springer, Berlin, Heidelberg, 2008), Vol. 7, p. 207.
- [20] H. Jobic, J. Kärger, and M. Bee, Phys. Rev. Lett. **82**, 4260 (1999).
- [21] D. Tzoulaki *et al.*, Angew. Chem. **48**, 3525 (2009).
- [22] J. Kärger and J. Caro, J. Chem. Soc., Faraday Trans. 1 **73**, 1363 (1977).
- [23] See supplementary material at <http://link.aps.org/supplemental/10.1103/PhysRevLett.104.085902> for more details about the material, IR microimaging, and the data analysis.
- [24] F. Schüth, K. S. W. Sing, and J. Weitkamp, *Handbook of Porous Solids* (Wiley-VCH, Weinheim, 2002).
- [25] M. J. Zaworotko, Nature Chem. Biol. **1**, 267 (2009).
- [26] F. J. Keil, R. Krishna, and M. O. Coppens, Rev. Chem. Eng. **16**, 71 (2000).
- [27] R. Krishna and D. Paschek, Phys. Chem. Chem. Phys. **4**, 1891 (2002).
- [28] D. M. Ruthven, S. Brandani, and M. Eic, in *Adsorption and Diffusion*, edited by H. G. Karge and J. Weitkamp (Springer, Berlin, Heidelberg, 2008), Vol. 7, p. 45.
- [29] K. Hahn, J. Kärger, and V. Kukla, Phys. Rev. Lett. **76**, 2762 (1996).
- [30] D. S. Sholl and K. A. Fichthorn, Phys. Rev. Lett. **79**, 3569 (1997).
- [31] S. Stapf, Nature Phys. **2**, 731 (2006).

4.2 Novel MOF-Membrane for Molecular Sieving Predicted by IR-Diffusion Studies and Molecular Modeling

H. Bux, C. Chmelik, J.M. van Baten, R. Krishna, and J. Caro, *Advanced Materials* **2010**, *22*, 4741-4743.

Novel MOF-Membrane for Molecular Sieving Predicted by IR-Diffusion Studies and Molecular Modeling

By Helge Bux,* Christian Chmelik, Jasper M. van Baten, Rajamani Krishna, and Jürgen Caro

Metal-organic frameworks (MOFs) are new microporous materials, which might revolutionize gas separation as molecular sieve membranes.^[1–3] The framework structure of these organic-inorganic coordination compounds is constructed of metal cations or clusters bridged by anionic organic linker molecules. Pore size and adsorption affinities can be altered by functionalizing the linker molecule, which is why MOFs are recommended as material for molecular sieving. From 1978 to 2010, the number of MOFs has grown exponentially,^[4] so that there is an extensive reservoir of new promising microporous membrane materials. However, MOF membrane preparation is usually associated with a high preparation effort and (possibly) high cost for rare linker molecules, while the separation performance is highly uncertain. One of the most important criteria for a molecular sieve membrane with reasonable performance is selectivity above the Knudsen separation. The Knudsen constant of a gas mixture is defined as the ratio of the reciprocal square root of the molar masses. Often pinholes and cracks of membranes as well as poorly performing microporous materials show this type of selectivity. Even though there have been increasing attempts to develop MOF-based molecular sieve membranes,^[5–10] only in recent publications membranes are reported, which perform better than the Knudsen separation.^[11–15] In view of the cost of development and the uncertainty of the performance of new MOFs, a computer-based screening and pre-selection method is desired.

Currently, there are several groups researching methods to predict selectivity of MOF membranes by theoretical approaches.^[16] Recently, in a pioneering work, Sholl et al. published a calculational screening method to estimate the H₂/CH₄ separation performance of several hundred MOF membranes.^[17] Their predictions agree remarkably well with permeation measurements of a MOF-5 membrane^[9,10] with pore apertures

of 8 Å^[1] which is larger than the kinetic diameter of CH₄ (3.8 Å). In contrast, recent measurements on narrow-pore ZIF-7 and ZIF-8 membranes^[18–20] show huge discrepancies with the predictions assuming rigid pore apertures.

As recently demonstrated, the permeation selectivity of a membrane can be estimated from the product of adsorption selectivity and diffusion selectivity.^[21] However, the experimental determination of gas mixture diffusivity and adsorption is still a great challenge. In consequence of the loading dependency of the diffusivity from guest–guest and guest–framework interactions, predictions by models based on pure species gas data can deviate from the gas mixture experiment. Hence, in this work we combine experimental measurements by IR microscopy (IRM) with theoretical studies by grand canonical Monte Carlo simulations (GCMC)^[22–24] to determine adsorption and diffusion data on ZIF-8. From these studies, we estimate the permeation selectivity of a ZIF-8 membrane as product of adsorption and diffusion selectivities and correlate the results with permeation data. As a member of the thermally and chemically stable family of zeolitic imidazolate frameworks (ZIFs),^[25] ZIF-8^[26–28] fulfills the basic stability requirement as membrane material. ZIF-8 crystallizes in a cubic sodalite type topology, where the large β -cages are connected by 6-membered ring windows. The sizes of the β -cages and the connecting 6-membered ring windows were estimated from XRD analysis to be 11.6 Å and 3.4 Å respectively.^[26] ZIF-8 is not only a promising membrane candidate, but also represents an appropriate model system for our adsorption and diffusion studies due to the simple, isotropic pore network. Aiming towards refining of natural gas, in this work we focus on separation of CO₂ (kinetic diameter 3.3 Å) from CH₄ (kinetic diameter 3.8 Å) in a binary, equimolar gas mixture.

GCMC simulations were performed for simulating the CH₄ and CO₂ adsorption equilibrium of pure compound gases and the equimolar binary mixture in ZIF-8 for different temperatures and pressures (see Supporting Information, Section S1). From these data, pure compound, and gas mixture sorption isotherms were obtained.

By employing time and space resolved IRM,^[29] we measured the sorption uptake/desorption of CO₂/CH₄ as a function of the partial pressures on large ZIF-8 single crystals, which were grown by a similar synthesis conditions as for the membrane preparation (Figure S2–1 in the Supporting Information). The GCMC studies were used to convert the IR adsorption data from arbitrary to absolute units. From the instantaneous sorption uptake/desorption profiles obtained by IRM, diffusion coefficients were determined by solving Fick's second law for the boundary conditions. For details of the method, see Supporting Information, Section S2.

[*] H. Bux, Prof. J. Caro
Institute of Physical Chemistry and Electrochemistry
Leibniz University Hannover
Callinstr. 3a, D-30167, Hannover (Germany)
E-mail: helge.bux@pci.uni-hannover.de
Dr. C. Chmelik
Faculty of Physics and Geosciences
Leipzig University
Linnéstr. 5, D-04103 Leipzig (Germany)
Dr. J. M. van Baten, Prof. R. Krishna
Van't Hoff Institute for Molecular Sciences
University of Amsterdam
Nieuwe Achtergracht 166
1018 WV Amsterdam (The Netherlands)

DOI: 10.1002/adma.201002066

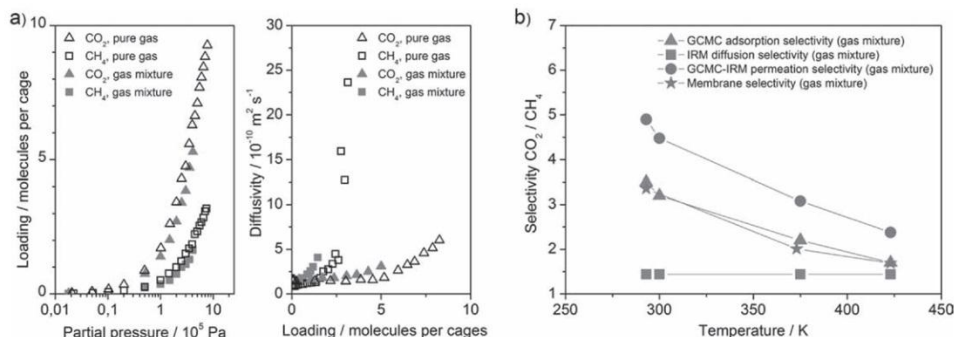


Figure 1. a) GCMC-IRM adsorption and diffusion results on ZIF-8 at room temperature. b) From GCMC-IRM studies estimated CO_2/CH_4 adsorption and diffusion selectivities as well as the mixture permeation selectivities of the ZIF-8 membrane shown in Figure 2a.

Figure 1a shows GCMC-IRM sorption isotherms and diffusivities for room temperature. The measured and simulated gas mixture sorption isotherms are in good agreement with the ideal adsorbed solution theory (IAST, Figure S2–4 in the Supporting Information). The IRM sorption studies also indicate a flexible nature of ZIF pore apertures, since CH_4 is adsorbed despite a kinetic diameter larger than the estimated crystallographic pore aperture size. Rather unexpected is the behavior of the diffusivity, since both the pure component and gas mixture diffusivities of CH_4 increase sharply with increasing loading, in contrast to CO_2 . Even with respect to the flexible pore apertures, a moderate energy barrier for a large molecule passing the pore window and, hence, a diffusion hindrance would be expected. The diffusion behavior of CH_4 might be correlated to its preferred localized adsorption near the pore apertures, as shown by GCMC in the Supporting Information, Section 1.4.

From the adsorption and diffusion data, the adsorption and diffusion selectivities have been calculated. Since for increasing partial pressures/loadings (i) the adsorption of CO_2 is favored over that of CH_4 , and (ii) the diffusion for CH_4 exceeds that of CO_2 , both selectivities behave contrarily (Figure S2–3 in the Supporting Information). The CO_2/CH_4 permeation selectivity of a ZIF-8 membrane, as product of adsorption and diffusion selectivity, is predicted to be 4.9 from an equimolar gas mixture at 1×10^5 Pa partial pressure difference at room temperature (Figure 1b). In contrary, a Knudsen mechanism would predict an opposed permeation selectivity of CH_4 above CO_2 of about 1.7.

For validating the predictions from GCMC-IRM, we measured the temperature dependent permeation of pure CO_2 and CH_4 gases and as mixture through a ZIF-8 membrane (for detailed preparation method, see Supporting Information, Section 3). An SEM image of the cross section of the continuous ZIF-8 layer on top of the titania support is shown in **Figure 2a**. The measurements were carried out by the Wicke–Kallenbach technique (Figure S3–2 in the Supporting Information) for 1×10^5 Pa partial pressure difference. From the permeances (Figure 2b, left axis), pure and mixture

gas selectivities (Figure 2b right axis) were calculated for different temperatures (see Supporting Information S3).

Both the CO_2/CH_4 pure and mixture gas selectivities at room temperature are about 3.5 and hence anti-Knudsen as predicted from GCMC-IRM studies. Although the predictions are based on a simple model, and the IRM data were obtained under ideal conditions on single crystals, the selectivity derived from the model is remarkably close to the selectivity of the ZIF-8 membrane (Figure 1b). For elevated temperatures, GCMC adsorption selectivity and membrane selectivity show almost coinciding trends. It is concluded that, therefore, permeation on the ZIF-8 membrane is adsorption controlled rather than diffusion controlled. In a good approximation the diffusion selectivity can be assumed constant over the narrow temperature range under study.

The slight overestimation of the GCMC-IRM permeation selectivity in respect to the membrane measurements can be explained by the non-ideal structure of the ZIF-8 membrane. In contrast to single crystals, the membrane layer is polycrystalline, where grain boundaries might contribute to an unknown mass transport.

In conclusion, we applied a combination of a theoretical (GCMC) and an experimental (IRM) method to estimate the CO_2/CH_4 permeation selectivity of a ZIF-8 molecular sieve membrane. The results fit the experimentally measured permeation selectivities of a recently developed ZIF-8 membrane remarkably well. As shown both in earlier works^[16,17] and this works, it is generally possible to predict the membrane selectivity,

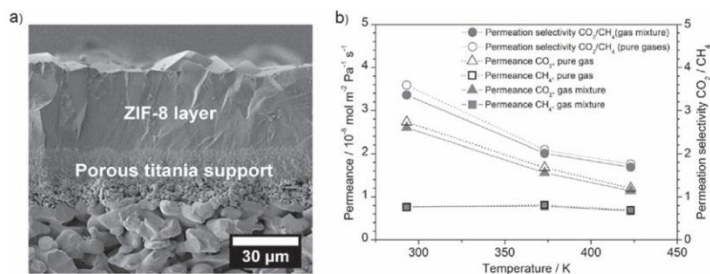


Figure 2. a) SEM image of the cross-section of the ZIF-8 membrane. b) Measured permeances of CO_2 and CH_4 as pure components and from their binary mixture as well as ideal and mixture permeation selectivities as a function of temperature.

either by experimental or theoretical approaches and, hence, screen porous materials for membrane applications, thus saving time and effort in R&D. Although there are similarities with other porous materials like zeolites, MOFs show unique features and behaviors. Although the pore aperture of ZIF-8 is estimated to be smaller than the diameter of CH₄, the larger molecule can pass through. A sharp molecular sieve separation is neither predicted from GCMC-IRM diffusivity data nor observed in the membrane permeation measurements. This findings might indicate the pore apertures are rather flexible than rigid. In consequence, models assuming rigid pores might show only limited accuracy in MOF membrane screening and, hence, should be evolved to take flexibility into consideration.

Experimental Section

Membrane synthesis and permeation measurements: A porous titania support was used in a microwave assisted solvothermal reaction of 2-methylimidazole (0.975 g), sodium formate (0.538 g) and zinc chloride (0.808 g) in methanol (80 ml). After 4 h at 100 °C, a dense layer of ZIF-8 formed on the surface. For detection in gas permeation experiments a HP Agilent 6890N gas chromatograph was used.

Infrared microscopy: The IR micro-imaging device used in this study consists of a spectrometer (Bruker Vertex 80 v) attached to an IR microscope (Bruker Hyperion 3000) equipped with a Focal Plane Array (FPA) detector. For measurements, several selected crystals were placed in an IR cell with IR transparent CaF₂ windows.

Grand Canonical Monte Carlo Simulations: The GCMC simulations were performed using the BIGMAC code developed by T.J.H. Vlucht (see Supporting Information, Section S2, Refs. [21–24]) as basis. The code was modified to handle rigid molecular structures and charges.

Scanning electron microscopy: The SEM image of the membrane cross section (Figure 2a) was taken on a JEOL JSM-6700F at 1 kV accelerating voltage, 5 µA current and a working distance of 15 mm.

Supporting Information

Detailed methods descriptions are available in Supporting Information. Supporting Information is available from the Wiley Online Library or from the author.

Acknowledgements

This work is part of DFG (Deutsche Forschungsgemeinschaft) Priority Program 1362 (Porous Metal-Organic Frameworks) organized by S. Kaskel. We gratefully acknowledge the financial support.

Received: June 4, 2010

Published online: September 2, 2010

- [1] O. M. Yaghi, M. O'Keeffe, N. W. Ockwig, H. K. Chae, M. Eddaoudi, J. Kim, *Nature* **2003**, 423, 705.
- [2] G. Férey, *Chem. Soc. Rev.* **2008**, 37, 191.
- [3] J.-R. Li, R. J. Kuppler, H.-C. Zhou, *Chem. Soc. Rev.* **2009**, 38, 1477.
- [4] O. M. Yaghi, J. R. Long, *Chem. Soc. Rev.* **2009**, 38, 1213.
- [5] D. Zacher, O. Shekha, C. Wöll, R. A. Fischer, *Chem. Soc. Rev.* **2009**, 38, 1418.
- [6] M. Arnold, P. Kortunov, D. J. Jones, Y. Nedellec, J. Kärger, J. Caro, *Eur. J. Inorg. Chem.* **2007**, 60.
- [7] Y. Yoo, H.-K. Jeong, *Chem. Commun.* **2008**, 2441.
- [8] J. Gascon, S. Aguado, F. Kapteijn, *Microporous Mesoporous Mater.* **2008**, 113, 132.
- [9] Y. Liu, Z. Ng, E. A. Khan, H.-K. Jeong, C.-B. Ching, Z. Lai, *Microporous Mesoporous Mater.* **2009**, 118, 296.
- [10] Y. Yoo, Z. Lai, H.-K. Jeong, *Microporous Mesoporous Mater.* **2009**, 123, 100.
- [11] H. Guo, G. Zhu, I. J. Hewitt, S. Qiu, *J. Am. Chem. Soc.* **2009**, 131, 1646.
- [12] R. Ranjan, M. Tsapatsis, *Chem. Mater.* **2009**, 21, 4920.
- [13] S. R. Venna, M. A. Carreon, *J. Am. Chem. Soc.* **2010**, 132, 76.
- [14] Y. Liu, E. Hu, E. A. Khan, Z. Lai, *J. Membr. Sci.* **2010**, 353, 36.
- [15] J. Gascon, F. Kapteijn, *Angew. Chem. Int. Ed.* **2010**, 49, 1530.
- [16] S. Keskin, J. Liu, R. B. Rankin, J. K. Johnson, D. S. Sholl, *Ind. Eng. Chem. Res.* **2009**, 48, 2355.
- [17] E. Haldoupis, S. Nair, D. S. Sholl, *J. Am. Chem. Soc.* **2010**, 132, 7528.
- [18] H. Bux, F.-Y. Liang, Y.-S. Li, J. Cravillon, M. Wiebcke, J. Caro, *J. Am. Chem. Soc.* **2009**, 131, 16000.
- [19] Y.-S. Li, F.-Y. Liang, H. Bux, W.-S. Yang, J. Caro, *J. Membr. Sci.* **2010**, 354, 48.
- [20] Y.-S. Li, F.-Y. Liang, H. Bux, A. Feldhoff, W.-S. Yang, J. Caro, *Angew. Chem. Int. Ed.* **2010**, 49, 548.
- [21] R. Krishna, *J. Phys. Chem. C* **2009**, 113, 19756.
- [22] R. Krishna, J. M. van Baten, *J. Membr. Sci.* **2010**, 360, 323.
- [23] R. Krishna, J. M. van Baten, *Chem. Eng. J.* **2007**, 133, 121.
- [24] R. Krishna, J. M. van Baten, *Sep. Purif. Technol.* **2007**, 55, 246.
- [25] A. Phan, C. J. Doonan, F. J. Uribe-Romo, C. B. Knobler, M. O'Keeffe, O. M. Yaghi, *Acc. Chem. Res.* **2010**, 43, 58.
- [26] K. S. Park, Z. Ni, A. P. Côté, J. Y. Choi, R. Huang, F. J. Uribe-Romo, H. K. Chae, M. O'Keeffe, O. M. Yaghi, *Proc. Natl. Acad. Sci. USA* **2006**, 103, 10186.
- [27] X.-C. Huang, Y.-Y. Lin, J.-P. Zhang, X.-M. Chen, *Angew. Chem. Int. Ed.* **2006**, 45, 1557.
- [28] J. Cravillon, S. Münzer, S.-J. Lohmeier, A. Feldhoff, K. Huber, M. Wiebcke, *Chem. Mater.* **2009**, 21, 1410.
- [29] C. Chmelik, H. Bux, J. Caro, L. Heinke, F. Hibbe, T. Titze, J. Kärger, *Phys. Rev. Lett.* **2010**, 104, 085902.

4.5 Ethene/Ethane Separation by the MOF Membrane ZIF-8: Molecular Correlation of Permeation, Adsorption, Diffusion

H. Bux, C. Chmelik, R. Krishna, and J. Caro, *Journal of Membrane Science* **2011**, 369, 284-289.



Ethene/ethane separation by the MOF membrane ZIF-8: Molecular correlation of permeation, adsorption, diffusion

Helge Bux^a, Christian Chmelik^b, Rajamani Krishna^c, Juergen Caro^{a,*}

^a Institute of Physical Chemistry and Electrochemistry, Leibniz University Hannover, Callinstr. 3A, D-30167 Hannover, Germany

^b Faculty of Physics and Geosciences, Leipzig University, Linnéstr. 5, D-04103 Leipzig, Germany

^c Van't Hoff Institute for Molecular Sciences, University of Amsterdam, Science Park 904, 1098 XH, Amsterdam, The Netherlands

ARTICLE INFO

Article history:

Received 27 September 2010

Received in revised form

29 November 2010

Accepted 2 December 2010

Available online 8 December 2010

Keywords:

MOF membrane

ZIF-8 membrane

Ethene/ethane separation

IR microscopy

GCMC simulations

ABSTRACT

The newly developed MOF membrane ZIF-8 separates an equimolar ethene/ethane mixture at room temperature for 1 and 6 bar feed pressure, respectively, with a selectivity of 2.8 and 2.4. Independent sorption uptake studies of an ethene/ethane mixture on a big ZIF-8 single crystal by IR microscopy detection show in combination with grand canonical Monte Carlo simulations that this moderate ethene selectivity of the ZIF-8 membrane can be explained by the interplay of a preferential ethane adsorption selectivity competing with a preferential ethene diffusion selectivity. This means, that ethane adsorbs stronger than ethene, but ethene diffuses faster and overcompensates the adsorption preference of ethane, resulting in a membrane permeation selectivity for ethene.

© 2010 Elsevier B.V. All rights reserved.

1. Introduction

The paraffin/olefin separation by cryogenic distillation is one of the most energy and cost intensive processes. Separation by adsorption is an energy-efficient alternative. Two concepts can be applied: (i) the preferential uptake of the olefin under equilibrium condition e.g. by Cu modified adsorbents and (ii) the kinetic based separation by different diffusion rates, which result in the extreme case to steric size exclusion.

As a new type of nanoporous materials, metal–organic frameworks (MOFs) have been examined inter alia in their olefin/paraffin separation performance by adsorption [1]. By chlorine or bromine functionalization of organic linker molecules, the pore openings of zeolitic imidazolate frameworks (ZIFs) could be fine-tuned. The modification resulted in different diffusion rates – propene is slightly smaller and hence is diffusing faster than propane – and allowed kinetic separation of the mixture [2]. In contrary, copper containing MOFs like Cu₃(BTC)₂ showed favored adsorption of i-butene above i-butane, allowing the separation of the binary mixture in packed bed adsorber [3]. For liquid C₅ paraffin/olefin mixtures, Cu₃(BTC)₂ shows a clear olefin selectivity as well [4].

Very recently, first MOF membranes with selectivities higher than the Knudsen selectivity have been developed [5–12]. In our recent works, we focused on the development of thermally stable and steam resistant ZIF membranes like ZIF-7 [13–15], ZIF-8 [16] and ZIF-22 [17]. Despite pioneering works in the field of computer modeling to predict separation behavior of MOF adsorbents [18] and membranes [19], the experimental separation factors often differ considerably from the predictions [20]. These deviations might be correlated to the framework flexibility of the MOFs.

The in situ study of sorption uptake/desorption of guest molecules on large MOF or zeolite crystals detected by IR microscopy (IRM) supported by theoretical studies by grand canonical Monte Carlo (GCMC) simulations appears to be a powerful tool for determining loading dependent transport diffusion coefficients under mixed gas conditions [20,21]. Using the well-known relationship “permeability = mobility × solubility” as a rough estimation, the membrane selectivity can be expressed as the product of a diffusion and adsorption selectivity [22]. Here, we study ethene/ethane separation on a supported ZIF-8 membrane and give a molecular interpretation of the adsorption and diffusion contributions from GCMC supported IRM (GCMC-IRM) studies on large ZIF-8 single crystals.

2. Experimental

As recently reported, continuous ZIF-8 layers can be grown as membrane on-top of porous titania supports [16]. However, the

* Corresponding author.

E-mail addresses: juergen.caro@pci.uni-hannover.de, caro@pci.uni-hannover.de (J. Caro).

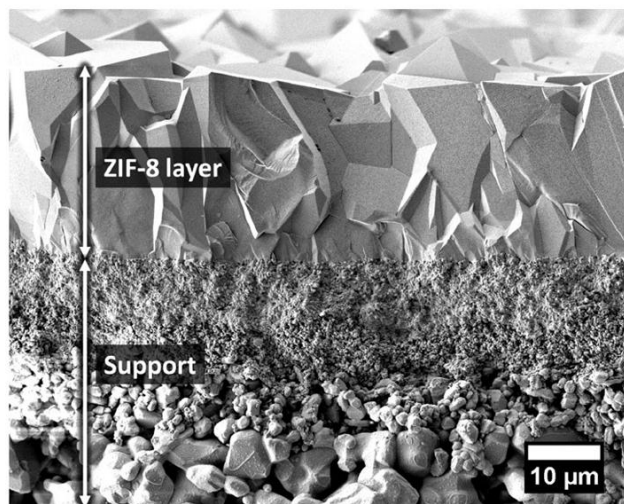


Fig. 1. Cross-section of the supported ZIF-8 membrane.

discoid titania supports of 1 mm thickness turned out to be too brittle for application at pressures difference across the membrane >3 bar. Hence, in this work a special composite support (Fraunhofer IKTS, Germany) consisting of a smooth titania layer on top of a mechanically strong alumina support was used for membrane preparation.

A typical synthesis solution contains 0.538 g (3.95 mmol) zinc chloride ($>99\%$ Merck), 0.486 g (5.92 mmol) 2-methylimidazole ($>99\%$, Sigma–Aldrich) and 0.268 g (3.95 mmol) sodium formate ($>99\%$, Sigma–Aldrich) solved by ultrasonic treatment in 80 ml methanol (99.9%, Roth). The solution together with the calcinated support was heated in a microwave oven for 4 h at 100°C forming ZIF-8 with the sum formula $\text{Zn}^{2+}(\text{mim}^-)_2$ ($\text{mim}^- = 2\text{-methylimidazolate}$). After synthesis the ZIF-8 membrane was cleaned with methanol and dried at room temperature overnight. For permeation measurements the membrane as shown in Fig. 1 is mounted in a permeation cell (cf. [16]).

Permeation measurements were carried out with two different methods. Pressure dependent permeation of an equimolar ethene/ethane gas mixture was measured by the Wicke–Kallenbach technique, permeate below the membrane was carried by a sweep gas to a gas chromatograph (HP Agilent 6890N with thermal conductivity detector), equipped with a HayeSep C packed column (15 ft, 1/8 in.). In addition, pure component permeation measurements were carried out at fixed feed pressure of 6 bar and atmospheric pressure (1 bar) on the permeate feed. The single gas permeation was performed without sweep gas and the flow rate was measured by bubble counter. Ideal and mixture separation factors were calculated following IUPAC definitions [23].

By IRM the time-resolved sorption uptake of the single gases and of the components of the binary mixture on a large ZIF-8 single crystal as shown in Fig. 3 is studied. The large ZIF-8 single crystals were grown similarly like the ZIF-8 membrane with the same stoichiometric ratio of the starting chemicals but using diffusion-controlled mixing of the chemicals. Zinc chloride and 2-methylimidazole dissolved in methanol were given into an autoclave. Sodium formate in methanol, however, was contained in a PTFE container inside this autoclave. Both solutions were able to counter-diffuse through an opening in the PTFE container of $\sim 1\text{ cm}^2$. After heating the autoclave to 140°C for 24 h in an air conditioned oven, large crystals could be collected from the inner of the PTFE container.

The gas uptake by the crystal is realized by only small step-changes of the gas phase to reduce the loading dependency of the diffusivity. The loading steps were less than 5% of the total loading for this temperature and, therefore, a constant diffusivity can be assumed for this “differential loading step”. By fitting the sorption uptake curves with appropriate solutions of Fick’s second law (spherical geometry, constant diffusivity, constant boundary conditions as given by Crank [24]), diffusion coefficients of ethane and ethene as pure component as well as in the mixture could be derived. The sorption uptake/desorption curves represent the relative loading averaged over the whole crystal under study as a function of time (for details see Refs. [20,21]). Furthermore, when measuring the time and space resolved IR absorbance, IRM provides the concentration profiles during ad/desorption as additional information. From these profiles (not shown here) we could state that sorption uptake/desorption is controlled by intracrystalline diffusion and not by surface barriers. The diffusivities thus determined without any corrections are called “transport diffusion coefficients D_T ” (D_T in Figs. 5 and 6). IRM makes it possible to distinguish the relative amounts of the adsorbed ethene and ethane as pure component as well as in mixture. Therefore, IRM allows the determination of transient adsorption and diffusion data for the components of a mixture. Using IRM, isotherms from individual crystals were obtained in relative units of the absorbance, and additional data are necessary for calibration in order to convert the arbitrary absorbance units into absolute amounts of adsorbed molecules. GCMC simulations have proven to be an accurate tool [25–27] for the prediction of adsorption isotherms. Very recently, we have shown GCMC data for ZIF-8 including pure component ethane and ethene [20]. For the calibration of IRM this GCMC data was used, by scaling the loading axis of the IRM sorption isotherm to the best visual fit with the GCMC sorption data.

3. Results and discussion

For the correlation of the permeation selectivity with the GCMC-IRM diffusion and adsorption data, it has to be ensured that only the ZIF-8 layer on-top of the macroporous support controls the permeation. Hence, a relative thick ZIF-8 layer of about $25\ \mu\text{m}$ has been prepared on top of the asymmetric titania support (Fig. 1). However, it should be noted that using secondary growth crystallization, ZIF-8 membrane layers with a few μm in thickness can be realized [13].

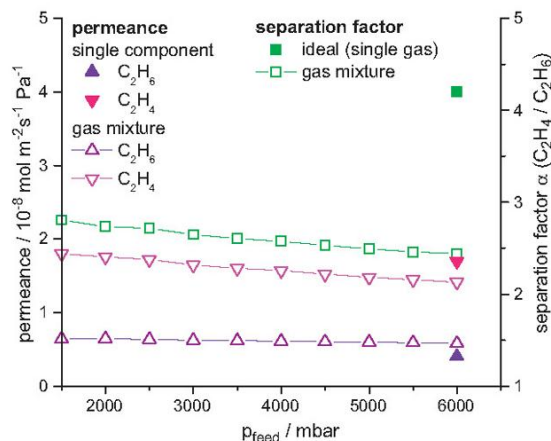


Fig. 2. Permeances and separation factors at $T=298$ K of the ZIF-8 membrane as shown in Fig. 1 for ethene and ethane as pure component as well as in equimolar mixture for different feed pressures. The mixture measurements were carried out by the Wicke–Kallenbach technique (partial pressure of the C_2 component ≈ 0 at the permeate side) while for the single gas measurement no sweep gas was used (partial pressure of the C_2 component ≈ 1 bar at the permeate side). For gas mixtures, the permeances were calculated at $T=293.15$ K and $p=1.013$ bar from the applied partial pressure difference (for equimolar composition this is 1/2 feed pressure) and for pure component from the total pressure difference ($\Delta p=5$ bar).

Fig. 2 shows the pressure dependency of the ethene/ethane separation factor α for the equimolar gas mixture measured by the Wicke–Kallenbach technique. A slight decrease in α from 2.8 to 2.4 with increasing feed gas pressure can be observed. In addition, from the pure component permeation measurements without sweep gas, an ideal separation factor of 4.2 as the ratio of the ethene flux ($1.24 \text{ ml cm}^{-2} \text{ min}^{-1}$) and the ethane flux ($0.29 \text{ ml cm}^{-2} \text{ min}^{-1}$) can be calculated. There are various reasons for the difference in separation efficiency between the pure component measurements and the mixed gas ones. First of all, both experiments were carried out under different conditions. Although for both experiments a total feed pressure of 6 bar was applied, for the mixture each gas only has a partial pressure of 3 bar. In the linear Henry region of the adsorption isotherm, equal pressure differences Δp result in equal concentration differences Δc in Fick's first law. Hence, in the Henry region experiments with and without sweep gas are generally comparable when Δp is equal. However, in our case both experiments were carried out significantly beyond this region. Hence, a direct relation of both experiments is not valid, since for both cases different Δc were present. In addition, the interplay of adsorption and diffusion effects such as mutual pore blocking as well as guest–guest interactions can highly influence the separation efficiency of gas mixtures in relation to the pure components.

The ethene selectivity of the ZIF-8 membrane can be understood in detail on the basis of the independent GCMC-IRM studies on a large ZIF-8 single crystal (Fig. 3). As shown in Fig. 4a, the pressure dependence of the amount adsorbed is captured well by both GCMC and IRM and, therefore, the adsorption data coincide, which make it possible to combine both techniques as explained in Section 2. Fig. 4b–d shows the increase in loading with increasing gas phase pressure for both single and mixed gas adsorption. Fig. 4b and c shows for the ethene/ethane mixtures of the compositions 1.9:1 and 1:1.5, that the mixture adsorption can be described very well by the ideal adsorption solution theory (IAST) [28]. The IAST data were calculated from an extended dual-site Langmuir fit of the single gas isotherms, the corresponding equation and parameters can be found in Table 1.

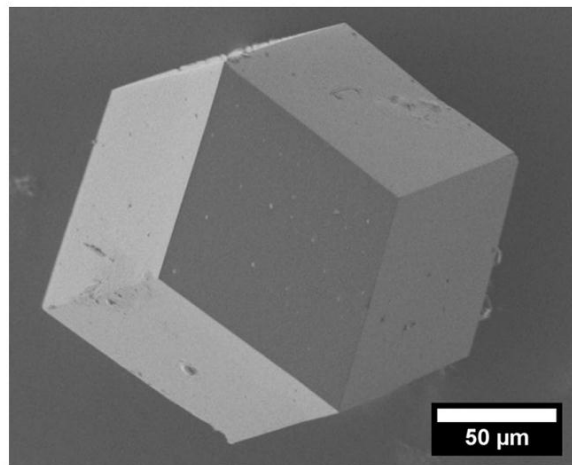


Fig. 3. Large ZIF-8 crystal with typical rhombic dodecahedral shape as used for IRM uptake/desorption measurements.

Table 1
Extended dual-site Langmuir model and parameters for ethene and ethane single gas isotherms (units: p in mbar, q in molecules/cage).

Equation	$q = A \frac{k_1 p^x}{1+k_1 p^x} + B \frac{k_2 p}{1+k_2 p}$
Parameter	$A=9, B=3, k_1=1.93004 \times 10^{-4}, k_2=1.95071 \times 10^{-6}, x=1.1100$
ethene	
Parameter	$A=8, B=3, k_1=4.46609 \times 10^{-4}, k_2=8.40412 \times 10^{-6}, x=1.1231$
ethane	

Although hard to see in pure component isotherms, ethane is notably stronger adsorbed compared to ethene. In mixture adsorption, the favored adsorption of ethane above ethene is much more obvious. For the ethene-rich mixture (ethene:ethane = 1.9:1) equal amounts of ethene and ethane are found in the adsorbed phase. For the ethene-poor mixture (ethene:ethane = 1:1.5) remarkably higher amounts of ethane are adsorbed. At first this finding of the preferential ethane adsorption in comparison with the ethene one seems surprising. However, for cation-free non-polar pore systems without specific interactions a thermodynamic selectivity for the adsorption of ethane over ethene is a common experimental finding¹ [29–31]. Whereas for the pure components, the amount of adsorbed ethane is only 5–10% higher than that of ethene (cf. Fig. 4a), for ethane-rich mixtures ethane is enriched by the factor of two in the adsorbed phase (cf. Fig. 4b). We cannot explain this experimental finding because of the quite similar Lennard–Jones parameters. Fig. 4d shows for the equimolar ethene/ethane mixture that the amount of adsorbed ethane is almost twice that of ethene. The pressure dependent adsorption selectivity can be obtained from the IAST model of an equimolar ethene/ethane mixture by the ratio of the adsorbed concentrations. For example, at a total pressure of 6 bar, 4.6 molecules ethane and 2.5 molecules ethene are adsorbed per cavity, giving a total loading of 7.1 C_2 molecules/cage and an ethene/ethane adsorption selectivity of around 0.5.

Fig. 5 shows the loading dependent transport diffusion coefficients D_T as obtained from the ethene and ethane sorption uptake curves from their binary mixtures. At least in the measured pressure range, ethene and ethane diffusivities are independent of the molar compositions of the gas mixtures i.e. the diffusivities for ethene and ethane from the mixtures of the ethene/ethane com-

¹ In a recent paper on ethane and ethane adsorption on ZIF-7, the preferred ethane adsorption is explained by a gate-opening mechanism [41].

4. Understanding Mass Transfer through MOF Membranes on the Basis of ZIF-8

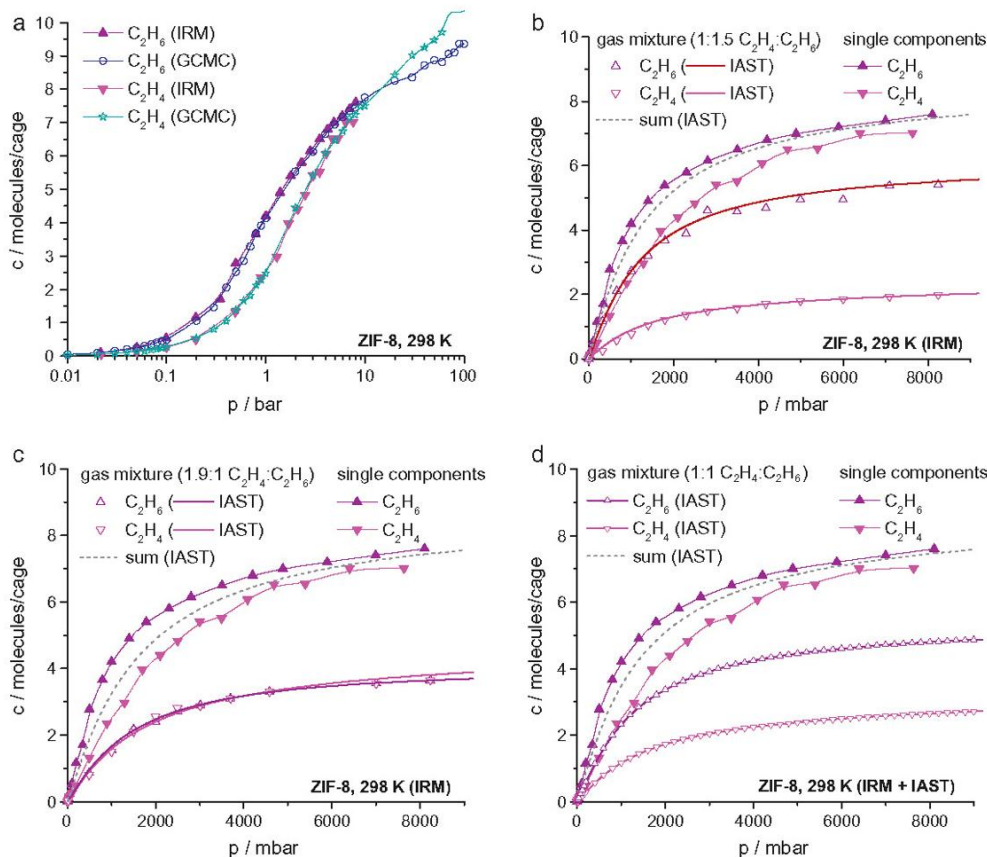


Fig. 4. (a) Ethene and ethane isotherms from pure component sorption uptake studies on a large ZIF-8 single crystal as shown in Fig. 3 were recorded by IRM at room temperature and calibrated by GCMC isotherms. (b and c) The GCMC-IRM mixture isotherms are compared with the partial ethene and ethane loadings for mixture adsorption computed by IAST (full lines). Composition of the ethene/ethane mixtures: 1:1.5 (b) and 1.9:1 (c). (d) The single gas adsorption data and the calculated partial loadings for a 1:1 ethene/ethane mixture as derived from IAST.

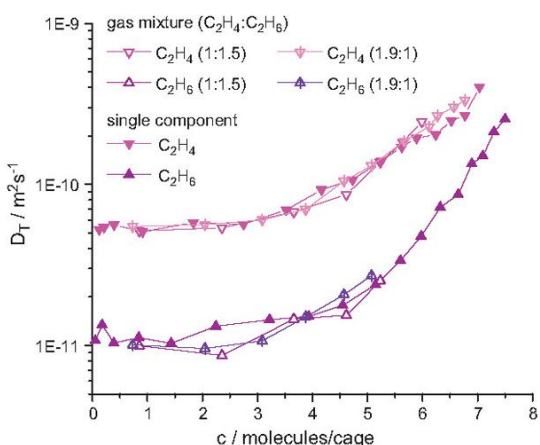


Fig. 5. Transport diffusion coefficients D_T at $T=298$ K of ethene and ethane from mixed gas sorption uptake experiments as derived from IRM on a big single crystal as shown in Fig. 3 for two ethene/ethane compositions of the gas mixture: 1:1.5 and 1.9:1 as function of total C_2 loading (sum of ethene + ethane molecules/cage). Calibration of the IRM by GCMC.

positions 1.9:1 and 1:1.5 coincide. In particular at low loadings, ethene diffuses around 5 times faster than ethane. However, with increasing loading ethane becomes more mobile. At a loading of 7.1 C_2 molecules/cage (partial loadings of 2.5 ethene and 4.6 ethane molecules/cage), the transport diffusion coefficient of ethene is found to be 2.7 times higher than that of the ethane. Multiplying the ethene/ethane adsorption selectivity (0.5) and diffusion selectivity (2.7), a total membrane selectivity of 1.4 is predicted for the ethene/ethane separation on a ZIF-8 membrane. This somewhat underestimates the measured ethene/ethane separation factor of 2.4 for an equimolar mixture at 6 bar (cf. Fig. 2). The derivation might be – at least partially – due to the highly simplified model, based on the Fick's first law assuming a constant diffusion coefficient and a linear concentration gradient. While assuming a linear concentration gradient might be appropriate, the diffusion coefficients however highly depend on loading (Fig. 5). It should be noted that the diffusion selectivity of ZIF-8 can be obtained as well exclusively by simulations as shown for ZIF-8 in comparison to the 8-ring window zeolites LTA, CHA, DDR [32] (Fig. 6).

In Fig. 7, some approximations are shown which account for the loading dependency of the diffusion coefficients in a rather simple way. Approach 1 refers to the above mentioned calculation method of choosing diffusion coefficient on the feed side of the membrane. In approach 2, we used the averaged loading at the feed and permeate side to determine the diffusion coefficient. While approach 1 leads to a slight underestimation, approach 2 slightly overestimates

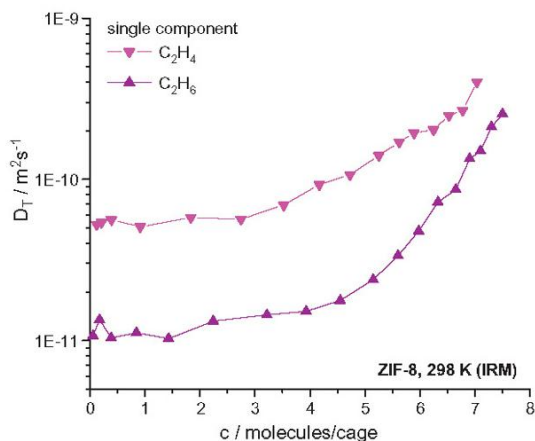


Fig. 6. Transport diffusion coefficients D_T at $T=298$ K as derived from sorption uptake experiments of the single gases ethene and ethane on a large ZIF-8 single crystal as shown in Fig. 3 with IRM detection. The relationship between loading and gas pressure follows from Fig. 4. Calibration of the IRM by GCMC.

the separation factor at higher loadings. For both approaches, the reason for the deviation is the sudden increase in the ethane and ethane diffusivities at a loading of around four C_2 molecules/cage. In contrast, the ethene/ethane adsorption ratio (adsorption selectivity) remains almost constant over the whole pressure range. For approach 1, this leads to a rapid drop in ethene/ethane separation factor, since the diffusivity of ethane increases somewhat faster with increasing loading as the diffusivity of ethene. The averaged concentration, used in approach 2, stays below the concentration of four C_2 molecules/cage and, hence, does not include the diffusivity increase at this concentration. This approach predicts a nearly constant separation factor. Apparently, both approximations fail in describing the real situation accurately. In a third approach, the averaged diffusion selectivity calculated from the diffusion selectivity at the feed and permeate side is used, which seems to fit quite good with the experiment. Although the decrease in diffusion selectivity on the feed side at high pressure is included, due to the

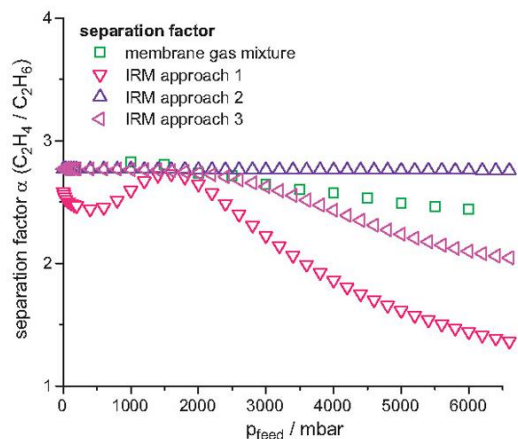


Fig. 7. Comparison of different simple approaches accounting in the loading dependency of the diffusion coefficient. Approach 1 is calculated using the diffusion coefficients D_T derived from the loading on the feed side of the ZIF-8 membrane. In approach 2, the averaged loadings across the membrane were used to determine the diffusion coefficients. For approach 3, an averaged selectivity was calculated by forming the ratio of the feed side selectivity (high loadings) and the permeate side selectivity (low loadings).

averaging with the constant diffusion selectivity of the permeate side, the drop in separation factor it is less rapid. This well working approach of a diffusivity at the average concentration similar to the one of Crank [24], who suggested to use an average diffusivity over the relevant range of concentration.

In addition to the interpretation and correlation of the mixture behavior so far discussed in this paper, the single component permeances can be predicted with sufficient accuracy from the GCMC-IRM single gas adsorption and diffusion data. In single gas permeation, ethene and ethane fluxes of $1.24 \text{ ml cm}^{-2} \text{ min}^{-1}$ and $0.29 \text{ ml cm}^{-2} \text{ min}^{-1}$ have been measured at room temperature for pressure differences of 5 bar (6 bar on the feed and 1 bar on the permeate side). Following Fick's first law with $j_i = -D_i \text{ grad } c_i$ the fluxes j_i of ethene and ethane through the membrane can be roughly estimated from the single gas GCMC-IRM data and compared with the above permeation measurements. The concentration gradient $\text{grad } c_i$ is approximated by the concentration difference Δc_i between the loadings of the ZIF-8 on the feed side at 6 bar and on the permeate side at 1 bar divided by the membrane thickness of $25 \mu\text{m}$ and assuming a u.c. volume of 4905.3 \AA^3 [20] or 4900 \AA^3 [33].

From Fig. 4, the concentration differences Δc_i between the ethene and ethane loading under aforementioned conditions are 4.2 and 2.9 molecules/cage,² respectively. Assuming an average loading of 4.6 molecules ethene/cage and 5.7 molecules ethane/cage, pure component diffusivities D_i of $1 \times 10^{-10} \text{ m}^2 \text{ s}^{-1}$ for ethene and $3.9 \times 10^{-11} \text{ m}^2 \text{ s}^{-1}$ for ethane are obtained from the loading dependency of diffusivity in Fig. 6. With this approximation, we estimate an ethene flux of $1.70 \text{ ml cm}^{-2} \text{ min}^{-1}$ and an ethane flux of $0.46 \text{ ml cm}^{-2} \text{ min}^{-1}$ which are near to the measured data.

This quite consistent picture of C_2 adsorption and diffusion in ZIF-8 single crystals and through membranes derived from membrane permeation, IRM adsorption/desorption and GCMC calculations is rather surprising. Similar correlations for zeolite membranes but using much more qualified models predicted much higher membrane fluxes than really measured e.g. using the Maxwell–Stefan-based models for silicalite-1 membranes [34,35] and for DDR membranes [36]. One reason for the fact that our simple approach works well might be that the ZIF-8 membrane layer shown in Fig. 1 consists of larger crystals with a low contribution of mass transport via grain boundaries in comparison with zeolite membranes. From the time and space resolved concentration profiles (not shown here) it can be concluded that sorption uptake/desorption is controlled by intracrystalline diffusion rather than by a surface transport resistance caused by an amorphous surface layer as it was found for Zn(tbip) – as a less stable MOF structure towards chemical degradation in comparison to ZIF-8 [37,38]. In another recent study on large FAU “single” crystals it was found that internal twin planes running through the crystal can reduce the translational mobility [39].

4. Conclusions

Membrane selectivities can be predicted with sufficient accuracy as the product of adsorption and diffusion selectivity. Both can be obtained from sorption uptake experiments on large single crystals by IR microscopy. We demonstrated this procedure for the ethene separation from an equimolar ethene/ethane mixture for different feed pressures at room temperature. At 6 bar feed pressure, the product of the ethene/ethane adsorption selectivity (0.5) and diffusion selectivity (2.7) gives an estimated permeation selectivity of 1.4 which is near to the measured ethene/ethane selectivity of 2.4. We ascribe this underestimation mainly to the assumption

² u.c. corresponds to 2 cages (cf. [20,33]).

of constant diffusion coefficients in the simple model. However, using averaged loading to determine diffusion coefficients or by calculating the averaged selectivity of feed and permeate side, the underestimation could be compensated. Furthermore, based on the diffusion coefficients and loadings derived from sorption uptake studies with IR detection, the single gas fluxes of ethene and ethane could be predicted with sufficient accuracy following Fick's first law. The good agreement might indicate that in the case of ZIF-8 inner transport barriers, like crystal defects and grain boundaries, as well as outer barriers like surface resistances, only slightly influence the macroscopic mass transport through the membrane. The preferential ethene diffusion competes with the preferential ethane adsorption thus reducing the ethene selectivity of the ZIF-8 membrane. The phenomena of opposed diffusion and adsorption selectivities might however be resolved by the very unique hybrid organic–inorganic character of ZIFs or MOFs in general. Functionalization of linker molecules – even post-synthesis [40] – might allow controlling interactions with olefins to improve the ethene/ethane adsorption selectivity of ZIFs.

Acknowledgements

This work is part of the DFG Priority Program SPP 1362 “Porous Metal–Organic Frameworks”, organized by S. Kaskel. The financial support is gratefully acknowledged.

References

- [1] J.-R. Li, R.J. Kuppler, H.-C. Zhou, Selective gas adsorption and separation in metal–organic frameworks, *Chem. Soc. Rev.* 38 (2009) 1477–1504.
- [2] K. Li, D.H. Olson, J. Seidel, T.J. Emge, H. Gong, H. Zeng, J. Li, Zeolitic imidazolate frameworks for kinetic separation of propane and propene, *J. Am. Chem. Soc.* 131 (2009) 10368–10369.
- [3] M. Hartmann, S. Kunz, D. Himsl, O. Tangermann, S. Ernst, A. Wagner, Adsorptive separation of isobutene and isobutane on $\text{Cu}_2(\text{BTC})_2$, *Langmuir* 24 (2008) 8634–8642.
- [4] M. Maes, L. Alaerts, F. Vermoortele, R. Ameloot, S. Couck, V. Finsy, J.F.M. Denayer, D.E. De Vos, Separation of C_5 -hydrocarbons on microporous materials: complementary performance of MOFs and zeolites, *J. Am. Chem. Soc.* 132 (2010) 2284–2292.
- [5] H. Guo, G. Zhu, I.J. Hewitt, S. Qiu, “Twin copper source” growth of metal–organic framework membrane: $\text{Cu}_2(\text{BTC})_2$ with high permeability and selectivity for recycling H_2 , *J. Am. Chem. Soc.* 131 (2009) 1646–1647.
- [6] R. Ranjan, M. Tsapatsis, Microporous metal organic framework membrane on porous support using the seeded growth method, *Chem. Mater.* 21 (2009) 4920–4924.
- [7] Y. Liu, E. Hu, E.A. Khan, Z. Lai, Synthesis and characterization of ZIF-69 membranes and separation for CO_2/CO mixture, *J. Membr. Sci.* 353 (2010) 36–40.
- [8] S.R. Venna, M.A. Carreon, Highly permeable zeolite imidazolate framework-8 membranes for CO_2/CH_4 separation, *J. Am. Chem. Soc.* 132 (2010) 76–78.
- [9] J. Gascon, F. Kapteijn, Metal–organic framework membranes–high potential, bright future? *Angew. Chem. Int. Ed.* 49 (2010) 1530–1532.
- [10] M.C. McCarthy, V. Varela-Guerrero, G.V. Barnett, H.-K. Jeong, Synthesis of zeolitic imidazolate framework films and membranes with controlled microstructures, *Langmuir* 26 (2010) 14636–14641.
- [11] V.V. Guerrero, Y. Yoo, M.C. McCarthy, H.-K. Jeong, *J. Mater. Chem.* 20 (2010) 3938–3943.
- [12] A. Huang, W. Dou, J. Caro, Steam-stable zeolitic imidazolate framework ZIF-90 membrane with hydrogen selectivity through covalent functionalization, *J. Am. Chem. Soc.* 132 (2010) 15562–15564.
- [13] Y. Li, F. Liang, H. Bux, A. Feldhoff, W. Yang, J. Caro, Molecular sieve membrane: supported metal–organic framework with high hydrogen selectivity, *Angew. Chem. Int. Ed.* 49 (2010) 548–551.
- [14] Y. Li, F. Liang, H. Bux, W. Yang, J. Caro, Zeolitic imidazolate framework ZIF-7 based molecular sieve membrane for hydrogen separation, *J. Membr. Sci.* 354 (2010) 48–54.
- [15] Y.-S. Li, H. Bux, A. Feldhoff, G.-L. Li, W.-S. Yang, J. Caro, Controllable synthesis of metal–organic frameworks: from MOF nanorods to oriented MOF membranes, *Adv. Mater.* 22 (2010) 3322–3326.
- [16] H. Bux, F. Liang, Y. Li, J. Cravillon, M. Wiebcke, J. Caro, Zeolitic imidazolate framework membrane with molecular sieve properties by microwave assisted solvothermal growth, *J. Am. Chem. Soc.* 131 (2009) 16000–16001.
- [17] A. Huang, H. Bux, F. Steinbach, J. Caro, Molecular sieve membrane with hydrogen permselectivity: ZIF-22 in LTA topology prepared with 3-aminopropyltriethoxysilane as covalent linker, *Angew. Chem. Int. Ed.* 49 (2010) 4958–4961.
- [18] S. Keskin, D.S. Sholl, Progress, Opportunities, and challenges for applying atomically detailed modeling to molecular adsorption and transport in metal–organic framework materials, *Ind. Eng. Chem. Res.* 48 (2009) 2355–2371.
- [19] E. Haldoupis, S. Nair, D.S. Sholl, Efficient calculation of diffusion limitations in metal organic framework materials: a tool for identifying materials for kinetic separations, *J. Am. Chem. Soc.* 132 (2010) 7528–7539.
- [20] H. Bux, C. Chmelik, J.M. van Baten, R. Krishna, J. Caro, Novel MOF-membrane for molecular sieving predicted by IR-diffusion studies and molecular modeling, *Adv. Mater.* 22 (2010) 4741–4743.
- [21] C. Chmelik, H. Bux, J. Caro, L. Heinke, F. Hibbe, T. Titze, J. Kärger, Mass transfer in a nanoscale material enhanced by an opposite flux, *Phys. Rev. Lett.* 104 (2010) 085902.
- [22] R. Krishna, Describing the diffusion of guest molecules inside porous structures, *J. Phys. Chem. C* 113 (2009) 19756–19781.
- [23] W.J. Koros, Y.H. Ma, T. Shimidzu, Terminology for membranes and membrane processes, *Pure Appl. Chem.* 68 (1996) 1479–1489.
- [24] J. Crank, *The Mathematics of Diffusion*, Oxford University Press, 1980, ISBN: 10:0198534116.
- [25] R. Krishna, J.M. van Baten, In silico screening of zeolite membranes for CO_2 capture, *J. Membr. Sci.* 360 (2010) 323–333.
- [26] R. Krishna, J.M. van Baten, Using molecular simulations for screening of zeolites for separation of CO_2/CH_4 mixtures, *Chem. Eng. J.* 133 (2007) 121–131.
- [27] R. Krishna, J.M. van Baten, Screening of zeolite adsorbents for separation of hexane isomers: a molecular simulation study, *Sep. Purif. Technol.* 55 (2007) 246–255.
- [28] A.L. Myers, J.M. Prausnitz, Thermodynamics of mixed-gas adsorption, *AIChE J.* 11 (1965) 121–127.
- [29] D.D. Do, H.D. Do, Cooperative and competitive adsorption of ethylene, ethane, nitrogen and argon on graphitized carbon black and in slit pores, *Adsorption* 11 (2005) 35–50.
- [30] M.C. Kroon, L.F. Vega, Selective paraffin removal from ethane/ethylene mixtures by adsorption into aluminum methylphosphonate- α : a molecular simulation study, *Langmuir* 25 (2009) 2148–2152.
- [31] D.H. Olsen, M.A. Cambor, L.A. Villaescusa, G.H. Kuehl, Light hydrocarbon sorption properties of pure silica SI-CHA and ITQ-3 and high silica ZSM-58, *Micropor. Mesopor. Mater.* 67 (2004) 27–33.
- [32] R. Krishna, J.M. Van Baten, A molecular dynamics investigation of the diffusion characteristics of cavity-type zeolites with 8-ring windows, *Micropor. Mesopor. Mater.* 137 (2011) 83–91.
- [33] S.A. Moggach, T.D. Bennett, A.K. Cheetham, The effect of pressure on ZIF-8: increasing pore size with pressure and the formation of a high-pressure phase at 1.47 GPa, *Angew. Chem. Int. Ed.* 48 (2009) 7087–7089.
- [34] J.M. van de Graaf, F. Kapteijn, J.A. Moulijn, Modeling permeation of binary mixtures through zeolite membranes, *AIChE J.* 45 (1999) 497–511.
- [35] J.M. van de Graaf, F. Kapteijn, J.A. Moulijn, Permeation of weakly adsorbing components through a silicalite-1 membrane, *Chem. Eng. Sci.* 54 (1999) 1081–1092.
- [36] J. van den Bergh, M. Mittelmanier-Hazeleger, F. Kapteijn, Modeling permeation of CO_2/CH_4 , N_2/CH_4 and CO_2/air mixtures across a DD3R zeolite membrane, *J. Phys. Chem. C* 114 (2010) 9379–9389.
- [37] C. Chmelik, F. Hibbe, D. Tzoulaki, L. Heinke, J. Caro, J. Li, J. Kärger, Exploring the nature of surface barriers on MOF Zn(tbp) by applying IR microscopy in high temporal and spatial resolution, *Micropor. Mesopor. Mater.* 129 (2010) 340–344.
- [38] D. Tzoulaki, L. Heinke, H. Lim, J. Li, D. Olson, J. Caro, R. Krishna, C. Chmelik, Assessing surface permeabilities from transient guest profiles in nanoporous host materials, *Angew. Chem. Int. Ed.* 48 (2009) 3525–3528.
- [39] A. Feldhoff, J. Caro, H. Jobic, J. Olivier, C.B. Krause, P. Galvosas, J. Kärger, Intracrystalline transport resistances in nanoporous zeolite X crystals, *PhysChemPhys* 10 (2009) 2429–2433.
- [40] W. Morris, C.J. Doonan, H. Furuikawa, R. Banerjee, O.M. Yaghi, Crystals as molecules: postsynthesis covalent functionalization of zeolitic imidazolate frameworks, *J. Am. Chem. Soc.* 130 (2008) 12626–12627.
- [41] C. Güçüyener, J. van den Bergh, J. Gascon, F. Kapteijn, Ethane/Ethene separation turned on its head: Selective ethane adsorption on the metal–organic framework ZIF-7 through a gate-opening mechanism, *J. Am. Chem. Soc.* 132 (2010) 17704–17706.

5 Closing Remarks

This work is dedicated to the preparation and characterization of microporous metal-organic framework (MOF) membranes, demonstrated by the examples of ZIF-7 and ZIF-8. As described in Section 1.1, molecular sieve membranes, although at the moment underrepresented in the membrane market, possess great potential to improve a broad range of industrial separation processes and can be used in membrane reactors for process intensification. Currently, and in the near future, membranes designed for clean environmental processes are increasingly important, for instance: the removal and subsequent storage of greenhouse gases, the carbon neutral production and concentration of bio fuels, and the large-scale hydrogen production as a clean energy source.

MOFs, with their remarkable properties, such as ultra-high inner surface areas, modifiable functionalization, customizable adsorption affinities, and directly accessible metal centers (see Section 1.2), are currently revolutionizing the field of porous materials and can introduce new aspects to molecular sieving. Although, not yet suitable for scale-up in the present form, this work demonstrates that the preparation of ZIF-7 and ZIF-8 membranes, at least on laboratory scale, is possible by different routes. The presented methods result in continuous, polycrystalline layers that are mechanically stabilized by macroporous, stiff ceramic supports. Oriented crystal growth relative to the support was observed for ZIF-8 after the secondary growth of previously seeded alumina supports (Section 2.2). The oriented growth for ZIF-7 was initially not observed for secondary growth, but took place after the modification of the synthesis recipe, which allowed the synthesis of crystals with a well-defined morphology (Section 2.3). Both processes could be consistently explained by the extended evolutionary selection model of van der Drift. The same model has been already be successfully used to explain the experimental findings of oriented growth of zeolite membranes, thus demonstrating that known principles from zeolite science are transferable to MOFs.

The unary and binary component mass transfer through MOF membranes was investigated in detail for ZIF-8. In this study, the presented membranes exhibit separation behaviors based on mass transport through micropores rather than exclusively through grain boundaries or other defects, such as cracks or pinholes. On the basis of the mass transfer studies, it was determined that the framework flexibility of MOFs is more relevant than originally expected. This flexibility is highly relevant and must be carefully considered for

5. Closing Remarks

possible applications that aim at sharp molecular sieving. Even though ZIF-7 and ZIF-8 are not subject to major breathing effects, which result in changes of the framework topology and related cage and pore geometries, both revealed only a “soft” micropore separation rather than a sharp cut-off in mass transport experiments of guests larger than the estimated pore sizes. This finding was explained by the apparently incorrect assumption of rigid pores and the consequently wrong estimation of pore sizes from the crystallographic structure derived from X-ray diffraction (XRD). XRD only provides averaged atomic positions and is not able to reflect the true rotational dynamics of the linkers in the framework.

The linker dynamics seem to limit the application of ZIF-8 in molecular sieving (e.g., carbon dioxide from methane). The corresponding, equimolar binary mass transfer experiment on a ZIF-8 membrane showed a separation of carbon dioxide from methane by a factor ~ 3.5 (at ambient temperature and 1 bar partial pressure difference, see Section 4.2). In theory, 100% separation of carbon dioxide from methane was expected because the kinetic diameter of methane (~ 3.8 Å) is much larger than the pore size of ZIF-8 (~ 3.4 Å; estimated for a rigid framework, see Section 1.2.6). The adsorption data from infrared microscopy (IRM) and grand canonical Monte Carlo (GCMC) simulations clearly show that methane and even larger molecules (e.g., propane) are adsorbed, thus demonstrating that the experimental finding on the ZIF-8 membrane was not an artifact. The corresponding diffusion coefficients, also obtained by IRM and GCMC, provided a detailed understanding of the experimentally observed separation. At low framework loadings, methane diffuses slightly slower than carbon dioxide but shows much higher transport diffusion coefficients with increasing loading than carbon dioxide. The preferred adsorption of carbon dioxide is opposed to the faster diffusion of methane, thus reducing the separation factor of the ZIF-8 membrane for carbon dioxide.

The finding of methane diffusing faster than carbon dioxide is in contrast to the expectation that the rate-limiting step in diffusion (which is the passing of the 6-membered ring pore windows) should at least exhibit a higher activation energy for the bulky methane compared to the slim carbon dioxide. Eventually, the GCMC simulations indicated a preferred adsorption of methane at sites near the pore windows. This possibly allows methane to jump more frequently through the pore windows, thus increasing its mobility within the framework. These findings demonstrate that insight on the molecular level is necessary to understand and optimize MOFs for molecular separation.

Although the very slow mass transfer of propane through the ZIF-8 membrane (Section 4.2) resulted in high separation factors > 300 for hydrogen in equimolar mixtures, this separation does not represent true molecular sieving because propane can still be adsorbed by ZIF-8. However, the experiment demonstrates that the structural concept of very large cavities (~ 11.6 Å in diameter for ZIF-8) connected by small windows can substantially reduce pore blocking in molecular sieving. Hence, from the perspective of molecular sieving, the focus should be to develop MOFs with large cavities that are connected by small pores.

In contrast to molecular sieving, another route used to separate molecules in a “soft” manner was demonstrated in Section 4.3. The ZIF-8 membrane showed the micropore separation of ethene from ethane by a factor of ~ 2 . As in the above-mentioned case of carbon dioxide and methane, the separation factor was interpreted as the result of opposing selectivities: ethene diffuses faster, whereas ethane was preferentially adsorbed. Nevertheless, this provides hope that MOFs can be fine-tuned to interact with π -bonds (e.g., by accessible metal centers or specific linker functionalization), and consequently show much better separation by improved adsorption of the olefin component.

As already mentioned in Section 1.1, gas separating membranes currently represent a relatively small, but growing field within the membrane market, whereas liquid separation dominates. Hence, the next reasonable step will be understanding the mass transfer from the liquid phase through MOF membranes (e.g., in laboratory scale pervaporation experiments). Microporous membranes in liquid phase separations operate at values close to the saturation range of the adsorption isotherm. Similar conditions can be achieved in gas separation (GS) only at high pressures. Hence, it can be expected that these completely different molecular situations result in a different, primarily adsorption-dominated behavior. Especially with respect to related problems of the framework flexibility in molecular sieving of gases through MOF membranes, adsorption-controlled mass transfer might result in much higher separation factors than observed in GS. By specific functionalization, 100% selectivity can potentially be reached by exclusive adsorption (e.g., of alcohols from water in hydrophobic MOF frameworks, such as ZIF-8).

5. Closing Remarks

Appendix

Publications Included in the Thesis

1. H. Bux*, F.Y. Liang, Y.S. Li, J. Cravillon, M. Wiebcke, and J. Caro, Zeolitic Imidazolate Framework Membrane with Molecular Sieving Properties by Microwave-Assisted Solvothermal Synthesis. *Journal of the American Chemical Society* **2009**, *131*, 16000-16001.
2. C. Chmelik*, H. Bux, J. Caro, L. Heinke, F. Hibbe, T. Titze, and J. Kärger, Mass Transfer in a Nanoscale Material Enhanced by an Opposing Flux. *Physical Review Letters* **2010**, *104*, 085902.
3. Y.S. Li*, F.Y. Liang, H. Bux, A. Feldhoff, W.S. Yang, and J. Caro, Molecular Sieve Membrane: Supported Metal-Organic Framework with High Hydrogen Selectivity. *Angewandte Chemie International Edition* **2010**, *49*, 548-551.
4. Y.S. Li*, H. Bux, A. Feldhoff, G.L. Li, W.S. Yang, and J. Caro, Controllable Synthesis of Metal-Organic Frameworks: From MOF Nanorods to Oriented MOF Membranes. *Advanced Materials* **2010**, *22*, 3322-3326.
5. H. Bux*, C. Chmelik, J.M. van Baten, R. Krishna, and J. Caro, Novel MOF-Membrane for Molecular Sieving Predicted by IR-Diffusion Studies and Molecular Modeling. *Advanced Materials* **2010**, *22*, 4741-4743.
6. H. Bux*, C. Chmelik, R. Krishna, and J. Caro, Ethene/Ethane Separation by the MOF Membrane ZIF-8: Molecular Correlation of Permeation, Adsorption, Diffusion. *Journal of Membrane Science* **2011**, *369*, 284-289.
7. H. Bux*, A. Feldhoff, J. Cravillon, M. Wiebcke, Y.S. Li, and J. Caro, Oriented Zeolitic Imidazolate Framework-8 Membrane with Sharp H₂/C₃H₈ Molecular Sieve Separation. *Chemistry of Materials* **2011**, *23*, 2262-2269.

Publications Not Included in the Thesis

8. Y.S. Li*, F.Y. Liang, H. Bux, W.S. Yang, and J. Caro, Zeolitic Imidazolate Framework ZIF-7 Based Molecular Sieve Membrane for Hydrogen Separation. *Journal of Membrane Science* **2010**, 354, 48-54.
9. A.S. Huang*, H. Bux, F. Steinbach, and J. Caro, Molecular-Sieve Membrane with Hydrogen Permselectivity: ZIF-22 in LTA Topology Prepared with 3-Aminopropyltriethoxysilane as Covalent Linker. *Angewandte Chemie International Edition* **2010**, 49, 4958-4961.
10. C. Chmelik*, H. Voß, H. Bux, and J. Caro, Adsorption and Diffusion - Basis for Molecular Understanding of Permeation through Molecular Sieve Membranes. *Chemie Ingenieur Technik* **2011**, 83, 104-112.
11. L. Hertäg, H. Bux, J. Caro, C. Chmelik, T. Remsungnen, M. Knauth*, and S. Fritzsche, Diffusion of CH₄ and H₂ in ZIF-8. *Journal of Membrane Science* **2011**, 15, 36-41.
12. C. Chmelik*, D. Freude, H. Bux, and J. Haase, Ethene/Ethane Mixture Diffusion in the MOF Sieve ZIF-8 Studied by MAS PFG NMR Diffusometry. *Microporous & Mesoporous Materials*, in Press, doi:10.1016/j.micromeso.2011.06.009.

Contributions to Conferences

1. H. Bux*, J. Cravillon, M. Wiebcke, and J. Caro, First Steps in the Preparation of ZIF-8 Membranes by Secondary Growth Crystallization, 21. *Deutsche Zeolith-Tagung*: 4th - 6th March **2009**, Kiel, poster presentation (George Kokotailo Award).
2. H. Bux*, F.Y. Liang, Y.S. Li, J. Cravillon, M. Wiebcke, C. Chmelik, J. Kärger, S. Fritzsche, and J. Caro, Transport through Zeolitic Imidazolate Frameworks: From Molecular Diffusion to Membrane Permeation. 22. *Deutsche Zeolith-Tagung*: 3rd - 5th March **2010**, Munich, oral presentation (George Kokotailo Award lecture).

-
3. T. Kirchner*, C. Chmelik, H. Bux, J. Caro, L. Heinke, F. Hibbe, T. Titze, and J. Kärger, Measuring Hindered Transport and Self-Diffusion by Means of Optical and NMR Methods. *22. Deutsche Zeolith-Tagung: 3rd - 5th March 2010*, Munich, poster presentation.
 4. C. Chmelik*, H. Bux, J. Caro, J.M. van Baten, R. Krishna, and J. Kärger, Characterizing Molecular Transport of CO₂ and CH₄ in MOF ZIF-8. *Deutsche Zeolith-Tagung: 3rd - 5th March 2010*, Munich, poster presentation.
 5. H. Bux*, F.Y. Liang, Y.S. Li, J. Cravillon, M. Wiebcke, and J. Caro, Zeolitic Imidazolate Framework Molecular Sieving Membrane, *5th International Zeolite Membrane Meeting: 23rd - 26th May 2010*, Loutraki, oral presentation.
 6. J. Cravillon*, F.Y. Liang, H. Bux, J. Caro, and M. Wiebcke, Room-Temperature Syntheses of Supported ZIF-8 Membranes. *5th International Zeolite Membrane Meeting: 23rd - 26th May 2010*, Loutraki, poster presentation.
 7. H. Bux, C. Chmelik, J. Kärger, S. Fritzsche, J. Cravillon, M. Wiebcke, R. Krishna, and J. Caro*, Adsorption, Diffusion and Membrane Permeation of the CO₂/CH₄ Mixture on the MOF Membrane of Type ZIF-8. *16th International Zeolite Conference: 4th - 9th July 2010*, Sorrento, poster presentation.
 8. J. Caro*, H. Bux, and Y.S. Li, Zeolite contra MOF Membranes - Loser and Winner. *16th International Zeolite Conference: 4th - 9th July 2010*, Sorrento, oral presentation.
 9. C. Chmelik*, H. Bux, J. Caro, L. Heinke, F. Hibbe, T. Titze, and J. Kärger, Faster by Opposing the Stream. *16th International Zeolite Conference: 4th - 9th July 2010*, Sorrento, oral presentation.
 10. H. Bux*, F.Y. Liang, Y.S. Li, J. Cravillon, M. Wiebcke, C. Chmelik, J. Kärger, L. Hertäg, S. Fritzsche, J. M. van Baten, R. Krishna, and J. Caro, Zeolitic Imidazolate Framework-8 Molecular Sieve Membrane: From Molecular Modelling to Membrane Permeation. *MOF2010 - Metal-Organic Frameworks: 5th - 9th September 2010*, Marseille, oral presentation.
 11. A. Huang*, H. Bux, F. Steinbach, and J. Caro, Molecular Sieve MOF Membrane with Hydrogen Permselectivity: ZIF-22 in LTA Topology Prepared Using 3-

-
- Aminopropyltriethoxysilane as Covalent. *MOF2010 - Metal-Organic Frameworks*: 5th - 8th September **2010**, Marseille, poster presentation.
- 12.** C. Chmelik*, J. Kärger, H. Bux, J. Caro, L. Hertäg, S. Fritzsche, J.M. van Baten, and R. Krishna, Characterizing Molecular Transport in MOF ZIF-8. *MOF2010 - Metal-Organic Frameworks*: 5th - 8th September **2010**, Marseille, poster presentation.
- 13.** M. Knauth*, K. Kirchner, S. Fritzsche, C. Chmelik, T. Remsungnen, K. Seeharmart, H. Bux, and J. Caro, Molecular Dynamics Investigation of the Influence of Lattice Flexibility and Partial Charges on the Migration of Guest Molecules in the Metal-Organic Framework ZIF-8. *MOF2010 - Metal-Organic Frameworks*: 5th - 8th September **2010**, Marseille, poster presentation.
- 14.** H. Bux*, Y.S. Li, J. Cravillon, M. Wiebcke, and J. Caro, Zeolitic Imidazolate Frameworks as Molecular Sieve Membranes. *23. Deutsche Zeolith-Tagung*: 2nd - 4th March **2011**, Erlangen, poster presentation.
- 15.** J. Cravillon, C.A. Schröder*, A. Rothkirch, H. Bux, J. Caro, and M. Wiebcke, Fast Synthesis of Big ZIF-8 Crystals Investigated Using Time-Resolved In-Situ Synchrotron EDXRD in Tandem with Ex-Situ SEM. *23. Deutsche Zeolith-Tagung*: 2nd - 4th March **2011**, Erlangen, poster presentation.
- 16.** H. Bux, A. Feldhoff, A. Huang, Y.S. Li, J. Cravillon, M. Wiebcke, C. Chmelik, J. Kärger, M. Knauth, S. Fritzsche, T. Remsungnen, and J. Caro, Preparation and Characterization of Zeolitic Imidazolate Framework Molecular Sieve Membranes. 5th International FEZA Conference: 3rd - 7th July, Valencia, oral presentation.

Curriculum Vitae

Personal data

Date of birth	March 20 th 1982
Place of birth	Hannover, Germany
Marital status	Unmarried, no children

Awards

March 2009	George Kokotailo Award Awarded for the best poster presentation (Fachsektion Zeolithe der DECHEMA, 21. Deutsche Zeolith-Tagung).
------------	--

Higher education

Since April 2009	Gottfried Wilhelm Leibniz University Hannover Research associate at the group of Prof. Dr. Jürgen Caro, Institute of Physical Chemistry and Electrochemistry
October 2008 - March 2009	Gottfried Wilhelm Leibniz University Hannover Degree: Diplom-Chemiker, mark: excellent Diploma thesis together with Prof. Dr. Jürgen Caro: Erste Schritte in der Präparation einer ZIF-8-Membran
October 2002 - November 2008	Gottfried Wilhelm Leibniz University Hannover Study of chemistry

Education

August 1992 - June 2001	IGS Mühlenberg, Hannover Degree: Abitur, mark: 1.7 Intense course: chemistry and music
Oktober 1990	Grundschule Wettbergen, Hannover
August 1988	Grundschule Alemannstraße, Hannover

Alternative civilian service

August 2001 - May 2002	KEKS e. V., Stuttgart
------------------------	------------------------------

Erklärung zur Dissertation

Hierdurch erkläre ich, dass ich meine Dissertation mit dem Titel

„Preparation and Characterization of Metal-Organic Framework Membranes for Gas Separation“

selbständig verfasst und die benutzten Hilfsmittel und Quellen sowie gegebenenfalls die zu Hilfeleistungen herangezogenen Institutionen vollständig angegeben habe.

Die Dissertation wurde nicht schon als Masterarbeit, Diplomarbeit oder andere Prüfungsarbeit verwendet.

Hannover, 15.07.2011

Dipl.-Chem. Helge Bux